New Directions in Cavity Quantum Electrodynamics

Simon James Whalen

A thesis submitted in fulfilment of the requirements
for the degree of Master of Science in Physics

The University of Auckland

2010

Abstract

Cavity quantum electrodynamics (cavity QED) is the study of systems in which atoms interact with the quantised electromagnetic modes of an optical cavity. We consider two new directions in cavity QED: two-mode cavity QED and circuit QED.

In two-mode cavity QED, an atom with Zeeman structure in its ground and excited states interacts with two orthogonal linear polarisation modes of an optical cavity, via an $F = 3 \leftrightarrow F' = 4$ transition. We consider the full atomic level structure for this transition, including the Zeeman energy shift, as well as the atom's coupling to the two orthogonal modes of the cavity. By approximating the driven mode of the cavity semiclassically, we are able to investigate quantum beats: interference fringes in the second-order photon correlation function caused by the Larmor precession of the atom in an applied magnetic field. We go on to simulate the strong driving behaviour of this system, and find that the mean photon number in the non-driven mode of the cavity begins to decrease beyond a certain threshold driving field strength. We explain this behaviour qualitatively by way of an analogy to a simple model involving an atom with just two relevant quantum states.

Circuit QED is an implementation of cavity QED in a superconducting circuit. We develop the background physics of one particular circuit QED system, which consists of a transmission line cavity coupled to a superconducting charge qubit. The type of qubit used in this system, known as a transmon, behaves in many ways more similarly to an anharmonic oscillator than a pure qubit. As an application of the model we develop, we investigate dispersive optical bistability in the circuit QED system. We perform a semiclassical treatment of the system, including a linearised stability analysis, which is indicative of bistability. We then carry out a full quantum treatment, plotting Q-functions to visualise the bimodality of the cavity field. Monte Carlo simulations based on a quantum trajectory unravelling of the master equation display the expected "tunnelling" between metastable states due to quantum fluctuations, confirming the presence of dispersive optical bistability in our model.

Acknowledgements

First and foremost, I would like to thank my supervisors Howard Carmichael, Matthew Collett and Scott Parkins for their invaluable help and guidance. I count myself lucky to have had the opportunity to learn from three such excellent teachers.

I would also like to thank Luis Orozco, David Norris, Pablo Barberis-Blostein and everyone else I met at the University of Maryland for making me feel welcome, and for many interesting discussions.

My thanks to Sophie Shamailov, whose intelligence is matched only by her irrepressible enthusiasm and thirst for knowledge, for several valuable conversations. I thank the rest of my fellow students for creating a great sense of community, and for making this last year so much fun. And finally to all my friends and family, thank you for your unwavering support.

Contents

1

Introduction

Cavity quantum electrodynamics (cavity QED) is the study of systems in which atoms interact with the quantised electromagnetic modes of an optical cavity [1, 2].

In quantum electrodynamics in general, the electromagnetic field may be quantised by considering a finite volume defined by conducting walls, where the field can be decomposed into a discrete, though infinite, set of modes. The field is quantised in the usual way, by imposing canonical commutation relations. Then, the mode volume is increased to infinity, and the continuous spectrum of the field is recovered. If, however, the conducting walls of the mode volume are retained in the form of a cavity, this imposes boundary conditions on the field, and the spectrum of the cavity field remains discrete. It is this discrete field that an atom interacts with in a cavity QED experiment. In its simplest form, cavity QED consists of a single atom with just two relevant quantum states, coupled to a single mode of the electromagnetic field.

In this thesis we consider two new directions in cavity quantum electrodynamics. The first is two-mode cavity QED, in which an atom with Zeeman structure in its ground and excited states interacts with two orthogonal linear polarisation modes of an optical cavity. The inclusion – in contrast to the prototypical form of cavity QED, which involves a two-level atom and a single cavity mode – of the additional cavity mode and magnetic substructure of the atomic energy levels gives rise to unique physics. The second new direction we investigate is circuit quantum electrodynamics, which is an implementation of cavity QED in a superconducting circuit. We consider a circuit QED system consisting of a transmission-line cavity coupled to a superconducting charge qubit, and make connections with the physics of traditional cavity QED.

This thesis is largely concerned with the modelling of *open quantum systems* [3]: systems which interact with the surrounding environment. Therefore in chapter 2 we develop the mathematical theory of open quantum systems, and derive the Lindblad master equation [4], which is the most general form of a large class of Markovian quantum master equations. The Lindblad master equation describes the non-unitary evolution of the density matrix which characterises the state of the open quantum system, and is put to much use in the following chapters. Additionally, we present an overview of *quantum trajectory theory* [5], which is an alternative conceptual and computational tool for analysing the dynamics of an open quantum system.

In chapter 3, we review the *Jaynes-Cummings model* [6], which describes the interaction of a two-level atom with a single quantised mode of the electromagnetic field. We derive the Jaynes-Cummings Hamiltonian for an isolated atom-cavity system; this Hamiltonian is readily

generalised to take driving of the system into account. The Lindblad master equation is used to describe the damping of the Jaynes-Cummings system which arises due to its interaction with the surrounding environment. Our consideration of the Jaynes-Cummings model underlies much of the following theory of cavity QED.

In chapter 4, we set out to model – using the Jaynes-Cummings model as a starting point – a two-mode cavity quantum electrodynamics experiment carried out by L. A. Orozco's group at the University of Maryland [7]. This system comprises a single Rubidium-85 atom within an optical cavity. Two optical cavity modes with orthogonal linear polarisations interact with the atom via the atom's $5S_{1/2}, F = 3 \leftrightarrow 5P_{3/2}, F' = 4$ transition; one of the cavity modes is resonantly driven by a periodic classical field. We consider the full atomic level structure for this transition, including the Zeeman energy shift, as well as the atom's coupling to the two orthogonal modes of the cavity. Chapter 5 is devoted to results obtained from the two-mode cavity QED model we have developed. We find that this system displays *quantum beats* [8]: interference fringes in the second-order photon correlation function, caused by the Larmor precession of the atom in an applied magnetic field. We find that we can approximate the driven mode of the cavity semiclassically, and use this approximation to further investigate quantum beat effects, as well as the strong driving behaviour of the system.

In chapter 6 we introduce *circuit quantum electrodynamics* [9]: a radical new implementation of cavity quantum electrodynamics, in a superconducting circuit. Circuit QED is of great interest due to potential applications in the field of quantum information processing [10, 11]. Chapter 7 is devoted to the detailed development of the background physics of one particular type of circuit QED system, starting from the basic principles of quantum mechanics and of electrical circuit theory. The particular implementation of circuit QED we consider consists of a one-dimensional transmission line cavity coupled to a superconducting charge qubit. This type of system fits the experimental requirements to achieve strong coupling between the qubit and the electromagnetic field, in which the rate of absorption or emission of a single photon by the qubit is more rapid than any of the rates of loss [11, 12]. In recent years, dramatic measurements showing the quantum mechanics of the Jaynes-Cummings model have been made in circuit QED systems: measurements which would never have been possible with real atoms [13, 14]. The type of qubit used in the circuit QED system we investigate is known as a *transmon* [15], and behaves in many ways more similarly to an anharmonic oscillator than a pure qubit. In chapter 8, as an application of the theory we have developed, we investigate dispersive optical bistability in our model of the circuit QED system.

Finally, a word on the subject of notation. Some aspects of the notation used in parts of this thesis are inconsistent. For example, we often use circumflexes to denote Hilbert space operators such as $\hat{a}$ or $\hat{\sigma}_-$; Hamiltonians, however, will generally not possess circumflexes. Where confusion is unlikely, we may omit the circumflexes altogether. Another example of a notational change is the omission of the subscript on the density operator ρ_S for an open quantum system. Where a notational change might cause confusion, we will introduce it explicitly.

References

[1] H. Walther, B. T. H. Varcoe, B.-G. Englert, and T. Becker. Cavity quantum electrodynamics. *Reports on Progress in Physics*, 69:1325–1382, 2006.

[2] R. Miller, T. E. Northup, K. M. Birnbaum, A. Boca, A. D. Boozer, and H. J. Kimble. Trapped atoms in cavity QED: coupling quantized light and matter. *Journal of Physics B*, 38:S551–S565, 2005.

[3] H.-P. Breuer and F. Pettruccione. *The theory of open quantum systems*. Oxford University Press, 2007.

[4] G. Lindblad. On the generators of quantum dynamical semigroups. *Communications in Mathematical Physics*, 48:119–130, 1976.

[5] H. J. Carmichael. *An Open Systems Approach to Quantum Optics*. Springer-Verlag, 1993.

[6] E. T. Jaynes and F. W. Cummings. Comparison of quantum and semiclassical radiation theories with application to the beam maser. *Proceedings of the IEEE*, 51:89–109, 1963.

[7] D. G. Norris, L. A. Orozco, P. Barberis-Blostein, and H. J. Carmichael. Observation of ground-state quantum beats in atomic spontaneous emission. To be published in *Physical Review Letters*, 2010.

[8] P. Barberis-Blostein, D. G. Norris, L. A. Orozco, and H. J. Carmichael. From quantum feedback to probabilistic error correction: manipulation of quantum beats in cavity QED. *New Journal of Physics*, 12:023002, 2010.

[9] R. J. Schoelkopf and S. M. Girvin. Wiring up quantum systems. *Nature*, 451:664–669, 2008.

[10] J. Q. You and F. Nori. Quantum information processing with superconducting qubits in a microwave field. *Phys. Rev. B*, 68:064509, 2003.

[11] A. Blais, R.-S. Huang, A. Wallraff, S. M. Girvin, and R. J. Schoelkopf. Cavity quantum electrodynamics for superconducting electrical circuits: An architecture for quantum computation. *Physical Review A*, 69:062320, 2004.

[12] A. Wallraff, D. I. Schuster, A. Blais, L. Frunzio, R.-S. Huang, J. Majer, S. Kumar, S. M. Girvin, and R. J. Schoelkopf. Strong coupling of a single photon to a superconducting qubit using circuit quantum electrodynamics. *Nature*, 431:162–167, 2004.

[13] J. M. Fink, M. Göppl, M. Baur, R. Bianchetti, P. J. Leek, A. Blais, and A. Wallraff. Climbing the Jaynes-Cummings ladder and observing its $\sqrt{n}$ nonlinearity in a cavity QED system. *Nature*, 454:315–318, 2008.

[14] L. S. Bishop, J. M. Chow, J. Koch, A. A. Houck, M. H. Devoret, E. Thuneberg, S. M. Girvin, and R. J. Schoelkopf. Nonlinear response of the vacuum Rabi resonance. *Nature Physics*, 5:105–109, 2009.

[15] J. Koch, T. M. Yu, J. Gambetta, A. A. Houck, D. I. Schuster, J. Majer, A. Blais, M. H. Devoret, S. M. Girvin, and R. J. Schoelkopf. Charge-insensitive qubit design derived from the Cooper pair box. *Physical Review A*, 76:042319, 2007.

2

Open quantum systems

Sections 2.1 and 2.2 will largely follow the course and notation of Breuer and Pettruccione [1]. Other treatments are available in Kronenwett [2] and Carmichael [3]. Throughout this chapter we will set $\hbar \equiv 1$.

2.1 Closed and open quantum systems

2.1.1 The von Neumann equation

The Schrödinger equation for the time evolution of the state vector $|\psi(t)\rangle$ is

$$\mathrm{i}\frac{\mathrm{d}}{\mathrm{d}t}|\psi(t)\rangle = H(t)|\psi(t)\rangle \,. \tag{2.1}$$

The solution of the Schrödinger equation with initial condition $|\psi(t_0)\rangle$ can be written

$$|\psi(t)\rangle = U(t,t_0)|\psi(t_0)\rangle \,, \tag{2.2}$$

where $U(t,t_0)$ is the unitary time evolution operator. The time evolution operator also satisfies the Schrödinger equation:

$$\mathrm{i}\frac{\partial}{\partial t}U(t,t_0) = H(t)U(t,t_0)\,, \tag{2.3}$$

with initial condition

$$U(t_0,t_0) = I\,. \tag{2.4}$$

The solution of (2.3) with initial condition (2.4) can be written as

$$U(t,t_0) = \mathrm{T}\exp\left[-\mathrm{i}\int_{t_0}^{t}\mathrm{d}s\,H(s)\right], \tag{2.5}$$

where the time ordering operator T orders products of time-dependent operators such that their time arguments increase from right to left: "earlier operators operate earlier". Obviously when the Hamiltonian is time-independent the above solution reduces to $U(t,t_0) = \exp[-\mathrm{i}H(t-t_0)]$.

It may be the case that the system under consideration is driven by external forces. If, however, the dynamics of the system can still be formulated solely in terms of a Hamiltonian $H(t)$ (which, as the notation suggests, may in general be time-dependent), the system is still

considered to be *closed*. A system whose Hamiltonian is independent of time is called an *isolated* system.

If the system under consideration is in a mixed state, we characterise it by way of the density matrix $\rho(t)$. As is well-known (and very easy to show), the equation of motion for the density matrix is the von Neumann equation,

$$\frac{\mathrm{d}}{\mathrm{d}t}\rho(t) = -\mathrm{i}\,[H(t), \rho(t)]\,. \tag{2.6}$$

The von Neumann equation can be written in a form analogous to the well-known classical Liouville equation,

$$\frac{\mathrm{d}}{\mathrm{d}t}\rho(t) = \mathcal{L}(t)\rho(t)\,, \tag{2.7}$$

where the *Liouville super-operator* (or simply *Liouvillian*) is defined by writing

$$\mathcal{L}(t)\hat{A} \equiv -\mathrm{i}[H(t), \hat{A}]\,. \tag{2.8}$$

If we assume that at some inital time t_0 the state of the system is characterised by the density matrix $\rho(t_0)$ we obtain, much as in (2.5), the formal solution

$$\rho(t) = \mathrm{T}\exp\left[\int_{t_0}^{t} \mathrm{d}s\,\mathcal{L}(s)\right]\rho(t_0)\,. \tag{2.9}$$

If the Hamiltonian is time-independent, then so is the Liouvillian, and we get

$$\rho(t) = \exp[\mathcal{L}(t - t_0)]\rho(t_0)\,. \tag{2.10}$$

2.1.2 Composite quantum systems

Consider two quantum systems S_A and S_B with Hilbert spaces $\mathcal{H}_A$ and $\mathcal{H}_B$ respectively. The state space of the combined system $S = S_A + S_B$ is given by

$$\mathcal{H} = \mathcal{H}_A \otimes \mathcal{H}_B\,. \tag{2.11}$$

If we take a fixed orthonormal basis $\{|\psi_{A,i}\rangle\}$ for $\mathcal{H}_A$ and $\{|\psi_{B,i}\rangle\}$ for $\mathcal{H}_B$, a general state in $\mathcal{H}$ can be written $|\Psi\rangle = \sum_{ij} \alpha_{ij}\,|\psi_{A,i}\rangle \otimes |\psi_{B,j}\rangle$. Thus, the elements $|\psi_{A,i}\rangle \otimes |\psi_{B,j}\rangle$ form a basis for $\mathcal{H}$.

If $\hat{O}_A$ and $\hat{O}_B$ are operators acting in $\mathcal{H}_A$ and $\mathcal{H}_B$ respectively, their tensor product is defined by

$$(\hat{O}_A \otimes \hat{O}_B)(|\psi_{A,i}\rangle \otimes |\psi_{B,j}\rangle) \equiv (\hat{O}_A\,|\psi_{A,i}\rangle) \otimes (\hat{O}_B\,|\psi_{B,j}\rangle)\,. \tag{2.12}$$

The action of an operator on an arbitrary state is defined by a linear extension of the above formula. Any operator $\hat{O}$ on $\mathcal{H}$ can be written $\hat{O} = \sum_\alpha \hat{O}_{A,\alpha} \otimes \hat{O}_{B,\alpha}$; specifically, the observables

of system S_A take the form $\hat{O}_A \otimes I_B$, and the observables of S_B take the form $I_A \otimes \hat{O}_B$. If one is only interested in observables of the subsystem S_A, say, one can make use of the reduced density matrix defined by

$$\rho_A \equiv \mathrm{tr}_B \rho \,, \tag{2.13}$$

where tr_B denotes the partial trace over $\mathcal{H}_B$. The reduced density matrix ρ_A completely describes the statistical properties of all observables belonging to S_A, that is observables of the form $\hat{O}_A \otimes I_B$; the expectation value of such an observable can be determined using the formula $\langle \hat{O} \rangle = \mathrm{tr}_A(\hat{O}_A \rho_A)$.

2.1.3 Open quantum systems

An open quantum system is a quantum system S (which we will frequently refer to as simply the *system*) which is coupled to another quantum system E, called the *environment*. The combined system $S + E$ is usually assumed to be closed, with dynamics described by the von Neumann equation. The dynamics of S however cannot, in general, be described in terms of unitary time-evolution as those of a closed system can. This is because the state of S will evolve as a consequence of both its internal dynamics and of its interaction with the environment, the interaction giving rise to correlations between the system and the environment.

If we denote the Hilbert spaces of S and E respectively by $\mathcal{H}_S$ and $\mathcal{H}_E$, then the Hilbert space of the combined system $S+E$ is given by $\mathcal{H} = \mathcal{H}_S \otimes \mathcal{H}_E$. The Hamiltonian of the combined system will take on the form

$$H(t) = H_S \otimes I_E + I_S \otimes H_E + H_I(t) \,, \tag{2.14}$$

where H_S and H_E are the free Hamiltonians for the system and environment respectively, and $H_I(t)$ describes the interaction between the two. If the environment E has infinitely many degrees of freedom, it is referred to as a *reservoir*. A reservoir in thermal equilibrium is a *bath*.

Sometimes a complete treatment of the dynamics of the combined system would be too complex to be practical. For example, a reservoir or bath consisting of infinitely many degrees of freedom has infinitely many equations of motion. Provided that all measurements of interest will pertain to the system S rather than its environment, we can develop a simpler description in the reduced state space $\mathcal{H}_S$. Referring back to section 2.1.2, all observables of S take the form $A_S \otimes I_E$, where A_S is an operator acting on $\mathcal{H}_S$. If the state of the combined system $S + E$ is described by ρ, then the expectation values of all observables acting on $\mathcal{H}_S$ are determined using

$$\langle A_S \rangle = \mathrm{tr}_S[A_S \rho_S] \,, \tag{2.15}$$

where

$$\rho_S = \mathrm{tr}_E(\rho) \tag{2.16}$$

is referred to as the reduced density matrix of the open quantum system S; tr_S and tr_E denote the partial traces over the system and environment respectively.

We see that the reduced density matrix $\rho_S(t)$ is obtained from the density matrix $\rho(t)$ of the combined system $S + E$ by taking the partial trace over the degrees of freedom of the environment. Since the evolution of $\rho(t)$ is determined by the von Neumann equation (2.6), we can take the partial trace on both sides to obtain

$$\frac{\mathrm{d}}{\mathrm{d}t}\rho_S(t) = -\mathrm{i}\,\mathrm{tr}_E\{[H(t), \rho(t)]\}\,. \tag{2.17}$$

Similarly, as $\rho(t)$ evolves unitarily, we have

$$\rho_S(t) = \mathrm{tr}_E\{U(t, t_0)\rho(t_0)U^\dagger(t, t_0)\}\,. \tag{2.18}$$

2.2 The Lindblad master equation

Here we will briefly outline the formal mathematics behind the Markovian quantum master equation known as the *Lindblad master equation*, or simply the *Lindblad equation*. The details are available in, for example, Breuer and Pettruccione [4], and references therein.

2.2.1 Quantum dynamical semigroups

An important property of a classical, homogeneous Markov process is the semigroup property [5]. In the same way, a quantum Markov processes may be described by way of quantum dynamical semigroups, which we will now introduce.

Suppose that the state of the combined system $S + E$ at initial time $t = 0$ can be expressed as an uncorrelated product state $\rho(0) = \rho_S(0) \otimes \rho_E$, where ρ_E is some reference state of the environment. From (2.18), the transformation describing the evolution of the reduced system from $t = 0$ to some $t > 0$ can be written

$$\rho_S(0) \mapsto \rho_S(t) = V(t)\rho_S(0) \equiv \mathrm{tr}_E\{U(t, t_0)[\rho_S(0) \otimes \rho_E]U^\dagger(t, t_0)\}\,. \tag{2.19}$$

If we take ρ_E and the final time $t > 0$ to be fixed, the above relation defines a map from the space of density matrices of the reduced system, $\mathcal{S}(\mathcal{H}_S)$, to itself: $V(t) : \mathcal{S}(\mathcal{H}_S) \to \mathcal{S}(\mathcal{H}_S)$. The map $V(t)$ is known as a *dynamical map*. It can be shown that the dynamical map $V(t)$ can always be written entirely in terms of operators in $\mathcal{H}_S$ [4].

If we allow t to vary, we get a one-parameter family of dynamical maps,

$$\{V(t) \,|\, t \geq 0\}\,, \tag{2.20}$$

with $V(0)$ the identity. This family of maps completely characterises the future time-evolution of the open quantum system.

Provided that the time scales over which the correlation functions of the environment decay are much smaller than the time scale of the system's evolution, we can neglect memory effects in

the dynamics of the reduced system: the dynamics of the reduced system will be Markovian. The dynamical map corresponding to a time-homogeneous Markov process satisfies the semigroup property,

$$V(t_1)V(t_2) = V(t_1 + t_2)\,, \quad t_1, t_2 \geq 0\,. \tag{2.21}$$

A *quantum dynamical semigroup* is a continuous, one-parameter family of dynamical maps satisfying the semigroup property (2.21). The physical conditions under which the dynamics of the system can be assumed to Markovian will be examined later.

2.2.2 Generator of a quantum dynamical semigroup

Given a quantum dynamical semigroup there exists, subject to certain mathematical conditions [6], a linear map $\mathcal{L}$ that is the infinitesimal generator of the semigroup. Thus, we can represent the dynamical map in exponential form,

$$V(t) = \exp(\mathcal{L}t)\,, \tag{2.22}$$

which yields the equation of motion

$$\frac{\mathrm{d}}{\mathrm{d}t}\rho_S(t) = \mathcal{L}\rho_S(t)\,, \tag{2.23}$$

known as the *Markovian quantum master equation*. The generator $\mathcal{L}$ is a super-operator – a generalisation of the Liouvillian introduced in section 2.1.1. When confusion is unlikely, we will refer to the generator $\mathcal{L}$ as the Liouvillian as well.

If $\dim \mathcal{H}_s = N$, the corresponding Liouville space[1] has dimension N^2, and we can define a basis for the Liouville space, comprising orthonormal operators F_j, $j = 1, 2, \ldots, N^2$. The most general form of the generator is given by

$$\mathcal{L}\rho_S = -\mathrm{i}\,[H, \rho_S] + \sum_{i=1}^{N^2-1} \gamma_i \left(A_i \rho_S A_i^\dagger - \frac{1}{2} A_i^\dagger A_i \rho_s - \frac{1}{2} \rho_s A_i^\dagger A_i \right), \tag{2.24}$$

where the so-called *Lindblad operators* A_k are linear combinations of the basis functions F_i of the Liouville space. The master equation (2.23) corresponding to this generator is known as the *master equation in Lindblad form*, or simply the *Lindblad equation*.

The form (2.24) for the generator is constructed in Breuer and Pettruccione [4], but the actual proof that it is the most general form for the generator of a quantum dynamical semigroup, in the case of a finite-dimensional Hilbert space, has been given by Gorini et al. [8]; a related theorem was proved by Lindblad [9], for whom the equation is named.

[1] The generator $\mathcal{L}$ is an operator on Liouville space. See Breuer and Pettruccione [7].

2.2.3 Time-dependent generator

If an open quantum system is subjected to an external time-dependent field, the generator may also be time-dependent. An obvious time-dependent generalisation of (2.24) is

$$\frac{\mathrm{d}}{\mathrm{d}t}\rho_S(t) = \mathcal{L}(t)\rho_S(t)\,, \tag{2.25}$$

where $\mathcal{L}(t)$ is the generator of a quantum dynamical semigroup for each *fixed* $t \geq 0$. The corresponding propagator is

$$V(t, t_0) = \mathrm{T}\exp\left[\int_{t_0}^{t} \mathrm{d}s\, \mathcal{L}(s)\right]. \tag{2.26}$$

Compare this to (2.9). The time-dependent generalisation of the semigroup property (2.21) is

$$V(t, t_1)V(t_1, t_0) = V(t, t_0)\,, \tag{2.27}$$

which reduces to the semigroup property for fixed t.

2.2.4 Microscopic derivation of the Lindblad master equation

Consider a quantum mechanical system S weakly coupled to a reservoir E. The combined system's Hamiltonian is of the form

$$H = H_S + H_E + H_I\,. \tag{2.28}$$

The von Neumann equation in the interaction picture is

$$\frac{\mathrm{d}}{\mathrm{d}t}\rho(t) = -\mathrm{i}\left[H_I(t), \rho(t)\right]\,, \tag{2.29}$$

where $H_I(t)$ is the interaction part of Hamiltonian, transformed into the interaction picture. Integrating, we obtain

$$\rho(t) = \rho(0) - \mathrm{i}\int_0^t \mathrm{d}s\, \left[H_I(s), \rho(s)\right]\,. \tag{2.30}$$

Substituting the integral form of the von Neumann equation back into the differential form (2.29) and tracing over the reservoir degrees of freedom gives

$$\frac{\mathrm{d}}{\mathrm{d}t}\rho_S(t) = -\int_0^t \mathrm{d}s\, \mathrm{tr}_E\left\{\left[H_I(t), \left[H_I(s), \rho(s)\right]\right]\right\}\,, \tag{2.31}$$

where we have assumed that

$$\mathrm{tr}_E\left\{\left[H_I(t), \rho(0)\right]\right\} = 0\,. \tag{2.32}$$

In order to eliminate the density matrix $\rho(t)$ of the combined system from the right-hand

side of (2.31), we make an approximation known as the *Born approximation*. Provided the coupling between the system and reservoir is weak, the influence of the system on the reservoir will be small, and we can assume that the effect of the interaction on the reduced density matrix ρ_E of the reservoir is negligible. Thus, we can approximate the state of the combined system by

$$\rho(t) \approx \rho_S(t) \otimes \rho_E \,. \tag{2.33}$$

This approximation does not mean that the open quantum system causes no excitations in the reservoir: the Markov approximation, which we introduce below, deals with this issue. Substituting (2.33) into (2.31), we get

$$\frac{\mathrm{d}}{\mathrm{d}t}\rho_S(t) = -\int_0^t \mathrm{d}s\, \mathrm{tr}_E \left\{[H_I(t), [H_I(s), \rho_S(s) \otimes \rho_E]]\right\} . \tag{2.34}$$

In (2.34), the time-evolution of the system state depends on all the past states of the system. We now make the *Markov approximation*: the approximation that the time-evolution of the state of the system at time t depends only on the present state $\rho_S(t)$, and not on all the past states. The Markov approximation amounts to replacing $\rho_S(s)$ in the integrand above with $\rho_S(t)$. The resulting equation,

$$\frac{\mathrm{d}}{\mathrm{d}t}\rho_S(t) = -\int_0^t \mathrm{d}s\, \mathrm{tr}_E \left\{[H_I(t), [H_I(t-s), \rho_S(t) \otimes \rho_E]]\right\} , \tag{2.35}$$

is known as the *Redfield equation* [10]. Note that we have substituted $t - s$ for s above. The Redfield equation is local in time: the future time-evolution does not depend on the history of the system. However, it is not yet a Markovian master equation, since the time-evolution does depend on the initial preparation of ρ_S at time $t = 0$. This dependence enters the Redfield equation by way of the upper integration limit, and so it can be removed by letting the upper limit of the integral go to infinity,

$$\frac{\mathrm{d}}{\mathrm{d}t}\rho_S(t) = -\int_0^\infty \mathrm{d}s\, \mathrm{tr}_E \left\{[H_I(t), [H_I(t-s), \rho_S(t) \otimes \rho_E]]\right\} . \tag{2.36}$$

This approximation is justified provided that the integrand disappears sufficiently fast for $s \gg \tau_E$, where τ_E is the reservoir correlation time. Thus we see that the relaxation time of the system τ_R, which defines the characteristic time-scale over which the system state varies appreciably, must be large compared with τ_E for the Markov approximation to apply.

The Markov approximation provides a description of the dynamics on a coarse-grained time-scale, larger than the time-scale of the reservoir correlations. The underlying assumption is that the reservoir excitations decay over times which are not resolved, justifying the Born approximation we made earlier. Indeed, any dynamical behaviour on time-scales of the order of magnitude of the reservoir correlation time τ_E is not resolved by a Markovian quantum master equation.

Before we continue with our derivation of the Lindblad master equation, we will make an interesting digression. To this end we characterise the strength of the interaction between

system and environment by a coupling strength α, writing

$$H_I \to \alpha H_I \,. \tag{2.37}$$

The Markov approximation simplifies the calculations substantially: equation (2.34), where only the Born approximation has been made, is a rather complicated integro-differential equation, and the Markov approximation removes much of the complexity. Despite this fact, to second order in the coupling strength α, omitting the Markov approximation (and making only the Born approximation) does not, in general, improve the accuracy of the calculation [11]. It is interesting to note that both the Born and Markov approximations are only valid to second order in the coupling strength.

The approximations made above in equations (2.33), (2.35) and (2.36) are known collectively as the *Born-Markov approximation*. However in general they do not guarantee that the equation of motion (2.36) defines the generator of a quantum dynamical semigroup [12, 13]. A further approximation is necessary: a secular approximation in which one averages over those terms in the master equation which oscillate rapidly. This approximation is known as the *rotating-wave approximation*. Before this approximation can be made, though, some additional steps are required.

In the Schrödinger picture, the interaction Hamiltonian can always be expanded in the form [14]

$$H_I = \sum_{\alpha,\omega} A_\alpha(\omega) \otimes B_\alpha \,, \tag{2.38}$$

where B_α are reservoir operators, and $A_\alpha(\omega)$ are degenerate eigenoperators of the system Hamiltonian H_S, such that

$$[H_S, A_\alpha(\omega)] = -\omega A_\alpha(\omega) \,, \tag{2.39a}$$
$$[H_S, A_\alpha^\dagger(\omega)] = \omega A_\alpha^\dagger(\omega) \,. \tag{2.39b}$$

Both $\sum_\omega A_\alpha(\omega)$ and B_α are Hermitian operators for all α. From these relations we find the corresponding interaction picture operators:

$$\mathrm{e}^{\mathrm{i}H_S t} A_\alpha(\omega) \mathrm{e}^{-\mathrm{i}H_S t} = \mathrm{e}^{-\mathrm{i}\omega t} A_\alpha(\omega) \,, \tag{2.40a}$$
$$\mathrm{e}^{\mathrm{i}H_S t} A_\alpha^\dagger(\omega) \mathrm{e}^{-\mathrm{i}H_S t} = \mathrm{e}^{\mathrm{i}\omega t} A_\alpha^\dagger(\omega) \,. \tag{2.40b}$$

The interaction Hamiltonian can now be written in the form

$$\begin{aligned} H_I(t) &= \sum_{\alpha,\omega} \mathrm{e}^{-\mathrm{i}\omega t} A_\alpha(\omega) \otimes B_\alpha(t) \\ &= \sum_{\alpha,\omega} \mathrm{e}^{\mathrm{i}\omega t} A_\alpha^\dagger(\omega) \otimes B_\alpha^\dagger(t) \,, \end{aligned} \tag{2.41}$$

where

$$B_\alpha(t) = \mathrm{e}^{\mathrm{i}H_E t} B_\alpha \mathrm{e}^{-\mathrm{i}H_E t}\,. \tag{2.42}$$

Note that the assumption (2.32) now becomes

$$\mathrm{tr}\{B_\alpha(t)\rho_E\} = \langle B_\alpha(t)\rangle = 0\,, \tag{2.43}$$

that is, we have in fact assumed the expectation values of $B_\alpha(t)$ in the reservoir vanish.

Substituting the form (2.41) of the interaction Hamiltonian into (2.36), we obtain

$$\begin{aligned}\frac{\mathrm{d}}{\mathrm{d}t}\rho_S(t) &= \int_0^\infty \mathrm{d}s\,\mathrm{tr}_E[H_I(t-s)\rho_S(t)\otimes\rho_E H_I(t) - H_I(t)H_I(t-s)\rho_S(t)\otimes\rho_E] + \text{h.c.}\\ &= \sum_{\alpha,\omega'}\sum_{\beta,\omega}\mathrm{e}^{\mathrm{i}(\omega'-\omega)t}\Gamma_{\alpha\beta}(\omega)[A_\beta(\omega)\rho_S(t)A_\alpha^\dagger(\omega') - A_\alpha^\dagger(\omega')A_\beta(\omega)\rho_S(t)] + \text{h.c.}\,,\end{aligned} \tag{2.44}$$

where

$$\Gamma_{\alpha\beta}(\omega) = \int_0^\infty \mathrm{d}s\,\mathrm{e}^{\mathrm{i}\omega s}\left\langle B_\alpha^\dagger(t)B_\beta(t-s)\right\rangle\,, \tag{2.45}$$

with the *reservoir correlation functions*

$$\left\langle B_\alpha^\dagger(t)B_\beta(t-s)\right\rangle = \mathrm{tr}_E[B_\alpha^\dagger(t)B_\beta(t-s)\rho_E]\,. \tag{2.46}$$

Supposing that ρ_E is a stationary state of the reservoir Hamiltonian, $[H_E,\rho_E]=0$, the reservoir correlation functions are homogeneous in time,

$$\left\langle B_\alpha^\dagger(t)B_\beta(t-s)\right\rangle = \left\langle B_\alpha^\dagger(s)B_\beta(0)\right\rangle\,, \tag{2.47}$$

which means that the quantities $\Gamma_{\alpha\beta}(\omega)$ do not depend on time.

In order for the Markov approximation to be justified, the time τ_E over which the reservoir correlation functions decay must, as we have already remarked, be much smaller than the system relaxation time τ_R. If we were dealing with a general environment consisting of a collection of harmonic oscillator modes with a discrete frequency spectrum, the reservoir correlation functions would be quasi-periodic in s [14]. Rapid decay of the reservoir correlations requires a continuum of frequencies, which is in fact the case when we consider a reservoir, which has infinitely many degrees of freedom.

We are now in a position to make the rotating-wave approximation we mentioned earlier. The typical time-scale τ_S on which the system S evolves is defined by a typical value of $|\omega'-\omega|^{-1}$, where $\omega'\neq\omega$. If $\tau_S \gg \tau_R$, then the terms for which $\omega'\neq\omega$ oscillate very rapidly over the typical time-scale on which the system state varies and can be neglected. Assuming that this

condition is satisfied, we obtain

$$\frac{\mathrm{d}}{\mathrm{d}t}\rho_S(t) = \sum_{\omega}\sum_{\alpha,\beta}\Gamma_{\alpha\beta}(\omega)[A_\beta(\omega)\rho_S(t)A_\alpha^\dagger(\omega) - A_\alpha^\dagger(\omega)A_\beta(\omega)\rho_S(t)] + \text{h.c.} \tag{2.48}$$

We perform the decomposition

$$\Gamma_{\alpha\beta}(\omega) = \frac{1}{2}\gamma_{\alpha\beta}(\omega) + \mathrm{i}S_{\alpha\beta}(\omega)\,, \tag{2.49}$$

such that, for fixed ω, the matrix formed by

$$S_{\alpha\beta}(\omega) = \frac{1}{2\mathrm{i}}[\Gamma_{\alpha\beta}(\omega) - \Gamma_{\beta\alpha}^*(\omega)] \tag{2.50}$$

is Hermitian, and the matrix formed by

$$\gamma_{\alpha\beta}(\omega) = \Gamma_{\alpha\beta}(\omega) + \Gamma_{\beta\alpha}^*(\omega) \tag{2.51}$$

is positive.[2] Seeing the indices α and β run over the same set, these definitions finally lead to the interaction picture master equation

$$\begin{aligned}\frac{\mathrm{d}}{\mathrm{d}t}\rho_S(t) = -\mathrm{i}\,[H_{LS}, \rho_S(t)] + \sum_{\omega}\sum_{\alpha,\beta}\gamma_{\alpha\beta}(\omega)\Big[&A_\beta(\omega)\rho_S(t)A_\alpha^\dagger(\omega) \\ &- \frac{1}{2}A_\alpha^\dagger(\omega)A_\beta(\omega)\rho_S(t) - \frac{1}{2}\rho_S(t)A_\alpha^\dagger(\omega)A_\beta(\omega)\Big],\end{aligned} \tag{2.52}$$

where

$$H_{LS} = \sum_{\omega}\sum_{\alpha,\beta}S_{\alpha\beta}(\omega)A_\alpha^\dagger A_\beta(\omega) \tag{2.53}$$

is known as the *Lamb shift* Hamiltonian, because it results in a Lamb shift-type renormalisation of the unperturbed energy levels, caused by the system-reservoir coupling.[3] From (2.40), it is easy to show that the Lamb shift Hamiltonian commutes with the system Hamiltonian, $[H_S, H_{LS}] = 0$.

Once the master equation (2.52) is transformed back into the Schrödinger picture, it can be brought into Lindblad form – corresponding to the generator (2.24) – by diagonalising the matrix $\gamma_{\alpha\beta}(\omega)$. The final form of the Lindblad equation is

$$\frac{\mathrm{d}}{\mathrm{d}t}\rho_S(t) = -\mathrm{i}\,[H_S + H_{LS}, \rho_S(t)] + \sum_i \gamma_i\Big[A_i\rho_S(t)A_i^\dagger - \frac{1}{2}A_i^\dagger A_i\rho_S(t) - \frac{1}{2}\rho_S(t)A_i^\dagger A_i\Big], \tag{2.54}$$

where the index i runs over the various independent decay channels.

[2] For the proof that $\gamma_{\alpha\beta}(\omega)$ is positive, see Breuer and Pettruccione [14] and references therein.
[3] See Breuer and Pettruccione [15] for a treatment of this term.

2.2.5 Jump operators

The master equation in Lindblad form, with generator given by (2.24), is also sometimes written in a different form, which we obtain by scaling the Lindblad operators,

$$\hat{\jmath}_i \equiv \sqrt{\gamma_i} A_i \,, \tag{2.55}$$

so that the master equation becomes

$$\frac{\mathrm{d}}{\mathrm{d}t}\rho_S(t) = -\mathrm{i}\left[H_S + H_{LS}, \rho_S(t)\right] + \sum_i \left(\hat{\jmath}_i \rho_S(t) \hat{\jmath}_i^\dagger - \frac{1}{2}\hat{\jmath}_i^\dagger \hat{\jmath}_i \rho_S(t) - \frac{1}{2}\rho_S(t)\hat{\jmath}_i^\dagger \hat{\jmath}_i\right). \tag{2.56}$$

The operators $\hat{\jmath}_i$ are sometimes called *jump operators*

2.3 The quantum regression formula

We now derive a useful formula which will allow us to evaluate, in a combined quantum system $S + E$, two-time averages of the form

$$\left\langle O_1(t) O_2(t') O_3(t)\right\rangle \quad \text{with} \quad t' - t \geq 0 \,, \tag{2.57}$$

where the operators O_i above act in $\mathcal{H}_S$. Clearly such an average cannot be evaluated in the Schrödinger picture, as Schrödinger picture operators are not general time dependent. We must write the average as a trace in the Heisenberg picture, and then transform it back into the Schrödinger picture. The average in the Heisenberg picture is given by[4]

$$\begin{aligned}\left\langle O_1(t) O_2(t') O_3(t)\right\rangle &= \mathrm{tr}_{S+E}\left[\rho^{(H)} O_1^{(H)}(t) O_2^{(H)}(t') O_3^{(H)}(t)\right] \\ &= \mathrm{tr}_{S+E}\left[\rho^{(H)} \mathrm{e}^{\mathrm{i}Ht} O_1^{(S)} \mathrm{e}^{\mathrm{i}H(t'-t)} O_2^{(S)} \mathrm{e}^{-\mathrm{i}H(t'-t)} O_3^{(S)} \mathrm{e}^{-\mathrm{i}Ht}\right],\end{aligned} \tag{2.58}$$

where we have taken the Hamiltonian to be constant in time. The total trace tr_{S+E} is equivalent to the partial traces over the system and environment separately: $\mathrm{tr}_{S+E} = \mathrm{tr}_S \mathrm{tr}_E$. Using the cyclic property of the trace, this becomes

$$\begin{aligned}\left\langle O_1(t) O_2(t') O_3(t)\right\rangle &= \mathrm{tr}_{S+E}\left[O_2^{(S)} \mathrm{e}^{-\mathrm{i}H(t'-t)} O_3^{(S)} \mathrm{e}^{-\mathrm{i}Ht} \rho^{(H)} \mathrm{e}^{\mathrm{i}Ht} O_1^{(S)} \mathrm{e}^{\mathrm{i}H(t'-t)}\right] \\ &= \mathrm{tr}_{S+E}\left[O_2^{(S)} \mathrm{e}^{-\mathrm{i}H(t'-t)} O_3^{(S)} \rho^{(S)}(t) O_1^{(S)} \mathrm{e}^{\mathrm{i}H(t'-t)}\right] \\ &= \mathrm{tr}_S\left\{O_2 \mathrm{tr}_E\left[\mathrm{e}^{-\mathrm{i}H(t'-t)} O_3 \rho(t) O_1 \mathrm{e}^{\mathrm{i}H(t'-t)}\right]\right\},\end{aligned} \tag{2.59}$$

[4] Heisenberg picture operators are denoted by a superscript (H), and Schrödinger picture operators by a superscript (S).

where in the last line we are now fully back in the Schrödinger picture. If we define the *collapsed* density matrix[5]

$$\rho_{O_3O_1}(\tau) \equiv \mathrm{e}^{-\mathrm{i}H\tau} O_3^{(S)} \rho^{(S)} O_1^{(S)} \mathrm{e}^{\mathrm{i}H\tau} \quad \text{with} \quad \tau \equiv t' - t\,, \tag{2.60}$$

the two-time average becomes

$$\left\langle O_1(t) O_2(t') O_3(t) \right\rangle = \mathrm{tr}_S \left\{ O_2 \mathrm{tr}_E \left[\rho_{O_3O_1}(\tau) \right] \right\} . \tag{2.61}$$

We also define

$$\rho_{O_3O_1,S}(\tau) = \mathrm{tr}_E \left[\rho_{O_3O_1}(\tau) \right] . \tag{2.62}$$

We can now make the Born approximation (2.33) for the collapsed density matrix (2.60), obtaining

$$\begin{aligned} \rho_{O_3O_1}(0) &= O_3 \rho(t) O_1 \\ &= O_3 \rho_S(t) O_1 \otimes \rho_E \\ &= \mathrm{tr}_E \left[O_3 \rho(t) O_1 \right] \otimes \rho_E \\ &= \rho_{O_3O_1,S}(0) \otimes \rho_E\,. \end{aligned} \tag{2.63}$$

We see that the Born approximation carries over into the collapsed system. Finally, the definition of the collapsed density matrix implies that it satisfies the von Neumann equation,

$$\frac{\mathrm{d}}{\mathrm{d}\tau} \rho_{O_3O_1}(\tau) = -\mathrm{i} \left[H, \rho_{O_3O_1}(\tau) \right] . \tag{2.64}$$

With the Born approximation and von Neumann equation applying to the collapsed system, we have the starting point of the microscopic derivation of the Lindblad equation of section (2.2.4), so clearly $\rho_{O_3O_1,S}$ obeys the same equation of motion as ρ_S,

$$\frac{\mathrm{d}}{\mathrm{d}\tau} \rho_{O_3O_1,S}(\tau) = \mathcal{L} \rho_{O_3O_1,S}(\tau)\,. \tag{2.65}$$

As we have noted, this equation has formal solution

$$\rho_{O_3O_1,S}(\tau) = \mathrm{e}^{\mathcal{L}\tau} \rho_{O_3O_1,S}(0) = \mathrm{e}^{\mathcal{L}\tau} \left[O_3 \rho_S(0) O_1 \right] . \tag{2.66}$$

Thus, (2.61) simplifies to give

$$\left\langle O_1(t) O_2(t+\tau) O_3(t) \right\rangle = \mathrm{tr}_S \left\{ O_2 \mathrm{e}^{\mathcal{L}\tau} \left[O_3 \rho_S(t) O_1 \right] \right\} , \tag{2.67}$$

the *quantum regression formula* [16].

[5] To clarify our terminology: the collapsed density matrix is not itself a density matrix, unless O_3 and O_1 are Hermitian adjoints of one another.

2.4 Quantum trajectory theory

Quantum trajectory theory provides an alternative conceptual and computational tool for analysing the master equation for some system. This section presents an overview of quantum trajectory theory, largely following Carmichael [17]. Further reading is available in Kronenwett [2], Carmichael [3, 18].

Quantum trajectory theory has been introduced by other authors in different ways;[6] it is part of the wider context of stochastic dynamics in Hilbert space [20].

2.4.1 Perturbation expansion for the density operator

The master equation describing the time-evolution of the system density operator $\rho(t)$ (where, for the remainder of this chapter, we drop the subscript on ρ_S to simplify the notation) may be written formally as in (2.23):

$$\dot{\rho}(t) = \mathcal{L}\rho(t)\,. \tag{2.68}$$

In general, the Liouvillian $\mathcal{L}$ can be written as the sum of an unperturbed part $\mathcal{L}_0$ and a small perturbation $\mathcal{S}$, such that

$$\mathcal{L}_0 \equiv \mathcal{L} - \mathcal{S}\,. \tag{2.69}$$

The formal solution of (2.68) is therefore

$$\rho(t) = e^{(\mathcal{L}_0+\mathcal{S})t}\rho(0)\,, \tag{2.70}$$

provided that $(\mathcal{L}_0 + \mathcal{S})$ is not explicitly time-dependent.[7] The first step towards obtaining a perturbation expansion for $\rho(t)$ is defining an auxiliary density operator $\rho'(t)$, given by

$$\rho'(t) \equiv e^{-\mathcal{L}_0 t}\rho(t)\,. \tag{2.71}$$

Taking the time derivative of (2.71), and substituting for $\mathcal{L}$ using (2.69) and for $\rho'(t)$ using (2.71), yields

$$\begin{aligned}\dot{\rho}'(t) &= -e^{-\mathcal{L}_0 t}\mathcal{L}_0\rho(t) + e^{-\mathcal{L}_0 t}\mathcal{L}\rho(t)\\ &= e^{-\mathcal{L}_0 t}\mathcal{S}\rho(t)\\ &= e^{-\mathcal{L}_0 t}\mathcal{S}e^{\mathcal{L}_0 t}\rho'(t)\,,\end{aligned} \tag{2.72}$$

the equation of motion for $\rho'(t)$.

We formally integrate the equation of motion (2.72), and substitute (2.72) into the result to

[6] See references in Carmichael [19].

[7] We consider only time-independent generators in this exposition of quantum trajectory theory.

obtain

$$\begin{aligned}\rho(t) &= e^{\mathcal{L}_0 t}\left[\rho'(0) + \int_0^t \mathrm{d}t' \dot{\rho}'(t')\right] \\ &= \rho(0) + \int_0^t \mathrm{d}t' e^{\mathcal{L}_0(t-t')}\mathcal{S}e^{\mathcal{L}_0 t'}\rho'(t')\,. \end{aligned} \tag{2.73}$$

Iterating this solution yields a Dyson series:

$$\rho(t) = \sum_{m=0}^{\infty}\int_0^t \mathrm{d}t_m \int_0^{t_m} \mathrm{d}t_{m-1}\cdots\int_0^{t_2} \mathrm{d}t_1 e^{\mathcal{L}_0(t-t_m)}\mathcal{S}e^{\mathcal{L}_0(t_m-t_{m-1})}\mathcal{S}\cdots\mathcal{S}e^{\mathcal{L}_0 t_1}\rho(0)\,, \tag{2.74}$$

with $\{t_m\}$ a monotonically increasing sequence. The integration kernel in (2.74) describes a single *quantum trajectory* for the initial state $\rho(0)$. The terms $e^{\mathcal{L}_0(t_m-t_{m-1})}$ represent continuous time-evolution in the intervals $[t_{m-1}, t_m)$, while $\mathcal{S}$ represents discontinuous quantum jumps (to be defined below) at the times $\{t_m\}$. One can interpret (2.74) as a generalised sum over all the possible "jump" pathways that the system might follow during its evolution from time $t = 0$ to time t. Specifically, (2.74) is a sum over all the possible numbers of jumps, $m = 0, \ldots, \infty$, and an integration over all possible times of these jumps within the interval $[0, t)$.

It may be the case that several distinguishable perturbations, each causing the system to "jump" in a different fashion at different times, will need to be taken into account. If in addition to the first perturbation $\mathcal{S}$ there is a second perturbation to $\mathcal{L}_0$, say $\mathcal{S}'$, each period of free evolution in the time intervals $[t_{m-1}, t_m)$ (that is, between the jumps due to $\mathcal{S}$) will be interrupted by some number of jumps due to $\mathcal{S}'$. As such, each free evolution term will need to be replaced by a Dyson series much like that in (2.74):

$$e^{\mathcal{L}_0(t_m-t_{m-1})} \to \sum_{n=0}^{\infty}\int_{t_{m-1}}^{t_m}\mathrm{d}t_n\int_{t_{m-1}}^{t_n}\mathrm{d}t_{n-1}\cdots\int_{t_{m-1}}^{t_2}\mathrm{d}t_1 e^{\mathcal{L}_0(t-t_n)}\mathcal{S}'e^{\mathcal{L}_0(t_n-t_{n-1})}\mathcal{S}'\cdots\mathcal{S}'e^{\mathcal{L}_0 t_1}\rho(0)\,. \tag{2.75}$$

Instead of substituting this Dyson series for every free evolution in (2.74), we redefine m as the total number of quantum jumps due to all $\mathcal{S}_i$, $i = 1, \ldots, N$, and sum over the N possibilities at each jump, giving a general Dyson series

$$\begin{aligned}\rho(t) = \sum_{m=0}^{\infty}\sum_{\nu_m=1}^{N}\sum_{\nu_{m-1}=1}^{N}\cdots\sum_{\nu_1=1}^{N}\int_0^t \mathrm{d}t_m\int_0^{t_m}\mathrm{d}t_{m-1}\cdots\int_0^{t_2}\mathrm{d}t_1 \\ e^{\mathcal{L}_0(t-t_m)}\mathcal{S}_{\nu_m}e^{\mathcal{L}_0(t_m-t_{m-1})}\mathcal{S}_{\nu_{m-1}}\cdots\mathcal{S}_{\nu_1}e^{\mathcal{L}_0 t_1}\rho(0)\,. \end{aligned} \tag{2.76}$$

The integration kernel of this Dyson series is a density operator, called the *unnormalised conditioned density operator*,

$$\tilde{\rho}_c(t) \equiv e^{\mathcal{L}_0(t-t_m)}\mathcal{S}_{\nu_m}e^{\mathcal{L}_0(t_m-t_{m-1})}\mathcal{S}_{\nu_{m-1}}\cdots\mathcal{S}_{\nu_1}e^{\mathcal{L}_0 t_1}\rho(0)\,; \tag{2.77a}$$

the normalised conditioned density operator is given by

$$\rho_c(t) \equiv \frac{\tilde{\rho}_c(t)}{\mathrm{tr}\left[\tilde{\rho}_c(t)\right]}, \tag{2.77b}$$

and describes the state of the system at time t with an initial state $\rho(0)$ *conditioned* on a particular sequence of jump times in the interval $[0, t)$.

Thus far, the quantum trajectory formalism has been developed in a general language, for any choice of $\mathcal{L}_0$ and $\mathcal{S}$, so long as $\mathcal{S}$ can be considered to be a small perturbation. The next section will be concerned more specifically with the unravelling of the master equation in Lindblad form.

2.4.2 Unravelling the Lindblad master equation

The master equation in Lindblad form [9] is given formally by (2.68) with the Liouvillian $\mathcal{L}$ given, as in (2.56), by

$$\mathcal{L}\rho = -\mathrm{i}\left[H, \rho\right] + \sum_i \left(\hat{\jmath}_i \rho \hat{\jmath}_i^\dagger - \frac{1}{2}\hat{\jmath}_i^\dagger \hat{\jmath}_i \rho - \frac{1}{2}\rho \hat{\jmath}_i^\dagger \hat{\jmath}_i\right). \tag{2.78}$$

The jump operators $\hat{\jmath}_i$ are determined by the particular system under consideration. The terms $-\frac{1}{2}\hat{\jmath}_i\hat{\jmath}_i^\dagger\rho$ and $-\frac{1}{2}\rho\hat{\jmath}_i\hat{\jmath}_i^\dagger$ in the Liouvillian describe the loss of population from the current states, while the terms $\hat{\jmath}_i\rho\hat{\jmath}_i^\dagger$ describe the gain of population of the states toward which the system propagates. As such, $\hat{\jmath}_i\rho\hat{\jmath}_i^\dagger$ can be understood as the density matrix after the transition described by $\hat{\jmath}_i$; such transitions can be interpreted as "quantum jumps" in the state of the system [21]. This suggests an unravelling of the master equation in which the terms $\hat{\jmath}_i \cdot \hat{\jmath}_i^\dagger$ are interpreted as causing quantum jumps in the trajectories of the reduced density operator. The remaining terms are interpreted as causing a modified coherent time-evolution.

As such, the master equation in Lindblad form is re-written

$$\dot{\rho}(t) = \left(\mathcal{L}_0 + \mathcal{S}\right)\rho(t), \tag{2.79}$$

with

$$\mathcal{L}_0\rho(t) = -\mathrm{i}\left[H, \rho(t)\right] - \frac{1}{2}\sum_i \left[\hat{\jmath}_i^\dagger\hat{\jmath}_i, \rho(t)\right]_+, \tag{2.80}$$

where $\left[\cdot,\cdot\right]_+$ denotes the anti-commutator; and

$$\mathcal{S} = \sum_i \mathcal{S}_i, \tag{2.81}$$

where

$$\mathcal{S}_i\rho(t) = \hat{\jmath}_i\rho(t)\hat{\jmath}_i^\dagger. \tag{2.82}$$

The unperturbed Liouvillian $\mathcal{L}_0$ can also be written

$$\mathcal{L}_0\rho(t) = -\mathrm{i}\left[H_{\mathrm{eff}}\,\rho(t) - \rho(t)\,H_{\mathrm{eff}}^{\dagger}\right], \tag{2.83}$$

where H_{eff} is an effective, *non-Hermitian Hamiltonian* given by

$$H_{\mathrm{eff}} \equiv H - \mathrm{i}\frac{1}{2}\sum_i \hat{\jmath}_i^{\dagger}\hat{\jmath}_i\,. \tag{2.84}$$

The non-Hermitian Hamiltonian generates non-unitary time-evolution, described by the *non-unitary Schrödinger equation*

$$\mathrm{i}\frac{\mathrm{d}}{\mathrm{d}t}|\Psi(t)\rangle = H_{\mathrm{eff}}|\Psi(t)\rangle\,. \tag{2.85}$$

This relation only holds *between* quantum jumps. The dual correspondence

$$H_{\mathrm{eff}}|\Psi(t)\rangle \overset{\mathrm{DC}}{\longleftrightarrow} \langle\Psi(t)|H_{\mathrm{eff}}^{\dagger} \tag{2.86}$$

gives the equation of motion for the state bra

$$\mathrm{i}\frac{\mathrm{d}}{\mathrm{d}t}\langle\Psi(t)| = -\langle\Psi(t)|H_{\mathrm{eff}}^{\dagger}\,. \tag{2.87}$$

Suppose that the density operator $\rho(t)$ factorises as a pure state,

$$\rho(t) = |\Psi(t)\rangle\langle\Psi(t)|\,. \tag{2.88}$$

Differentiating this density operator and substituting in the equations of motion for the intervals between jumps, (2.85) and (2.87), yields

$$\begin{aligned}\frac{\mathrm{d}}{\mathrm{d}t}\rho(t) &= \left[\frac{\mathrm{d}}{\mathrm{d}t}|\Psi(t)\rangle\right]\langle\Psi(t)| + |\Psi(t)\rangle\left[\frac{\mathrm{d}}{\mathrm{d}t}\langle\Psi(t)|\right]\\ &= -\mathrm{i}\left[H_{\mathrm{eff}}|\Psi(t)\rangle\langle\Psi(t)| - |\Psi(t)\rangle\langle\Psi(t)|H_{\mathrm{eff}}^{\dagger}\right]\\ &= \mathcal{L}_0\rho(t)\,.\end{aligned} \tag{2.89}$$

This confirms that, provided the density operator factorises as a pure state, the non-Hermitian Hamiltonian generates the non-unitary coherent time-evolution for that state.

2.4.3 Stochastic wavefunctions

Equations (2.77) define a quantum trajectory for a prescribed sequence of emission times. However, the times of the quantum jumps – the emissions of photons into the reservoir – are not deterministic. The time intervals between two consecutive jumps $(t_m - t_{m-1})$ in the exponentials of (2.76) have to follow a quantum-mechanical randomness. Specifically, if the conditioned density operator at time t, as defined in (2.77), is $\rho_c(t)$, then the probability for a

jump due to $\mathcal{S}_i$ to occur in the interval $[t, t + \Delta t)$ is given by [22]

$$p_{c,i}(t) = \mathrm{tr}\left[\mathcal{S}_i \rho_c(t)\right] \Delta t\,. \tag{2.90}$$

Using the cyclicity of the trace, we obtain

$$\mathrm{tr}\left[\mathcal{S}_i \rho_c(t)\right] = \mathrm{tr}\left[\hat{\jmath}_i \rho_c(t) \hat{\jmath}_i^\dagger\right] = \mathrm{tr}\left[\hat{\jmath}_i^\dagger \hat{\jmath}_i \rho_c(t)\right] \tag{2.91}$$

it is clear that, in a quantum optical system where the jump operators $\hat{\jmath}_i$ represent photon emissions, (2.90) is the product of the conditioned mean photon flux due to $\mathcal{S}_i$ at time t and the time interval Δt. The probability to find at least one jump in the time interval $[t, t + \Delta t)$ due to any $\mathcal{S}_i$ is given by

$$p_c(t) = \sum_i p_{c,i}(t) = \mathrm{tr}\left[\mathcal{S} \rho_c(t)\right] \Delta t\,, \tag{2.92}$$

with $\mathcal{S}$ given by (2.81).

Often, the form of the various superoperators $\mathcal{L}_0$ and $\mathcal{S}_i$ allows the conditioned density operator $\rho_c(t)$ to be factorised as a pure state, as in (2.88); as such, one can define

$$\rho_c(t) = |\Psi_c(t)\rangle\langle\Psi_c(t)|\,, \tag{2.93a}$$

and

$$\bar{\rho}_c(t) = |\bar{\Psi}_c(t)\rangle\langle\bar{\Psi}_c(t)|\,. \tag{2.93b}$$

The particular unravelling of the Lindblad master equation presented in section 2.4.2 has the property that if the conditioned density operator factorises as a pure state initially, then it does so for all times [23, 24].

In the intervals between the quantum jumps, the motion of the unnormalised ket is governed by the non-unitary Schrödinger equation (2.85); as a result the propagation without photon emission over a time Δt is given by

$$|\bar{\Psi}_c(t + \Delta t)\rangle = e^{-\mathrm{i}H_{\mathrm{eff}}\Delta t}|\bar{\Psi}_c(t)\rangle\,, \tag{2.94}$$

where H_{eff} is the non-Hermitian Hamiltonian given by (2.84). At the times of the quantum jumps, the unnormalised ket evolves discontinuously. If a jump due to $\mathcal{S}_i$ occurs at a time t, then

$$|\bar{\Psi}_c(t)\rangle \longrightarrow \hat{\jmath}_i|\bar{\Psi}_c(t)\rangle\,. \tag{2.95}$$

The probability for a jump due to $\mathcal{S}_i$ to occur in the interval $[t, t + \Delta t)$ is

$$p_{c,i}(t) = \langle\Psi_c(t)|\hat{\jmath}_i^\dagger \hat{\jmath}_i|\Psi_c(t)\rangle \Delta t\,. \tag{2.96}$$

2.4.4 Monte Carlo simulation

Clearly, using the quantum trajectory formalism as an analytic tool will, for all but the most simple examples, be impractical or impossible (although this could also be said to be the case for any other formalism). Monte Carlo simulations provide the most useful implementation of quantum trajectory ideas. This section outlines a Monte Carlo algorithm for the generation of stochastic quantum trajectories, based on the unravelling of the Lindblad master equation developed thus far. The trajectories produced are statistically equivalent to the solution of the master equation.[8]

In the Monto-Carlo simulation, time is discrete with a time-step Δt. Given the conditioned state ket at time t_n, $|\Psi_c(t_n)\rangle$, the state ket at time $t_{n+1} = t_n + \Delta t$ is calculated using the following algorithm:

1. Calculate the N probabilities $p_{c,i}(t_n)$ $(i = 1, \ldots, N)$ for a quantum jump to occur in the interval $[t_n, t_n + \Delta t)$ using

$$p_{c,i}(t_n) = \langle \Psi_c(t_n)|\hat{j}_i^\dagger \hat{j}_i|\Psi_c(t_n)\rangle \Delta t\,, \tag{2.97}$$

   as well as the total probability for any jump to occur,

$$p_c(t_n) = \sum_i p_{c,i}(t_n)\,. \tag{2.98}$$

2. Draw a uniformly distributed (pseudo)random number r_n from the interval $[0,1)$, and compare $p_c(t_n)$ with r_n.

   (a) If $p_c(t_n) \geq r_n$, a jump occurs. Subdivide the unit interval into N sub-intervals in proportion to the individual jump probabilities $p_{c,i}(t_n)$, and draw a second uniformly distributed random number r_n' from the interval $[0,1)$. The random number r_n' will fall into one of the N sub-intervals. For the sub-interval i in which r_n' falls, calculate $|\bar{\Psi}_c(t_{n+1})\rangle$ using

$$|\bar{\Psi}_c(t_{n+1})\rangle = \hat{j}_i|\Psi_c(t_n)\rangle\,. \tag{2.99}$$

   (b) If $p_c(t_n) < r_n$, no jump occurs. Calculate $|\bar{\Psi}_c(t_{n+1})\rangle$ using

$$|\bar{\Psi}_c(t_{n+1})\rangle = e^{-\mathrm{i}H_{\mathrm{eff}}\Delta t}|\Psi_c(t_n)\rangle\,. \tag{2.100}$$

3. Normalise the new state:

$$|\Psi_c(t_{n+1})\rangle = \frac{|\bar{\Psi}_c(t_{n+1})\rangle}{\sqrt{\langle\bar{\Psi}_c(t_{n+1})|\bar{\Psi}_c(t_{n+1})\rangle}}\,. \tag{2.101}$$

[8] Refer to Carmichael [25, 26] and the references therein for a mathematical justification of the statistical equivalence between the stochastic quantum trajectories produced by Monte Carlo simulation and the master equation.

4. Go to 1.

One final thing to note is that for the superoperator $\mathcal{S}$ in the Dyson series (2.76) to be a small enough perturbation for this derivation – and this Monte Carlo algorithm – to apply, the probability for a quantum jump to occur in a time interval Δt must be very small. This can be ensured by choosing Δt small enough that each jump is separated by many time steps, $\Delta t \ll t_m - t_{m-1}$, so that most of the time the system evolves coherently.

References

[1] H.-P. Breuer and F. Pettruccione. *The theory of open quantum systems*, chapter 3. Oxford University Press, 2007.

[2] M. Kronenwett. *Photon Correlations in Two-Mode Cavity Quantum Electrodynamics*. Master's thesis, The University of Auckland, 2007.

[3] H. J. Carmichael. *An Open Systems Approach to Quantum Optics*. Springer-Verlag, 1993.

[4] H.-P. Breuer and F. Pettruccione. *The theory of open quantum systems*, section 3.2. Oxford University Press, 2007.

[5] H.-P. Breuer and F. Pettruccione. *The theory of open quantum systems*, section 1.4. Oxford University Press, 2007.

[6] H.-P. Breuer and F. Pettruccione. *The theory of open quantum systems*, pages 118–119. Oxford University Press, 2007.

[7] H.-P. Breuer and F. Pettruccione. *The theory of open quantum systems*, page 74. Oxford University Press, 2007.

[8] V. Gorini, A. Kossakowski, and E. C. G. Sudarshan. Completely positive dynamical semigroups of N-level systems. *Journal of Mathematical Physics*, 17:821–825, 1976.

[9] G. Lindblad. On the generators of quantum dynamical semigroups. *Communications in Mathematical Physics*, 48:119–130, 1976.

[10] A. G. Redfield. On the theory of relaxation processes. *IBM Journal of Research and Development*, 1:19–31, 1957.

[11] H.-P. Breuer, B. Kappler, and F. Petruccione. Stochastic wave-function method for non-markovian quantum master equations. *Physical Review A*, 59:1633–1643, 1999.

[12] E. B. Davies. Markovian master equations. *Communications in Mathematical Physics*, 39: 91–110, 1974.

[13] R. Dümcke and H. Spohn. The proper form of the generator in the weak coupling limit. *Zeitschrift für Physik B Condensed Matter*, 34:419–422, 1979.

[14] H.-P. Breuer and F. Pettruccione. *The theory of open quantum systems*, section 3.3. Oxford University Press, 2007.

[15] H.-P. Breuer and F. Pettruccione. *The theory of open quantum systems*, section 12.2.3.2. Oxford University Press, 2007.

[16] H. J. Carmichael. *Statistical Methods in Quantum Optics 1: Master Equations and Fokker-Planck Equations*, section 1.5. Springer, 1999.

[17] H. J. Carmichael. *An Open Systems Approach to Quantum Optics*, lecture 7. Springer-Verlag, 1993.

[18] H. J. Carmichael. *Statistical Methods in Quantum Optics 2: Non-Classical Fields*. Springer, 2008.

[19] H. J. Carmichael. *Statistical Methods in Quantum Optics 2: Non-Classical Fields*, chapter 17. Springer, 2008.

[20] H.-P. Breuer and F. Pettruccione. *The theory of open quantum systems*, chapter 6. Oxford University Press, 2007.

[21] M. Kronenwett. *Photon Correlations in Two-Mode Cavity Quantum Electrodynamics*, section 2.1.5. Master's thesis, The University of Auckland, 2007.

[22] H. J. Carmichael. *An Open Systems Approach to Quantum Optics*, section 7.5. Springer-Verlag, 1993.

[23] H. J. Carmichael. *Statistical Methods in Quantum Optics 2: Non-Classical Fields*, section 17.2.5. Springer, 2008.

[24] M. Kronenwett. *Photon Correlations in Two-Mode Cavity Quantum Electrodynamics*, section 2.2.2. Master's thesis, The University of Auckland, 2007.

[25] H. J. Carmichael. *An Open Systems Approach to Quantum Optics*, lectures 7–10. Springer-Verlag, 1993.

[26] H. J. Carmichael. *Statistical Methods in Quantum Optics 2: Non-Classical Fields*, chapters 17–19. Springer, 2008.

3

The Jaynes-Cummings model

The *Jaynes-Cummings model* [1, 2] describes the interaction of a two-level atom with a single quantised mode of the electromagnetic field.

3.1 The Jaynes-Cummings Hamiltonian

In the Coulomb gauge [3], where $\nabla \cdot \mathbf{A} = 0$, the Hamiltonian for an atom (with electron positions $\mathbf{r}_i$ and momenta $\mathbf{p}_i$) coupled to a radiation field characterised by the vector and scalar potentials $\mathbf{A}$ and Φ is [4, 5]

$$H = \frac{1}{2m}\sum_{i=1}^{Z}\left[\hat{\mathbf{p}}_i + e\hat{\mathbf{A}}(\mathbf{r}_i)\right]^2 + \frac{1}{2}\int_V \mathrm{d}\mathbf{r}\,\sigma(\mathbf{r})\Phi(\mathbf{r}) + \frac{1}{2}\int_V \mathrm{d}\mathbf{r}\left[\epsilon_0\hat{\mathbf{E}}_\mathrm{T}(\mathbf{r})^2 + {\mu_0}^{-1}\hat{\mathbf{B}}(\mathbf{r})^2\right]. \quad (3.1)$$

This is known as the *minimal coupling* form of the Hamiltonian. The quantity $\sigma(\mathbf{r})$ is the charge density of the atomic system, and V is the mode volume occupied by the field.

The complete Hamiltonian for a system described by the Jaynes-Cummings model consists of parts describing the two-level atomic excitation, the radiation field, and the interaction between the two:

$$H_\mathrm{JCM} = H_A + H_F + H_g\,. \quad (3.2)$$

We are going to use the minimal coupling form of the Hamiltonian to derive each of the three parts of the Jaynes-Cummings Hamiltonian.

3.1.1 The Hamiltonian of the atom

The first term in (3.1) includes the kinetic energies of the electrons; the second term is the electrostatic energy of the charges that constitute the atom, and does not involve any quantum operators of the transverse radiation field. The electrostatic interaction combines with the kinetic energy terms mentioned above to give the energy of the atom in the absence of its coupling to the transverse part of the electromagnetic field. The Hamiltonian of the electrons in the atom can, however, be simplified by considering a simple energy level structure, which we will do below.

Consider an atom with n energy eigenstates $|E_n\rangle$ having energies E_n. The Hamiltonian for such an atom would be written $H_A = \sum_n E_n |E_n\rangle\langle E_n|$. However for the purposes of the Jaynes-Cummings model, we make the two-level approximation: we consider only two non-degenerate

energy levels satisfying

$$E_e - E_g = \hbar\omega_A\,, \tag{3.3}$$

where ω_A is the frequency of the atomic transition in question. All other energy levels are ignored. This approximation is valid in the case where the frequency of the light with which the atom interacts is close to ω_A, while being far from resonance with any other atomic transition, and where the Zeeman substructure of the levels can be ignored.

For a two-level atom with ground state $|g\rangle$ and excited state $|e\rangle$, the atomic Hamiltonian can be expressed as $H = E_g\,|g\rangle\langle g| + E_e\,|e\rangle\langle e|$. If we take the zero of energy to be half way between the energies of the ground and excited states, the atomic Hamiltonian becomes

$$H_A = \frac{\hbar\omega_A}{2}\left(|e\rangle\langle e| - |g\rangle\langle g|\right)\,. \tag{3.4}$$

Here we introduce the atomic raising and lowering operators

$$\hat{\sigma}_+ = |e\rangle\langle g|\,, \quad \hat{\sigma}_- = |g\rangle\langle e|\,, \tag{3.5}$$

along with

$$\hat{\sigma}_z = \left[\hat{\sigma}_+, \hat{\sigma}_-\right]\,. \tag{3.6}$$

Thus, the Hamiltonian of the two-level atom becomes

$$H_A = \frac{1}{2}\hbar\omega_A\hat{\sigma}_z\,. \tag{3.7}$$

3.1.2 The Hamiltonian of the radiation field

As is well-known, the second-quantised form of the Hamiltonian for the full, multi-mode radiation field is given by [6]

$$H_F = \sum_{\mathbf{k}}\sum_{\lambda}\hbar\omega_{\mathbf{k}}\left(\hat{a}^\dagger_{\mathbf{k}\lambda}\hat{a}_{\mathbf{k}\lambda} + \frac{1}{2}\right)\,, \tag{3.8}$$

where $\hat{n}_{\mathbf{k}\lambda} \equiv \hat{a}^\dagger_{\mathbf{k}\lambda}\hat{a}_{\mathbf{k}\lambda}$ is the occupation number of the field mode specified by the wavevector $\mathbf{k}$ and the polarisation state λ: $\lambda = 1$ and $\lambda = 2$ denote the two transverse polarisations. The third term in the minimal coupling Hamiltonian (3.1) is the transverse field energy, which can be shown to be identical with (3.8). The boundary conditions imposed by the presence of an optical cavity determine what modes $\mathbf{k}\lambda$ are supported.

The term $\sum_{\mathbf{k}}\sum_{\lambda}\frac{1}{2}\hbar\omega_{\mathbf{k}}$ is due to the zero-point energy, and does not contribute to the energy of the electromagnetic field as measured by way of photon detection. As such, we shift the zero of energy in order to eliminate this term. This does not affect the equations of motion, as all operators commute with a constant.

In the Jaynes-Cummings model, only a single cavity mode is to be considered; specifically,

we neglect all modes from which the two-level atomic transition is far from resonance, leaving only a single mode to which the atom couples. As such we drop the mode indices for simplicity of notation. The resulting single-mode radiation field Hamiltonian is written

$$H_F = \hbar\omega_F \hat{a}^\dagger \hat{a}\,. \tag{3.9}$$

3.1.3 The interaction Hamiltonian

The first step in deriving the Hamiltonian for the interaction between the atom and the radiation field is to perform an harmonic decomposition of the vector potential of the electromagnetic field [6–8]:

$$\hat{\mathbf{A}}(\mathbf{r}) = \sum_{\mathbf{k}}\sum_{\lambda}\left(\frac{\hbar}{2\omega_{\mathbf{k}}\epsilon_0}\right)^{\frac{1}{2}}\left[\hat{a}_{\mathbf{k}\lambda}\mathbf{u}_{\mathbf{k}\lambda}(\mathbf{r}) + \hat{a}^\dagger_{\mathbf{k}\lambda}\mathbf{u}^*_{\mathbf{k}\lambda}(\mathbf{r})\right], \tag{3.10}$$

where, assuming the field is contained in a mode volume V, the spatial mode functions $\mathbf{u}_{\mathbf{k}\lambda}(\mathbf{r})$ are given by

$$\mathbf{u}_{\mathbf{k}\lambda}(\mathbf{r}) = V^{-\frac{1}{2}}\mathbf{e}_{\mathbf{k}\lambda} f_{\mathbf{k}}(\mathbf{r})\,. \tag{3.11}$$

Here $\mathbf{e}_{\mathbf{k}\lambda}$ is the unit polarisation vector. In free space, $f_{\mathbf{k}}(\mathbf{r}) = \exp(\mathrm{i}\mathbf{k}\cdot\mathbf{r})$; in a cavity the mode functions will depend on the particular geometry of the cavity considered.

The first term in (3.1) includes the kinetic energies of the electrons (which we have already considered in section 3.1.1), as well as additional terms

$$H_I = \frac{e}{2m}\sum_i\left[\hat{\mathbf{p}}_i\cdot\hat{\mathbf{A}}(\mathbf{r}_i) + \hat{\mathbf{A}}(\mathbf{r}_i)\cdot\hat{\mathbf{p}}_i\right] + \frac{e^2}{2m}\sum_i\hat{\mathbf{A}}(\mathbf{r}_i)^2, \tag{3.12}$$

which represent the interaction between the atom and the radiation field. Terms in the interaction Hamiltonian involving $\hat{\mathbf{A}}^2$ refer to two-photon processes which make a contribution much smaller than one-photon processes; thus, they can be neglected. The resulting interaction Hamiltonian is

$$\begin{aligned} H_I &= \frac{e}{m}\sum_i\hat{\mathbf{p}}_i\cdot\hat{\mathbf{A}}(\mathbf{r}_i) \\ &= \frac{e}{m}\sum_i\sum_{\mathbf{k}}\sum_{\lambda}\left(\frac{\hbar}{2\omega_{\mathbf{k}}\epsilon_0}\right)^{\frac{1}{2}}\hat{\mathbf{p}}_i\cdot\left[\hat{a}_{\mathbf{k}\lambda}\mathbf{u}_{\mathbf{k}\lambda}(\mathbf{r}_i) + \hat{a}^\dagger_{\mathbf{k}\lambda}\mathbf{u}^*_{\mathbf{k}\lambda}(\mathbf{r}_i)\right]. \end{aligned} \tag{3.13}$$

The momentum operators $\hat{\mathbf{p}}_i$ can be expressed in terms of the corresponding position operators $\hat{\mathbf{r}}_i$ using Heisenberg's equation of motion,

$$\hat{\mathbf{p}}_i = m\dot{\hat{\mathbf{r}}}_i = \frac{m}{\mathrm{i}\hbar}\left[\hat{\mathbf{r}}_i, H_A\right], \tag{3.14}$$

which yields the result that the matrix elements $\langle g|\hat{\mathbf{p}}_i|g\rangle$ and $\langle e|\hat{\mathbf{p}}_i|e\rangle$ are both identically zero.

Furthermore we obtain the result that

$$\langle g|\hat{\mathbf{p}}_i|e\rangle = -\mathrm{i}m\omega_A \langle g|\hat{\mathbf{r}}_i|e\rangle \,, \tag{3.15a}$$

$$\langle e|\hat{\mathbf{p}}_i|g\rangle = \mathrm{i}m\omega_A \langle e|\hat{\mathbf{r}}_i|g\rangle \,. \tag{3.15b}$$

We can now use these results, along with closure over the atomic ground and excited states, to obtain

$$\begin{aligned}
\hat{\mathbf{p}}_i &= \sum_{\alpha=g,e}\sum_{\alpha'=g,e} \left(|\alpha\rangle\langle\alpha|\,\hat{\mathbf{p}}_i\,|\alpha'\rangle\langle\alpha'|\right) \\
&= |g\rangle\langle g|\hat{\mathbf{p}}_i|g\rangle\langle g| + |e\rangle\langle e|\hat{\mathbf{p}}_i|e\rangle\langle e| + |g\rangle\langle g|\hat{\mathbf{p}}_i|e\rangle\langle e| + |e\rangle\langle e|\hat{\mathbf{p}}_i|g\rangle\langle g| \\
&= -\mathrm{i}m\omega_A(\langle g|\hat{\mathbf{r}}_i|e\rangle\,|g\rangle\langle e| - \langle e|\hat{\mathbf{r}}_i|g\rangle\,|e\rangle\langle g|) \\
&= \frac{m\omega_A}{e}\left(\mathrm{i}\mathbf{d}_{ge,i}\hat{\sigma}_- - \mathrm{i}\mathbf{d}^*_{ge,i}\hat{\sigma}_+\right) \,,
\end{aligned} \tag{3.16}$$

where we have defined $\mathbf{d}_{ge,i} \equiv -e\langle g|\hat{\mathbf{r}}_i|e\rangle$.

Substituting (3.16) in (3.13) yields

$$H_I = \hbar\sum_i\sum_{\mathbf{k}}\sum_{\lambda}\left(\frac{{\omega_A}^2}{2\hbar\omega_{\mathbf{k}}\epsilon_0}\right)^{\frac{1}{2}}\left(\mathrm{i}\mathbf{d}_{ge,i}\hat{\sigma}_- - \mathrm{i}\mathbf{d}^*_{ge,i}\hat{\sigma}_+\right)\cdot\left[\hat{a}_{\mathbf{k}\lambda}\mathbf{u}_{\mathbf{k}\lambda}(\mathbf{r}_i) + \hat{a}^\dagger_{\mathbf{k}\lambda}\mathbf{u}^*_{\mathbf{k}\lambda}(\mathbf{r}_i)\right] . \tag{3.17}$$

Now, consider the case where the spatial variation of the vector potential $\hat{\mathbf{A}}$ is slow compared with the size of the atom. This is usually the case in quantum optical experiments, where the wavelength of the electromagnetic field interacting with the atom is much larger than the size of the atom itself. Under these conditions, one can expand $f_{\mathbf{k}}(\mathbf{r})$ in $\mathbf{u}_{\mathbf{k}\lambda}$ around the position of the atom, which we denote $\mathbf{R}$. Writing $\mathbf{r} = \mathbf{R} + \delta\mathbf{r}$, we obtain (for the case of the free space mode functions; the argument is easily adapted to take into account general mode functions)

$$\begin{aligned}
\exp(\mathrm{i}\mathbf{k}\cdot\mathbf{r}) &= \exp(\mathrm{i}\mathbf{k}\cdot\mathbf{R})\exp(\mathrm{i}\mathbf{k}\cdot\delta\mathbf{r}) \\
&= \exp(\mathrm{i}\mathbf{k}\cdot\mathbf{R})\left[1 + \mathrm{i}\mathbf{k}\cdot\delta\mathbf{r} - \frac{1}{2}(\mathbf{r}\cdot\delta\mathbf{r})^2 + \cdots\right] .
\end{aligned} \tag{3.18}$$

The *dipole approximation* amounts to keeping the only the leading term. It is clear that this approximation is valid when the wavelength of the electromagnetic field is much larger than the characteristic length scale of the atom, that is when $2\pi/|\mathbf{k}| \gg |\delta\mathbf{r}|$. Making the dipole approximation, we can evaluate the electromagnetic field at the position $\mathbf{R}$ of the atom rather than the position $\mathbf{r}_i$ of the electron. This allows us to re-write the interaction Hamiltonian (3.17) as

$$H_I = \hbar\sum_{\mathbf{k}}\sum_{\lambda}\left(\frac{{\omega_A}^2}{2\hbar\omega_{\mathbf{k}}\epsilon_0}\right)^{\frac{1}{2}}\left(\mathrm{i}\mathbf{d}_{ge}\hat{\sigma}_- - \mathrm{i}\mathbf{d}^*_{ge}\hat{\sigma}_+\right)\cdot\left[\hat{a}_{\mathbf{k}\lambda}\mathbf{u}_{\mathbf{k}\lambda}(\mathbf{R}) + \hat{a}^\dagger_{\mathbf{k}\lambda}\mathbf{u}^*_{\mathbf{k}\lambda}(\mathbf{R})\right] , \tag{3.19}$$

where we have defined the dipole matrix element $\mathbf{d}_{ge} \equiv \sum_i \mathbf{d}_{ge,i}$.

3.1.4 Rotating-wave approximation

We consider a near-resonant atom-cavity system with a Hamiltonian consisting of two parts, $H = H_0 + H_I$. The interaction part is given by (3.19), while the unperturbed Hamiltonian is

$$H_0 = \frac{1}{2}\hbar\omega_A\hat{\sigma}_z + \sum_{\mathbf{k}}\sum_{\lambda}\hbar\omega_{\mathbf{k}}\hat{a}^\dagger_{\mathbf{k}\lambda}\hat{a}_{\mathbf{k}\lambda}\,. \tag{3.20}$$

We transform into the interaction picture, recalling that in this picture the time-dependence of operators is given by the transformation

$$\hat{A}(t) = \exp(\mathrm{i}H_0 t/\hbar)\hat{A}\exp(-\mathrm{i}H_0 t/\hbar)\,, \tag{3.21}$$

where $\hat{A}$ is an arbitrary Schrödinger picture operator. From this we obtain,[1]

$$\hat{\sigma}_-(t) = \hat{\sigma}_-\mathrm{e}^{-\mathrm{i}\omega_A t}\,, \qquad \hat{\sigma}_+(t) = \hat{\sigma}_+\mathrm{e}^{\mathrm{i}\omega_A t}\,, \tag{3.22a}$$

$$\hat{a}_{\mathbf{k}\lambda}(t) = \hat{a}_{\mathbf{k}\lambda}(t)\mathrm{e}^{-\mathrm{i}\omega_{\mathbf{k}} t}\,, \qquad \hat{a}^\dagger_{\mathbf{k}\lambda}(t) = \hat{a}^\dagger_{\mathbf{k}\lambda}(t)\mathrm{e}^{\mathrm{i}\omega_{\mathbf{k}} t}\,. \tag{3.22b}$$

Transforming the coupling Hamiltonian (3.19) into the interaction picture, we obtain

$$H_I(t) = \hbar\sum_{\mathbf{k}}\sum_{\lambda}\left(\frac{{\omega_A}^2}{2\hbar\omega_{\mathbf{k}}\epsilon_0}\right)^{\frac{1}{2}}\big[\mathrm{i}\mathbf{d}_{ge}\hat{\sigma}_-\cdot\mathbf{u}_{\mathbf{k}\lambda}(\mathbf{R})\hat{a}_{\mathbf{k}\lambda}\mathrm{e}^{-\mathrm{i}(\omega_A+\omega_{\mathbf{k}})t} \tag{3.23}$$

$$+\,\mathrm{i}\mathbf{d}_{ge}\hat{\sigma}_-\cdot\mathbf{u}^*_{\mathbf{k}\lambda}(\mathbf{R})\hat{a}^\dagger_{\mathbf{k}\lambda}\mathrm{e}^{-\mathrm{i}(\omega_A-\omega_{\mathbf{k}})t} \tag{3.24}$$

$$-\,\mathrm{i}\mathbf{d}^*_{ge}\hat{\sigma}_+\cdot\mathbf{u}_{\mathbf{k}\lambda}(\mathbf{R})\hat{a}_{\mathbf{k}\lambda}\mathrm{e}^{\mathrm{i}(\omega_A-\omega_{\mathbf{k}})t} \tag{3.25}$$

$$-\,\mathrm{i}\mathbf{d}^*_{ge}\hat{\sigma}_+\cdot\mathbf{u}^*_{\mathbf{k}\lambda}(\mathbf{R})\hat{a}^\dagger_{\mathbf{k}\lambda}\mathrm{e}^{\mathrm{i}(\omega_A+\omega_{\mathbf{k}})t}\big]\,. \tag{3.26}$$

There are two types of oscillatory terms present in the interaction picture Hamiltonian (3.23), whose frequencies have magnitudes $|\omega_A \pm \omega_{\mathbf{k}}|$. The interactions most effective in absorption and emission of photons are those which occur near resonance, with $\omega_A \approx \omega_{\mathbf{k}}$. As such, for those processes which make large contributions to the interaction, $|\omega_A - \omega_{\mathbf{k}}| \ll |\omega_A + \omega_{\mathbf{k}}|$.

The slowly oscillating terms with frequencies of magnitude $|\omega_A - \omega_{\mathbf{k}}|$ contain operator combinations $\hat{\sigma}_+\hat{a}_{\mathbf{k}\lambda}$ and $\hat{\sigma}_-\hat{a}^\dagger_{\mathbf{k}\lambda}$, while the rapidly oscillating terms with frequencies of magnitude $|\omega_A + \omega_{\mathbf{k}}|$ contain operators $\hat{\sigma}_+\hat{a}^\dagger_{\mathbf{k}\lambda}$ and $\hat{\sigma}_-\hat{a}_{\mathbf{k}\lambda}$. The latter processes are much less probable than those corresponding to the former type; thus, we can neglect the rapidly oscillating terms, making the *rotating-wave approximation*. The interaction Hamiltonian in the rotating-wave approximation is denoted H_g, and is given by

$$H_g = \hbar\sum_{\mathbf{k}}\sum_{\lambda}(-\mathrm{i}\mathbf{d}^*_{ge}\cdot\mathbf{u}_{\mathbf{k}\lambda}(\mathbf{R})\hat{\sigma}_+\hat{a}_{\mathbf{k}\lambda} + \mathrm{i}\mathbf{d}_{ge}\cdot\mathbf{u}^*_{\mathbf{k}\lambda}(\mathbf{R})\hat{\sigma}_-\hat{a}^\dagger_{\mathbf{k}\lambda})\,. \tag{3.27}$$

This Hamiltonian admits an intuitive physical explanation, wherein the atom absorbs a photon from, or emits a photon into, the cavity.

[1] With the use of, for example, the Baker-Hausdorff lemma [9].

If we now define

$$d_{ge} \equiv -\mathrm{i}\left(\frac{{\omega_A}^2}{2\hbar\omega_{\mathbf{k}}\epsilon_0 V}\right)^{\frac{1}{2}} \mathbf{d}_{ge}^* \cdot \mathbf{e}_{\mathbf{k}\lambda}\,, \tag{3.28}$$

as well as the *dipole coupling constant*

$$g_{\mathbf{k}\lambda} = d_{ge} f_{\mathbf{k}}(\mathbf{R})\,, \tag{3.29}$$

then the interaction Hamiltonian can be re-written

$$H_g = \hbar \sum_{\mathbf{k}} \sum_{\lambda} (g_{\mathbf{k}\lambda}\hat{\sigma}_+ \hat{a}_{\mathbf{k}\lambda} + g^*_{\mathbf{k}\lambda}\hat{\sigma}_- \hat{a}^\dagger_{\mathbf{k}\lambda})\,. \tag{3.30}$$

We may here absorb the complex phase of the dipole coupling constant into the cavity creation and annihilation operators (while preserving commutation relations), to yield a real coupling constant $g_{\mathbf{k}\lambda} = \left|d_{ge} f_{\mathbf{k}}(\mathbf{R})\right|$. This results in the Hamiltonian

$$H_g = \hbar \sum_{\mathbf{k}} \sum_{\lambda} g_{\mathbf{k}\lambda} (\hat{\sigma}_+ \hat{a}_{\mathbf{k}\lambda} + \hat{\sigma}_- \hat{a}^\dagger_{\mathbf{k}\lambda})\,. \tag{3.31}$$

We see that the dipole coupling constant depends on the position of the atom. In the Jaynes-Cummings model we consider a stationary atom, so this dependence is not usually written out explicitly, being of no importance. In more complicated cavity QED systems we may need to take the dependence on position into account.

Considering only a single cavity mode, as we did in section 3.1.2, the interaction Hamiltonian reduces to

$$H_g = \hbar g (\hat{\sigma}_+ \hat{a} + \hat{\sigma}_- \hat{a}^\dagger)\,. \tag{3.32}$$

We now combine the various Hamiltonians for the two-level atom, the single-mode radiation field, and the interaction between the two, to obtain the *Jaynes-Cummings Hamiltonian*:

$$H_{\mathrm{JCM}} = \frac{1}{2}\hbar\omega_A \hat{\sigma}_z + \hbar\omega_F \hat{a}^\dagger \hat{a} + \hbar g (\hat{\sigma}_+ \hat{a} + \hat{\sigma}_- \hat{a}^\dagger)\,. \tag{3.33}$$

3.2 The Jaynes-Cummings ladder

In this section we diagonalise the Jaynes-Cummings Hamiltonian (3.33), closely following Carmichael [10] and Whalen [11]. For simplicity we set $\hbar \equiv 1$:

$$H = \frac{1}{2}\omega_A \hat{\sigma}_z + \omega_F \hat{a}^\dagger \hat{a} + g(\hat{\sigma}_+ \hat{a} + \hat{\sigma}_- \hat{a}^\dagger)\,. \tag{3.34}$$

The ground state of the system is $|g, 0\rangle \equiv |g\rangle \otimes |0\rangle$, where the atom is in its ground state and the cavity is empty. The ground state energy is $-\frac{1}{2}\omega_A$. In the rotating-wave approximation, the

interaction couples the states in pairs:

$$H\,|g,n\rangle = \left(-\frac{1}{2}\omega_A + n\omega_F\right)|g,n\rangle + g\sqrt{n}\,|e,n-1\rangle \tag{3.35a}$$

$$H\,|e,n-1\rangle = \left(\frac{1}{2}\omega_A + (n-1)\omega_F\right)|e,n-1\rangle + g\sqrt{n}\,|g,n\rangle\ . \tag{3.35b}$$

In the two-dimensional subspace defined by

$$|g,n\rangle \doteq \begin{pmatrix}0\\1\end{pmatrix}, \quad |e,n-1\rangle \doteq \begin{pmatrix}1\\0\end{pmatrix}, \tag{3.36}$$

the Hamiltonian can be written

$$H \doteq \begin{pmatrix}\frac{1}{2}\omega_A + (n-1)\omega_F & g\sqrt{n}\\ g\sqrt{n} & -\frac{1}{2}\omega_A + n\omega_F\end{pmatrix}. \tag{3.37}$$

We want to find the energy eigenvalues, so we must solve $H\,|E_n\rangle = E_n\,|E_n\rangle$. If we define

$$\lambda_n \equiv E_n - \left(n - \frac{1}{2}\right)\omega_F\,, \tag{3.38a}$$

and

$$\Delta\omega_{AF} \equiv \omega_A - \omega_F\,, \tag{3.38b}$$

then we obtain the equations

$$\begin{pmatrix}\frac{1}{2}\Delta\omega_{AF} - \lambda_n & g\sqrt{n}\\ g\sqrt{n} & -\frac{1}{2}\Delta\omega_{AF} - \lambda_n\end{pmatrix}|E_n\rangle = \mathbf{0}\,. \tag{3.39}$$

From the above we derive a characteristic equation, which has solutions

$$\lambda_n = \pm\sqrt{\frac{{\Delta\omega_{AF}}^2}{4} + g^2 n}\,. \tag{3.40}$$

Therefore the excited state energies are given by

$$E_n^{\pm} = \left(n - \frac{1}{2}\right)\omega_F \pm \sqrt{\frac{{\Delta\omega_{AF}}^2}{4} + g^2 n}\,. \tag{3.41}$$

The corresponding energy eigenstates, also known as the *dressed states* [12], are easily obtained. The dressed states are:

$$|E_n^+\rangle = \frac{1}{\sqrt{2}\left(\frac{\Delta\omega_{AF}{}^2}{4} + g^2 n\right)^{\frac{1}{4}}}\left[\sqrt{\left(\frac{\Delta\omega_{AF}{}^2}{4} + g^2 n\right)^{\frac{1}{2}} + \frac{\Delta\omega_{AF}}{2}}\,|e, n-1\rangle + \sqrt{\left(\frac{\Delta\omega_{AF}{}^2}{4} + g^2 n\right)^{\frac{1}{2}} - \frac{\Delta\omega_{AF}}{2}}\,|g, n\rangle\right], \quad (3.42a)$$

$$|E_n^-\rangle = \frac{1}{\sqrt{2}\left(\frac{\Delta\omega_{AF}{}^2}{4} + g^2 n\right)^{\frac{1}{4}}}\left[\sqrt{\left(\frac{\Delta\omega_{AF}{}^2}{4} + g^2 n\right)^{\frac{1}{2}} - \frac{\Delta\omega_{AF}}{2}}\,|e, n-1\rangle - \sqrt{\left(\frac{\Delta\omega_{AF}{}^2}{4} + g^2 n\right)^{\frac{1}{2}} + \frac{\Delta\omega_{AF}}{2}}\,|g, n\rangle\right]. \quad (3.42b)$$

When the atom is resonant with the cavity ($\Delta\omega_{AF} = 0$) the energy eigenvalues are

$$E_n^{\pm} = \left(n - \frac{1}{2}\right)\omega \pm g\sqrt{n}\,, \quad (3.43)$$

where we have defined $\omega \equiv \omega_A = \omega_F$. The dressed states are given by

$$|E_n^+\rangle = \frac{1}{\sqrt{2}}\left(|e, n-1\rangle + |g, n\rangle\right), \quad (3.44a)$$

$$|E_n^-\rangle = \frac{1}{\sqrt{2}}\left(|e, n-1\rangle - |g, n\rangle\right). \quad (3.44b)$$

The eigenvalue spectrum of the Jaynes-Cummings Hamiltonian is referred to as the *Jaynes-Cummings ladder*. The ladder of energy eigenvalues is depicted for the resonant case in Fig. 3.1.

3.3 Driving

The Jaynes-Cummings Hamiltonian (3.33) by itself is not usually sufficient to describe experiments. It is useful to describe the case where the combined system of atom and cavity is driven by a periodic classical field. The Hamiltonian for such a driven system can be written

$$H = H_0 + H_{\mathcal{E}}(t)\,, \quad (3.45)$$

where H_0 is the unperturbed Hamiltonian for the standard Jaynes-Cummings system, given by (3.33), and $H_{\mathcal{E}}(t)$ is the Hamiltonian for the periodic interaction with the driving field [13]. The driving field may couple to either the cavity or the atom. In the former case the driving

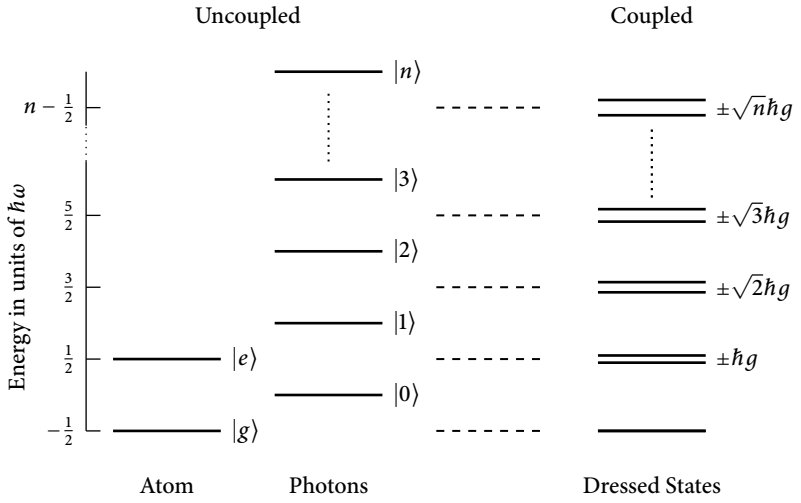

FIGURE 3.1: The Jaynes-Cummings ladder. Shown on the left are the energies of the uncoupled states of the atom and the field modes. Shown on the right is the ladder of dressed states, which describes a coupled atom-photon system with dipole coupling constant g. Each "rung" of the ladder, except for the very lowest, comprises two dressed states.

Hamiltonian is given by

$$H_{\mathcal{E}}(t) = \hbar\mathcal{E}\left(\hat{a}^\dagger e^{-i\omega_L t} + \hat{a}e^{i\omega_L t}\right), \tag{3.46}$$

and in the latter case by

$$H_{\mathcal{E}}(t) = \hbar\mathcal{E}\left(\hat{\sigma}_+ e^{-i\omega_L t} + \hat{\sigma}_- e^{i\omega_L t}\right). \tag{3.47}$$

In both cases we have denoted the frequency of the driving laser by ω_L.

The above Hamiltonians for the interaction with the driving laser field are obtained by a procedure which is broadly similar to that employed in section 3.1.3. If the laser frequency ω_L is near resonance with the atomic transition or cavity mode (whichever of the two the laser couples to), then the interaction is well-approximated by a linear coupling similar to the $\mathbf{p}\cdot\mathbf{A}$-type coupling we considered above [4, 14]. Making the rotating-wave approximation then leads to the interaction Hamiltonians (3.46) and (3.47).

3.4 The rotating frame

Let us consider the case of a driven Jaynes-Cummings system. Such a system is described by the Hamiltonian

$$H = H_{\mathcal{E}}(t) + \frac{1}{2}\omega_A\hat{\sigma}_z + \omega_F\hat{a}^\dagger\hat{a} + g(\hat{\sigma}_+\hat{a} + \hat{\sigma}_-\hat{a}^\dagger). \tag{3.48}$$

Once again we have defined $\hbar \equiv 1$. It is desirable to remove the time-dependence involved in the driving Hamiltonian, so we transform to the so-called *rotating frame*. This is like an

interaction picture transformation, with an unperturbed Hamiltonian

$$H_{\omega_L} = \frac{1}{2}\omega_L \hat{\sigma}_z + \omega_L \hat{a}^\dagger \hat{a}\,. \tag{3.49}$$

The resulting Hamiltonian, transformed into the rotating frame, is

$$H = H_{\mathcal{E}} + \frac{1}{2}\Delta\omega_A \hat{\sigma}_z + \Delta\omega_F \hat{a}^\dagger \hat{a} + g(\hat{\sigma}_+ \hat{a} + \hat{\sigma}_- \hat{a}^\dagger)\,, \tag{3.50}$$

where $\Delta\omega_A \equiv \omega_A - \omega_L$ and $\Delta\omega_F \equiv \omega_F - \omega_L$. In the rotating frame, the now time-independent driving Hamiltonian $H_{\mathcal{E}}$ is given by

$$H_{\mathcal{E}} = \mathcal{E}(\hat{a}^\dagger + \hat{a})\,, \tag{3.51}$$

in the case where the driving field couples to the cavity, or

$$H_{\mathcal{E}} = \mathcal{E}(\hat{\sigma}_+ + \hat{\sigma}_-)\,, \tag{3.52}$$

in the case where the driving field couples directly to the atom.

3.5 Master equation for the Jaynes-Cummings system

Consider a Jaynes-Cummings system described by the driven Hamiltonian (3.48). We want to describe the coupling of this system to a reservoir; in order to use the Lindblad equation (2.54), we must define the decay channels by which the system couples to the reservoir, and investigate the effect of the Lamb shift Hamiltonian (2.53).

3.5.1 Damping of the cavity field

We consider a system S comprising a collection of uncoupled harmonic oscillators, each representing a single cavity mode. This system will have a Hamiltonian of the same form as (3.8), but for our purposes here it will be useful to write the Hamiltonian in the form

$$H_S = \sum_i \hbar\omega_i \hat{a}_i^\dagger \hat{a}_i\,, \tag{3.53}$$

where we have referred the energy of each oscillator to its ground state. The index i runs over all modes supported by the cavity, including those degenerate in energy $\hbar\omega_i$. The reservoir, too, is modelled as a collection of harmonic oscillators, so its Hamiltonian is written in the same form,

$$H_E = \sum_j \hbar\omega_j \hat{r}_j^\dagger \hat{r}_j\,. \tag{3.54}$$

Just as with the interaction between the driving field and the cavity, we assume a linear coupling between the cavity and reservoir fields. The interaction Hamiltonian, in the form (2.38), is

$$H_I = \hbar \sum_i \sum_j (\hat{a}_i + \hat{a}_i^\dagger)(\kappa_{ij}\hat{r}_j + \kappa_{ij}^*\hat{r}_j^\dagger)\,, \tag{3.55}$$

where κ_{ij} characterises the strength of the interaction. In the interaction picture this becomes

$$H_I(t) = \hbar \sum_i \left[\mathrm{e}^{-\mathrm{i}\omega_i t}\hat{a}_i + \mathrm{e}^{\mathrm{i}\omega_i t}\hat{a}_i^\dagger\right] B_i(t)\,, \tag{3.56}$$

where $B_i(t) = \sum_j[\kappa_{ij}\hat{r}_j(t) + \kappa_{ij}^*\hat{r}_j^\dagger(t)]$. We assume that each eigenoperator $\hat{a}_\alpha$ couples to its own group of reservoir modes, statistically independent from the reservoir modes that all other $\hat{a}_\beta$ (with $\alpha \neq \beta$) couple to. This assumption means that $\kappa_{\alpha j}\kappa_{\beta j}^*$ is non-zero only when $\alpha = \beta$, a condition we will make use of later.

The master equation (2.52) is immediately adapted to the case of the interaction (3.56), giving

$$\begin{aligned}\frac{\mathrm{d}}{\mathrm{d}t}\rho_S(t) = \frac{1}{\mathrm{i}\hbar}\left[H_{LS}, \rho_S(t)\right] + \sum_{\alpha,\beta}\gamma_{\alpha\beta}^-\left[\hat{a}_\beta\rho_S(t)\hat{a}_\alpha^\dagger - \frac{1}{2}\hat{a}_\alpha^\dagger\hat{a}_\beta\rho_S(t) - \frac{1}{2}\rho_S(t)\hat{a}_\alpha^\dagger\hat{a}_\beta\right] \\ + \sum_{\alpha,\beta}\gamma_{\alpha\beta}^+\left[\hat{a}_\beta^\dagger\rho_S(t)\hat{a}_\alpha - \frac{1}{2}\hat{a}_\alpha\hat{a}_\beta^\dagger\rho_S(t) - \frac{1}{2}\rho_S(t)\hat{a}_\alpha\hat{a}_\beta^\dagger\right],\end{aligned} \tag{3.57}$$

where

$$H_{LS} = \hbar \sum_{\alpha,\beta}\left(S_{\alpha\beta}^-\hat{a}_\alpha^\dagger\hat{a}_\beta + S_{\alpha\beta}^+\hat{a}_\alpha\hat{a}_\beta^\dagger\right), \tag{3.58}$$

with

$$\Gamma_{\alpha\beta}^\pm = \int_0^\infty \mathrm{d}s\,\mathrm{e}^{\mp\mathrm{i}\omega_\alpha s}\mathrm{tr}_E[B_\alpha^\dagger(t)B_\beta(t-s)\rho_E] = \frac{1}{2}\gamma_{\alpha\beta}^\pm + \mathrm{i}S_{\alpha\beta}^\pm\,. \tag{3.59}$$

Note that the coefficient $\Gamma_{\alpha\beta}^\pm$ is only non-zero when the modes denoted by α and β are degenerate in frequency ($\omega_\alpha = \omega_\beta$), by the rotating wave approximation.

The correlation functions in $\Gamma_{\alpha\beta}^\pm$ are homogeneous in time, so we obtain

$$\begin{aligned}\Gamma_{\alpha\beta}^\pm = \sum_j\sum_{j'}\int_0^\infty \mathrm{d}s\Big[\kappa_{\alpha j}\kappa_{\beta j'}\langle\hat{r}_j\hat{r}_{j'}\rangle\mathrm{e}^{-\mathrm{i}(\omega_j\pm\omega_\alpha)s} + \kappa_{\alpha j}\kappa_{\beta j'}^*\langle\hat{r}_j\hat{r}_{j'}^\dagger\rangle\mathrm{e}^{-\mathrm{i}(\omega_j\pm\omega_\alpha)s} \\ + \kappa_{\alpha j}^*\kappa_{\beta j'}\langle\hat{r}_j^\dagger\hat{r}_{j'}\rangle\mathrm{e}^{\mathrm{i}(\omega_j\mp\omega_\alpha)s} + \kappa_{\alpha j}^*\kappa_{\beta j'}^*\langle\hat{r}_j^\dagger\hat{r}_{j'}^\dagger\rangle\mathrm{e}^{\mathrm{i}(\omega_j\mp\omega_\alpha)s}\Big].\end{aligned} \tag{3.60}$$

If we assume that the reference state of the environment ρ_E is the vacuum,[2]

$$\rho_E = |0\rangle\langle 0|\,, \tag{3.61}$$

[2]This approximation is reasonable, since at optical frequencies $\hbar\omega_j \gg k_B T$, and thermal excitations of the reservoir can be neglected [15].

then of the four expectation values in (3.60) above, the only non-zero one is

$$\langle \hat{r}_j \hat{r}_{j'}^\dagger \rangle = \delta_{jj'} \,. \tag{3.62}$$

Thus, we obtain

$$\Gamma_{\alpha\beta}^{\pm} = \sum_j \kappa_{\alpha j} \kappa_{\beta j}^* \int_0^\infty \mathrm{d}s \, \exp[-\mathrm{i}(\omega_j \pm \omega_\alpha)s] \,. \tag{3.63}$$

Using the assumption of statistical independence discussed earlier, with the result that $\kappa_{\alpha j}\kappa_{\beta j}^* \neq 0$ only when $\alpha = \beta$, we can insert a delta function into the relation above, obtaining

$$\Gamma_{\alpha\beta}^{\pm} = \delta_{\alpha\beta} \sum_j \kappa_{\alpha j} \kappa_{\beta j}^* \int_0^\infty \mathrm{d}s \, \exp[-\mathrm{i}(\omega_j \pm \omega_\alpha)s] \,. \tag{3.64}$$

As the modes of the reservoir, in this case the electromagnetic field, form a continuum, we go over into the continuum limit,

$$\Gamma_{\alpha\beta}^{\pm} = \delta_{\alpha\beta} \int_0^\infty \mathrm{d}\omega' \, g(\omega') \kappa_\alpha(\omega') \kappa_\beta^*(\omega') \int_0^\infty \mathrm{d}s \, \exp[-\mathrm{i}(\omega' \pm \omega_\alpha)s] \,, \tag{3.65}$$

where we have introduced the density of states $g(\omega')$: there are $g(\omega')\mathrm{d}\omega$ oscillators with frequencies in the interval $(\omega', \omega' + \mathrm{d}\omega')$. Using the relation

$$\int_0^\infty \mathrm{d}s \, \exp(-\mathrm{i}\epsilon s) = \pi\delta(\epsilon) - \mathrm{i}\mathrm{P}\frac{1}{\epsilon} \,, \tag{3.66}$$

where P denotes the Cauchy principal value, we obtain

$$\Gamma_{\alpha\beta}^{\pm} = \delta_{\alpha\beta} \left[\int_0^\infty \mathrm{d}\omega' \, g(\omega') \kappa_\alpha(\omega') \kappa_\beta^*(\omega') \pi\delta(\omega' \pm \omega_\alpha) \right. \\ \left. -\mathrm{i}\mathrm{P} \int_0^\infty \mathrm{d}\omega' \, g(\omega') \kappa_\alpha(\omega') \kappa_\beta^*(\omega') \frac{1}{\omega' \pm \omega_\alpha} \right] . \tag{3.67}$$

Simplifying, we obtain

$$\Gamma_{\alpha\beta}^{-} = \delta_{\alpha\beta} \left[\pi g(\omega_\alpha) \left|\kappa_\alpha(\omega_\alpha)\right|^2 + \mathrm{i}\mathrm{P} \int_0^\infty \mathrm{d}\omega' \, \frac{g(\omega') \left|\kappa_\alpha(\omega')\right|^2}{\omega_\alpha - \omega'} \right] \tag{3.68a}$$

and

$$\Gamma_{\alpha\beta}^{+} = \delta_{\alpha\beta} \mathrm{i}\mathrm{P} \int_0^\infty \mathrm{d}\omega' \, \frac{g(\omega') \left|\kappa_\alpha(\omega')\right|^2}{\omega_\alpha + \omega'} \tag{3.68b}$$

Thus, we obtain a master equation in the interaction picture

$$\frac{\mathrm{d}}{\mathrm{d}t}\rho_S(t) = \frac{1}{\mathrm{i}\hbar}\left[H_{LS}, \rho_S(t)\right] + \sum_i \gamma_i \left[\hat{a}_i \rho_S(t) \hat{a}_i^\dagger - \frac{1}{2}\hat{a}_i^\dagger \hat{a}_i \rho_S(t) - \frac{1}{2}\rho_S(t)\hat{a}_i^\dagger \hat{a}_i \right] , \tag{3.69}$$

with a Lamb shift Hamiltonian

$$H_{LS} = \hbar \sum_i S_i \left(\hat{a}_i^\dagger \hat{a}_i + \hat{a}_i \hat{a}_i^\dagger \right) , \tag{3.70}$$

where

$$\gamma_i = 2\pi g(\omega_i) \left| \kappa_i(\omega_i) \right|^2 , \tag{3.71}$$

and

$$S_i = \mathrm{P} \int_0^\infty \mathrm{d}\omega' \, g(\omega') \left| \kappa_i(\omega') \right|^2 \left[\frac{1}{\omega_i - \omega'} + \frac{1}{\omega_i + \omega'} \right] . \tag{3.72}$$

In the case of an atom coupled to an external electromagnetic field, the Lamb shift Hamiltonian leads to a renormalisation of the system Hamiltonian H_S which is induced by the vacuum fluctuations of the radiation field (the Lamb shift) and by thermally induced processes (the Stark shift). In the present context of a cavity coupled to a reservoir, the Lamb shift Hamiltonian leads to an analogous renormalisation of the unperturbed energy levels of the cavity. As can be seen from the expression for S_i above, the contribution from H_{LS} is formally infinite, and must be renormalised according to the renormalisation procedure from relativistic quantum electrodynamics [16]. We are not going to do this here. Fortunately for us, the contribution from the Lamb shift Hamiltonian is typically very small, and can be neglected (or at least absorbed into the definition of some transition frequency). We will neglect such contributions throughout this thesis.

3.5.2 Damping of the two-level atom

We now turn to a two-level atom with Hamiltonian

$$H_S = \frac{1}{2} \hbar \omega_A \hat{\sigma}_+ \hat{\sigma}_- , \tag{3.73}$$

coupled to a reservoir via the same type of coupling as in (3.19). If we follow the steps of the last section – the only real difference being that instead of summing over reservoir oscillators, we sum over polarisation states and integrate over wave-vectors – we obtain a master equation in the interaction picture for the decay of this two-level system

$$\frac{\mathrm{d}}{\mathrm{d}t} \rho_S(t) = \gamma \left[\hat{\sigma}_- \rho_S(t) \hat{\sigma}_+ - \frac{1}{2} \hat{\sigma}_+ \hat{\sigma}_- \rho_S(t) - \frac{1}{2} \rho_S(t) \hat{\sigma}_+ \hat{\sigma}_- \right] , \tag{3.74}$$

where we have neglected the Lamb shift and Stark shift contributions discussed above, and

$$\gamma = 2\pi \sum_\lambda \int \mathrm{d}^3 k \, g(\mathbf{k}) \left| \kappa(\mathbf{k}, \lambda) \right|^2 \delta(\omega_k - \omega_A) , \tag{3.75}$$

where

$$\kappa(\mathbf{k},\lambda) \equiv -\mathrm{i}e^{\mathrm{i}\mathbf{k}\cdot\mathbf{R}}\left(\frac{{\omega_A}^2}{2\hbar\omega_k\epsilon_0 L^3}\right)^{\frac{1}{2}}\mathbf{d}_{ge}^{*}\cdot\mathbf{e}_{\mathbf{k}\lambda}\,. \tag{3.76}$$

The plane waves that fit into a box of side length L, with periodic boundary conditions, have wave numbers $\mathbf{k} = 2\pi(n_x, n_y, n_z)/L$. Thus, the mode density $g(\mathbf{k})$ used above is given by

$$g(\mathbf{k}) = \left(\frac{L}{2\pi}\right)^3, \tag{3.77}$$

From this we obtain

$$\begin{aligned} g(\mathbf{k})\mathrm{d}^3k &= \left(\frac{L}{2\pi}\right)^3 k^2\sin\theta\mathrm{d}k\mathrm{d}\theta\mathrm{d}\phi \\ &= \frac{\omega_k^2 L^3}{8\pi^3c^3}\sin\theta\mathrm{d}\omega_k\mathrm{d}\theta\mathrm{d}\phi\,, \end{aligned} \tag{3.78}$$

and thus

$$\gamma = \frac{{\omega_A}^2}{8\pi^2\hbar\epsilon_0 c^3}\sum_{\lambda}\iiint\omega_k\delta(\omega_k-\omega_A)\left|\mathbf{d}_{ge}^{*}\cdot\mathbf{e}_{\mathbf{k}\lambda}\right|^2\sin\theta\mathrm{d}\omega_k\mathrm{d}\theta\mathrm{d}\phi\,. \tag{3.79}$$

With the help of the relations [17, 18]

$$\sum_{\lambda=1,2} e_{\mathbf{k}\lambda i}e_{\mathbf{k}\lambda j} = \delta_{ij} - \frac{k_i k_j}{|\mathbf{k}|^2}\,, \quad i,j = 1,2,3\,, \tag{3.80}$$

and

$$\iint\sin\theta\mathrm{d}\theta\mathrm{d}\phi\left(\delta_{ij} - \frac{k_i k_j}{|\mathbf{k}|^2}\right) = \frac{8\pi}{3}\delta_{ij}\,, \tag{3.81}$$

we obtain

$$\left|\mathbf{d}_{ge}^{*}\cdot\mathbf{e}_{\mathbf{k}\lambda}\right|^2 = \frac{8\pi}{3}\left|\mathbf{d}_{ge}\right|^2\,. \tag{3.82}$$

Thus we obtain the *spontaneous emission rate*,

$$\gamma = \frac{{\omega_A}^3\left|\mathbf{d}_{ge}\right|^2}{3\pi\hbar\epsilon_0 c^3}\,. \tag{3.83}$$

3.5.3 The damped Jaynes-Cummings model

For the case of a single-mode cavity, there is loss through both mirrors, and thus the cavity mode couples to two reservoir modes. From (3.69) we obtain (neglecting the Lamb shift term)

$$\frac{\mathrm{d}}{\mathrm{d}t}\rho_S(t) = (\gamma_{a1}+\gamma_{a2})\left[\hat{a}\rho_S(t)\hat{a}^\dagger - \frac{1}{2}\hat{a}^\dagger\hat{a}\rho_S(t) - \frac{1}{2}\rho_S(t)\hat{a}^\dagger\hat{a}\right]. \tag{3.84}$$

It is convenient to define the *cavity mode damping rate*,

$$\kappa \equiv \frac{\gamma_{a1} + \gamma_{a2}}{2} . \tag{3.85}$$

We now consider a system consisting of a two-level atom coupled to a single-mode cavity, which couples to the surrounding environment, and may in general be driven by a periodic classical field.

We have two decay channels: loss of light through the cavity mirrors, and spontaneous emission from the atom into modes other than that of the cavity. The dissipation terms corresponding to these decay channels are those we have already described, relating to the two-level atom (3.74) and to the cavity mode (3.84) respectively. Adding these gives the master equation in the interaction picture for the undriven Jaynes-Cummings system.

Transforming to the Schrödinger picture, and appending a term to the Hamiltonian to take into account the classical driving field, as in (3.48), we obtain the complete master equation

$$\begin{aligned}\frac{\mathrm{d}}{\mathrm{d}t}\rho_S(t) = \frac{1}{\mathrm{i}\hbar}\left[H_S, \rho_S(t)\right] + 2\kappa\left[\hat{a}\rho_S(t)\hat{a}^\dagger - \frac{1}{2}\hat{a}^\dagger\hat{a}\rho_S(t) - \frac{1}{2}\rho_S(t)\hat{a}^\dagger\hat{a}\right] \\ + \gamma\left[\hat{\sigma}_-\rho_S(t)\hat{\sigma}_+ - \frac{1}{2}\hat{\sigma}_+\hat{\sigma}_-\rho_S(t) - \frac{1}{2}\rho_S(t)\hat{\sigma}_+\hat{\sigma}_-\right],\end{aligned} \tag{3.86}$$

with

$$H_S = H_{\mathcal{E}}(t) + \frac{1}{2}\omega_A\hat{\sigma}_z + \omega_F\hat{a}^\dagger\hat{a} + g(\hat{\sigma}_+\hat{a} + \hat{\sigma}_-\hat{a}^\dagger) . \tag{3.87}$$

If we transform into the rotating frame (section 3.4) rather than into the Schrödinger picture, we obtain for the system Hamiltonian

$$H_S = H_{\mathcal{E}} + \frac{1}{2}\Delta\omega_A\hat{\sigma}_z + \Delta\omega_F\hat{a}^\dagger\hat{a} + g(\hat{\sigma}_+\hat{a} + \hat{\sigma}_-\hat{a}^\dagger) . \tag{3.88}$$

The driving Hamiltonians $H_{\mathcal{E}}(t)$ and $H_{\mathcal{E}}$ are as given in section 3.3 and 3.4.

We introduce the notation

$$\begin{aligned}\mathcal{D}\left[\hat{A}\right]\rho &= \frac{1}{2}\left(\left[\hat{A}\rho, \hat{A}^\dagger\right] + \left[\hat{A}, \rho\hat{A}^\dagger\right]\right) \\ &= \hat{A}\rho\hat{A}^\dagger - \frac{1}{2}\hat{A}^\dagger\hat{A}\rho - \frac{1}{2}\rho\hat{A}^\dagger\hat{A}\end{aligned} \tag{3.89}$$

for the Lindblad damping superoperator $\mathcal{D}$ (also sometimes called the *dissipator*). Using this notation, we write (3.86) in the form

$$\frac{\mathrm{d}}{\mathrm{d}t}\rho_S(t) = \frac{1}{\mathrm{i}\hbar}\left[H_S, \rho_S(t)\right] + \mathcal{D}[\sqrt{2\kappa}\hat{a}]\rho_S(t) + \mathcal{D}[\sqrt{\gamma}\hat{\sigma}_-]\rho_S(t) . \tag{3.90}$$

References

[1] E. T. Jaynes and F. W. Cummings. Comparison of quantum and semiclassical radiation theories with application to the beam maser. *Proceedings of the IEEE*, 51:89–109, 1963.

[2] B. W. Shore and P. L. Knight. The Jaynes-Cummings model. *Journal of Modern Optics*, 40:1195–1238, 1993.

[3] R. Loudon. *The quantum theory of light*, section 4.1. Oxford University Press, third edition, 2000.

[4] R. Loudon. *The quantum theory of light*, section 4.8. Oxford University Press, third edition, 2000.

[5] M. Kronenwett. *Photon Correlations in Two-Mode Cavity Quantum Electrodynamics*, section 1.3.2. Master's thesis, The University of Auckland, 2007.

[6] R. Loudon. *The quantum theory of light*, section 4.4. Oxford University Press, third edition, 2000.

[7] C. Anastopoulos and B. L. Hu. Two-level atom-field interaction: Exact master equations for non-Markovian dynamics, decoherence, and relaxation. *Physical Review A*, 62:033821, 2000.

[8] M. Kronenwett. *Photon Correlations in Two-Mode Cavity Quantum Electrodynamics*. Master's thesis, The University of Auckland, 2007.

[9] J. J. Sakurai. *Modern Quantum Mechanics*, page 96. Addison-Wesley, revised edition, 1994.

[10] H. J. Carmichael. Unpublished lecture notes. 2008.

[11] S. J. Whalen. *Photon correlation functions and photon blockade in two-mode cavity QED*. BSc (Honours) dissertation, The University of Auckland, 2008.

[12] D. F. Walls and G. J. Milburn. *Quantum Optics*, section 10.2. Springer-Verlag, second edition, 2008.

[13] P. Alsing, D.-S. Guo, and H. J. Carmichael. Dynamic Stark effect for the Jaynes-Cummings system. *Physical Review A*, 45:5135, 1992.

[14] M. Kronenwett. *Photon Correlations in Two-Mode Cavity Quantum Electrodynamics*, section 1.3.4. Master's thesis, The University of Auckland, 2007.

[15] M. Kronenwett. *Photon Correlations in Two-Mode Cavity Quantum Electrodynamics*, section 3.2. Master's thesis, The University of Auckland, 2007.

[16] H.-P. Breuer and F. Pettruccione. *The theory of open quantum systems*, section 12.2.3.2. Oxford University Press, 2007.

[17] R. Loudon. *The quantum theory of light*, section 4.5. Oxford University Press, third edition, 2000.

[18] H.-P. Breuer and F. Pettruccione. *The theory of open quantum systems*, section 3.4. Oxford University Press, 2007.

4

Two-mode cavity QED I: theory

Starting from the Jaynes-Cummings model, we set out to model a two-mode cavity quantum electrodynamics experiment carried out by L. A. Orozco's group at the University of Maryland, College Park [1–3]. This chapter considers a model originally developed by Kronenwett [4], and developed further by Viveros [5] and Whalen [6].

4.1 Schematic experimental set-up

The system we consider comprises a single Rubidium-85 atom within an optical cavity. Two optical cavity modes with orthogonal linear polarisations interact with the atom via the $5S_{1/2}, F = 3 \leftrightarrow 5P_{3/2}, F' = 4$ transition (the D_2-line of ^{85}Rb). An external magnetic field defines a quantisation axis, perpendicular to the axis of the cavity, such that one cavity mode couples the $F = 3$ atomic ground state to the $F' = 4$ excited state via $\Delta m_F = 0$ transitions. This mode is driven by a coherent laser field. The other cavity mode, having orthogonal polarisation to the driven mode, couples the atomic states via $\Delta m_F = \pm 1$ transitions.

Light escaping from the system by way of spontaneous emission from the atom leaks out the side of the cavity without necessarily being detected. Light leaking out through one of the cavity mirrors, on the other hand, is passed through a polarising beam splitter, such that the output from each cavity mode might be detected separately. In this experiment, we are interested in measurements pertaining to the non-driven mode in particular. A schematic diagram of the experimental setup is shown in Fig. 4.1.

4.2 Photon correlation measurements

In the following chapter we will calculate second-order photon correlation functions for the non-driven mode of the two-mode cavity QED system. Therefore we review some of the background of these correlation measurements.

4.2.1 The classical second-order intensity correlation function

In order to quantitatively investigate temporal fluctuations in the intensity $I(t)$ of a classical light beam, as originally measured in the Hanbury Brown-Twiss experiment [7], it is useful to introduce the second-order intesity correlation function,

$$g^{(2)}(\tau) = \frac{\langle I(t) I(t+\tau) \rangle}{\langle I(t) \rangle \langle I(t+\tau) \rangle} . \tag{4.1}$$

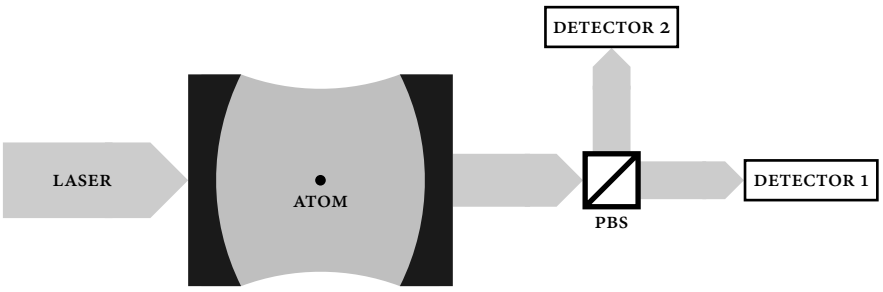

FIGURE 4.1: Schematic set-up of the two-mode cavity QED experiment, as described in section 4.1. The abbreviation 'PBS' refers to a polarising beam splitter.

Here the symbols $\langle\cdots\rangle$ denote an average with respect to t, computed by integrating over a long time period. Let us consider light with a constant mean intensity, such that $\langle I(t)\rangle = \langle I(t+\tau)\rangle$. We can write the intensity of such light as the sum of its mean and a fluctuation,

$$I(t) = \langle I\rangle + \Delta I(t)\,, \tag{4.2}$$

with $\langle \Delta I(t)\rangle = 0$. The second-order intensity correlation function therefore takes on the form,

$$g^{(2)}(\tau) = 1 + \frac{\langle \Delta I(t)\Delta I(t+\tau)\rangle}{\langle I\rangle^2}\,. \tag{4.3}$$

It is clear that $g^{(2)}(0)$ satisfies the inequality

$$g^{(2)}(0) = \frac{\langle I(t)^2\rangle}{\langle I(t)\rangle^2} = 1 + \frac{\langle \Delta I(t)^2\rangle}{\langle I\rangle^2} \geq 1\,. \tag{4.4}$$

Furthermore, it can be shown that $g^{(2)}(\tau)$ has a global maximum at $\tau = 0$ [8].

The time-scale of the intensity correlations is characterised by the coherence time τ_c of the source. For $\tau \gg \tau_c$, fluctuations at times t and $t+\tau$ will be completely uncorrelated, giving

$$\langle \Delta I(t)\Delta I(t+\tau)\rangle_{\tau\gg\tau_c} = 0\,. \tag{4.5}$$

Therefore, for light with constant mean intensity, and for sufficiently large τ, we have

$$g^{(2)}(\tau \gg \tau_c) = 1 + \frac{\langle \Delta I(t)\Delta I(t+\tau)\rangle_{\tau\gg\tau_c}}{\langle I\rangle^2} = 1\,. \tag{4.6}$$

A limiting case of note is that of perfectly coherent, monochromatic light with a constant intensity I_0. For such light, it is trivial to see that

$$g^{(2)}(\tau) = \frac{{I_0}^2}{{I_0}^2} = 1\,, \tag{4.7}$$

for all τ, because $I_0 = I(t) = I(t+\tau)$ is a constant.

4.2.2 The second-order photon correlation function

For quantum light, comprising a stream of photons, the number of counts registered on a photon-counting detector is is proportional to the intensity, so the second-order photon correlation function is given by

$$g^{(2)}(\tau) = \frac{\langle : \hat{n}_1(t)\hat{n}_2(t+\tau) : \rangle}{\langle \hat{n}_1(t) \rangle \langle \hat{n}_2(t+\tau) \rangle} = \frac{\left\langle \hat{a}_1^\dagger(t)\hat{a}_2^\dagger(t+\tau)\hat{a}_2(t+\tau)\hat{a}_1(t) \right\rangle}{\left\langle \hat{a}_1^\dagger(t)\hat{a}_1(t) \right\rangle \left\langle \hat{a}_2^\dagger(t+\tau)\hat{a}_2(t+\tau) \right\rangle}, \tag{4.8}$$

where $\hat{n}_i(t) = \hat{a}_i^\dagger(t)\hat{a}_i(t)$ is the occupation number of the light impinging on detector $i = 1, 2$ at time t. The reason we must now explicitly distinguish between the two detectors is that once a photon has been detected by one detector it cannot be detected by the other. In the classical case, we can split a beam in two and send half to each detector, but we cannot split a photon in two; each photon goes to one detector or the other, and hence the detectors must be distinguished. Note that the two detectors $i = 1, 2$ here do not necessarily correspond to the two detectors in Fig. 4.1; they can refer to measurements made on the same mode or on two different modes as the case may be. In the case of the photon correlation function, $\langle \cdots \rangle$ denotes a quantum-mechanical expectation value, obtained by taking the trace of the product of the operator in question and the density operator of the light beam.

The symbols $: \cdots :$ denote *normal ordering*, where all photon annihilation operators are written to the right of the creation operators in the expansion of the photon occupation operators. This is a consequence of the photoelectric detection process, which relies on the absorption of light, or the annihilation of photons [9].

The second-order photon correlation function is positive,

$$g^{(2)}(\tau) \geq 0\,, \tag{4.9}$$

but it does not in general satisfy either of the classical inequalities $g^{(2)}(0) \geq 1$ or $g^{(2)}(0) \geq g^{(2)}(\tau)$ [10]. It is possible to classify light according to the properties of the second-order photon correlation function; one such classification is whether the light satisfies the classical inequalities above, or whether it is "non-classical". Classifying light in this way leads to a rich and interesting field of study, but it is not the subject of this thesis, so we will not consider it here, instead referring the interested reader to other literature [4, 6, 11, 12].

4.3 Extensions of the Jaynes-Cummings model

4.3.1 Two-mode cavity

In section 3.5.1 we derived a master equation, and in 3.5.3 we specialised to the case of a single-mode cavity. Here, we consider a cavity which supports two modes of the electromagnetic field, degenerate in energy and orthogonal in polarisation. The Hamiltonian for the cavity field is

$$H_F = \hbar\omega_F \hat{a}^\dagger \hat{a} + \hbar\omega_F \hat{b}^\dagger \hat{b}\,. \tag{4.10}$$

From (3.69), the interaction picture master equation describing the loss for such a cavity is

$$\dot{\rho} = (\gamma_{a1} + \gamma_{a2})\mathcal{D}[\hat{a}]\rho + (\gamma_{b1} + \gamma_{b2})\mathcal{D}[\hat{b}]\rho\,, \tag{4.11}$$

where we have written ρ in place of $\rho_S(t)$ in the interests of simplifying our notation.

Light is lost through the cavity mirrors at rates γ_{ai} and γ_{bi} $(i = 1, 2)$ for the two orthogonal cavity modes. These rates are equal, that is to say $\gamma_{ai} = \gamma_{bi}$. Thus, (4.11) may be re-written

$$\dot{\rho} = 2\kappa\left(\mathcal{D}[\hat{a}]\rho + \mathcal{D}[\hat{b}]\rho\right)\,, \tag{4.12}$$

where

$$\kappa \equiv \frac{\gamma_{a1} + \gamma_{a2}}{2} = \frac{\gamma_{b1} + \gamma_{b2}}{2}\,. \tag{4.13}$$

4.3.2 Selection rules

The minimal coupling Hamiltonian (3.1) can be transformed under a unitary transformation into an alternative form which results in the same physical predictions [13]. The resulting interaction Hamiltonian in its complete form is known as the Power-Zienau-Woolley, or multipolar, Hamiltonian, and contains terms which take into account electric and magnetic potential energy, as well as nonlinear terms [14, 15]. The electric potential energy Hamiltonian has the form

$$H = \int_V \mathrm{d}\mathbf{r}\,\mathbf{P}(\mathbf{r})\cdot\hat{\mathbf{E}}_{\mathrm{T}}(\mathbf{r})\,, \tag{4.14}$$

where the atomic polarisation is given by [13]

$$\mathbf{P}(\mathbf{r}) = -e\sum_i \mathbf{r}_i \int_0^1 \mathrm{d}\zeta\,\delta(\mathbf{r} - \zeta\mathbf{r}_i)\,; \tag{4.15}$$

this integral form of the polarisation is obtained by solving the usual relation $\sigma(\mathbf{r}) = -\nabla\cdot\mathbf{P}(\mathbf{r})$ [16], where $\sigma(\mathbf{r}) = Ze\delta(\mathbf{r}) - e\sum_i \delta(\mathbf{r} - \mathbf{r}_i)$ is the atomic charge density. Keeping only the dominant dipole interaction term in the multipole expansion of (4.14) is equivalent to the dipole approximation of section 3.1.3, and results in the well-known electric dipole interaction Hamiltonian,

$$H_{ED} = -\hat{\mathbf{d}}\cdot\hat{\mathbf{E}}_{\mathrm{T}}(\mathbf{R})\,, \tag{4.16}$$

where

$$\hat{\mathbf{d}} = -e\hat{\mathbf{D}} = -e\sum_i \mathbf{r}_i\,. \tag{4.17}$$

We remind ourselves that $\mathbf{R}$ is the position of the atom. The transverse electric field operator is given by

$$\hat{\mathbf{E}}_{\mathrm{T}}(\mathbf{r}) = \mathrm{i}\sum_{\mathbf{k}}\sum_{\lambda}\left(\frac{\hbar\omega_{\mathbf{k}}}{2\epsilon_0}\right)^{\frac{1}{2}}\left[\hat{a}_{\mathbf{k}\lambda}\mathbf{u}_{\mathbf{k}\lambda}(\mathbf{r}) - \hat{a}^{\dagger}_{\mathbf{k}\lambda}\mathbf{u}^{*}_{\mathbf{k}\lambda}(\mathbf{r})\right]. \tag{4.18}$$

In first-order time-dependent perturbation theory, Fermi's golden rule states that the probability per unit time for a transition from an initial state $|\phi_i\rangle$ with energy E_i to a final state $|\phi_f\rangle$ with energy E_f, due to a perturbation V, is

$$P_{i\to f} = \frac{2\pi}{\hbar}\left|\langle\phi_f|V|\phi_i\rangle\right|^2\delta(E_f - E_i), \tag{4.19}$$

where this expression is integrated over a continuum of states $\int \mathrm{d}E_f\,\rho(E_f)$, with density of final states $\rho(E_f)$. Assuming that the interaction between the atom and the electromagnetic field provides only a small contribution to the total Hamiltonian, Fermi's golden rule can be applied. In this case, it is clear that the electric dipole interaction Hamiltonian (4.16) induces no transition between states $|\phi_i\rangle$ and $|\phi_f\rangle$ if the matrix element

$$M_{fi} \equiv \langle\phi_f|H_{ED}|\phi_i\rangle \tag{4.20}$$

vanishes. Transitions for which this matrix element vanishes are termed *forbidden* in the electric dipole interaction, but may occur due to another interaction (the magnetic dipole or electric quadrupole interactions, for example). Investigation of the matrix element (4.20) therefore yields the selection rules for electric-dipole transitions.

Now we must evaluate the matrix element M_{fi}. We find, considering only a single mode $\mathbf{k}\lambda$ of the transverse electric field,

$$\begin{aligned} M_{fi} &= \langle\phi_i|-\hat{\mathbf{d}}\cdot\hat{\mathbf{E}}_{\mathrm{T}}(\mathbf{R})|\phi_f\rangle \\ &= \left\langle\phi_f\middle|\mathrm{i}e\left(\frac{\hbar\omega_{\mathbf{k}\lambda}}{2\epsilon_0}\right)^{\frac{1}{2}}\hat{\mathbf{D}}\cdot\left[\hat{a}_{\mathbf{k}\lambda}\mathbf{u}_{\mathbf{k}\lambda}(\mathbf{R}) - \hat{a}^{\dagger}_{\mathbf{k}\lambda}\mathbf{u}^{*}_{\mathbf{k}\lambda}(\mathbf{R})\right]\middle|\phi_i\right\rangle \\ &= \mathrm{i}e\left(\frac{\hbar\omega_{\mathbf{k}\lambda}}{2\epsilon_0 V}\right)^{\frac{1}{2}}\left[\langle\phi_f|\hat{\mathbf{D}}\cdot\mathbf{e}_{\mathbf{k}\lambda}f_{\mathbf{k}}(\mathbf{R})\hat{a}_{\mathbf{k}\lambda}|\phi_i\rangle - \langle\phi_f|\hat{\mathbf{D}}\cdot\mathbf{e}_{\mathbf{k}\lambda}f^{*}_{\mathbf{k}}(\mathbf{R})\hat{a}^{\dagger}_{\mathbf{k}\lambda}|\phi_i\rangle\right] \end{aligned} \tag{4.21}$$

If we define

$$|\phi_i\rangle \equiv |\psi_i\rangle\,|n_{\mathbf{k}\lambda,i}\rangle\,, \quad \text{and} \quad |\phi_f\rangle \equiv |\psi_f\rangle\,|n_{\mathbf{k}\lambda,f}\rangle\,, \tag{4.22}$$

we obtain

$$\begin{aligned} M_{fi} = \mathrm{i}e\left(\frac{\hbar\omega_{\mathbf{k}\lambda}}{2\epsilon_0 V}\right)^{\frac{1}{2}}\Big[&\langle\psi_f|\hat{\mathbf{D}}|\psi_i\rangle\cdot\mathbf{e}_{\mathbf{k}\lambda}f_{\mathbf{k}}(\mathbf{R})\,\langle n_{\mathbf{k}\lambda,f}|\hat{a}_{\mathbf{k}\lambda}|n_{\mathbf{k}\lambda,i}\rangle \\ &- \langle\psi_f|\hat{\mathbf{D}}|\psi_i\rangle\cdot\mathbf{e}_{\mathbf{k}\lambda}f^{*}_{\mathbf{k}}(\mathbf{R})\,\langle n_{\mathbf{k}\lambda,f}|\hat{a}^{\dagger}_{\mathbf{k}\lambda}|n_{\mathbf{k}\lambda,i}\rangle\Big]. \end{aligned} \tag{4.23}$$

Note that $\langle n_{\mathbf{k}\lambda,f}|\hat{a}_{\mathbf{k}\lambda}|n_{\mathbf{k}\lambda,i}\rangle$ is non-zero only when $n_{\mathbf{k}\lambda,f} = n_{\mathbf{k}\lambda,i} - 1$, and $\langle n_{\mathbf{k}\lambda,f}|\hat{a}^\dagger_{\mathbf{k}\lambda}|n_{\mathbf{k}\lambda,i}\rangle$ is non-zero only when $n_{\mathbf{k}\lambda,f} = n_{\mathbf{k}\lambda,i} + 1$.

Energy conservation requires that

$$E_f - E_i \approx 0\,. \tag{4.24}$$

The change of energy of the atom must be approximately equal and opposite to that of the field (a mismatch on the order of the atomic linewidth being allowed). If the energies of the atom in its initial and final states are $E_{A,i}$ and $E_{A,f}$ respectively, we get

$$E_{A,f} - E_{A,i} \approx -(n_{\mathbf{k}\lambda,f} - n_{\mathbf{k}\lambda,i})\hbar\omega_{\mathbf{k}}\,. \tag{4.25}$$

From (4.23), we see that the matrix element M_{fi} is proportional to the atomic dipole matrix element

$$\mathbf{D}_{fi} \equiv \langle\psi_f|\hat{\mathbf{D}}|\psi_i\rangle\,, \tag{4.26}$$

and we find the transition probability per unit time

$$P_{i\to f} = 4\pi^2\frac{e^2}{4\pi\hbar c\epsilon_0}\frac{c}{V}\hbar\omega_{\mathbf{k}\lambda}\left|\mathbf{D}_{fi}\cdot\mathbf{e}_{\mathbf{k}\lambda}f_{\mathbf{k}}(\mathbf{R})\langle n_{\mathbf{k}\lambda,f}|\hat{a}_{\mathbf{k}\lambda}|n_{\mathbf{k}\lambda,i}\rangle - \mathbf{D}_{fi}\cdot\mathbf{e}_{\mathbf{k}\lambda}f^*_{\mathbf{k}}(\mathbf{R})\langle n_{\mathbf{k}\lambda,f}|\hat{a}^\dagger_{\mathbf{k}\lambda}|n_{\mathbf{k}\lambda,i}\rangle\right|^2\rho(E_f)\,. \tag{4.27}$$

We see that in fact the quantity of interest is $\mathbf{D}_{fi}$, because when $\mathbf{D}_{fi} = 0$, $P_{i\to f} = 0$ and the corresponding transition is forbidden.

In the case of a single-electron (hydrogenic) atom, we have

$$\mathbf{D}_{fi} = \mathbf{r}_{fi} = \langle\psi_f|\mathbf{r}|\psi_i\rangle\,, \tag{4.28}$$

where $\mathbf{r}$ is the position of the electron. The hydrogenic atom is a pretty good approximation to atoms with a single valence ("optical") electron, if we neglect perturbations due to screening [17, 18], and the results gained from looking at hydrogenic atoms are readily generalised to many-electron atoms [19].

The *Wigner-Eckart theorem* [20] states that the matrix elements of a spherical tensor operator $T^{(k)}_q$ (of rank k with $2k+1$ components $\{q\}$) with respect to angular momentum eigenstates satisfy

$$\langle\alpha', j', m'|T^{(k)}_q|\alpha, j, m\rangle = \langle j, k; m, q|j, k; j', m'\rangle\frac{\langle\alpha', j'\|T^{(k)}\|\alpha, j\rangle}{\sqrt{2j+1}}\,, \tag{4.29}$$

where the double-bar matrix element $\langle\alpha', j'\|T^{(k)}\|\alpha, j\rangle$ is independent of m and m', and of q. The quantity $\langle j, k; m, q|j, k; j', m'\rangle$ is a Clebsch-Gordan coefficient for adding j and k to get j'.

Using the Wigner-Eckart theorem, we can evaluate the matrix element $\mathbf{r}_{fi}$ via its spherical

vector components. Each of these components is obtained by finding the components of $\mathbf{r}$ in the direction of a polarisation vector, denoted $\mathbf{e}$ [21]. Let $\mathbf{e}_x$, $\mathbf{e}_y$ and $\mathbf{e}_z$ be unit vectors in the directions of the x-, y- and z-axes. For linear polarisation in the z-direction, $\mathbf{e} = \mathbf{e}_z$, and

$$\mathbf{e}\cdot\mathbf{r} = \mathbf{e}_z\cdot\mathbf{r} = z = r\cos\theta = r\left(\frac{4\pi}{3}\right)^{\frac{1}{2}} Y_1^0(\theta,\phi)\,. \tag{4.30}$$

For circularly polarised photons in the xy-plane, which possess ±1 unit of angular momentum about the z-axis, the polarisation vectors are $\mathbf{e} = (\mathbf{e}_x \pm \mathrm{i}\mathbf{e}_y)/\sqrt{2}$, giving

$$\mathbf{e}\cdot\mathbf{r} = \frac{1}{\sqrt{2}}(\mathbf{e}_x \pm \mathrm{i}\mathbf{e}_y)\cdot\mathbf{r} = \frac{1}{\sqrt{2}}(x \pm \mathrm{i}y) = \mp r\left(\frac{4\pi}{3}\right)^{\frac{1}{2}} Y_1^{\pm1}(\theta,\phi)\,. \tag{4.31}$$

Thus, we denote the spherical vector components of $\mathbf{r}$,

$$r_0 \equiv z \quad \text{and} \quad r_{\pm1} \equiv \frac{1}{\sqrt{2}}(x \pm \mathrm{i}y)\,. \tag{4.32}$$

A spherical vector such as $\mathbf{r}$ is a spherical tensor of rank one. Thus in the case of the position operator $\mathbf{r}$, we have $k = 1$ in (4.29). Hence the Wigner-Eckart theorem gives us

$$\left\langle \alpha', j', m' \middle| r_q \middle| \alpha, j, m \right\rangle = \left\langle j, 1; m, q \middle| j, 1; j', m' \right\rangle \frac{\langle \alpha', j' \| \mathbf{r} \| \alpha, j \rangle}{\sqrt{2j+1}}\,, \tag{4.33}$$

with $q = 0, \pm1$ corresponding to the three spherical vector components of $\mathbf{r}$. Referring back to (4.27), we see that the allowed transitions are those with non-vanishing Clebsch-Gordan coefficients $\langle j, 1; m, q | j, 1; j', m' \rangle$. The known properties (recursion relations) of the Clebsch-Gordan coefficients [22, 23] yield the well-known selection rules for fine structure [21, 24]. The selection rules for fine structure are:

$$\Delta j = 0, \pm1\,, \tag{4.34a}$$

$$\Delta m = 0, \pm1 \tag{4.34b}$$

are allowed transitions, but

$$j = 0 \nleftrightarrow j' = 0 \tag{4.34c}$$

$$m = 0 \nleftrightarrow m' = 0 \quad \text{if} \quad \Delta j = 0 \tag{4.34d}$$

are forbidden transitions.

If we include the spin of the atomic nucleus, F and m_F are good quantum numbers, and the angular momentum eigenstates are labelled $|\alpha, F, m_F\rangle$. Following the same procedure as we did for the selection rules for the fine structure, the Clebsch-Gordan coefficient which leads to the hyperfine structure selection rules is $\langle F, 1; m_F, q | F, 1; F', m'_F \rangle$. The resulting selection

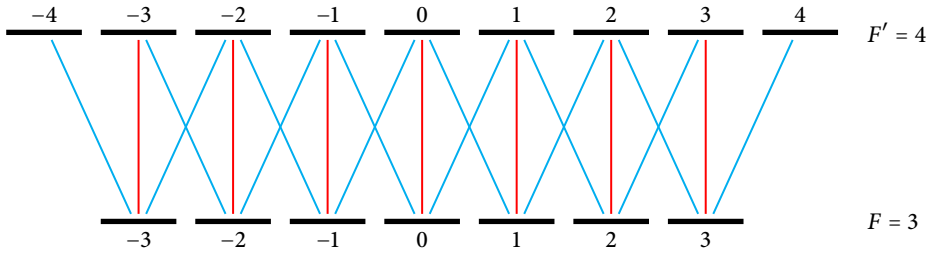

FIGURE 4.2: Atomic level structure and allowed electric dipole transitions for an $F = 3$ to $F' = 4$ transition. The relative transition strengths are determined by appropriate Clebsch-Gordan coefficients. The driven cavity mode interacts with the atom via $\Delta m_F = 0$ transitions (red lines), and the non-driven mode via $\Delta m_F = \pm 1$ transitions (blue lines).

rules for hyperfine structure are:

$$\Delta F = 0, \pm 1 \tag{4.35a}$$

$$\Delta m_F = 0, \pm 1 \tag{4.35b}$$

are allowed, but

$$F = 0 \nleftrightarrow F' = 0 \tag{4.35c}$$

$$m_F = 0 \nleftrightarrow m_F' = 0 \quad \text{if} \quad \Delta F = 0 \tag{4.35d}$$

are forbidden. The allowed transitions for an $F = 3$ to $F' = 4$ transition are shown in Fig. 4.2.

4.3.3 Two-level atom with magnetic substructure

We now consider the Hamiltonian for a two-level atom with magnetic substructure. We assume a quantisation axis such that the driven mode a couples the atomic ground and excited states via $\Delta m_F = 0$ (π) transitions, and the non-driven mode b (which, like a, is linearly polarised) couples the states via $\Delta m_F = \pm 1$ ($\sigma_+ + \sigma_-$) transitions. Such a quantisation axis may be imposed by, for example, a weak magnetic field with negligible Zeeman effect. Stronger magnetic fields, for which the energy level splitting due to the Zeeman effect will need to be taken into account, will be considered later.

The maximum dipole coupling strength of the atomic F to F' transition is denoted by g. To take into account the additional cavity mode and the more complicated level structure, the Jaynes-Cummings interaction Hamiltonian (3.32) for the two-level atom coupled to a single-mode cavity will need to be modified based on the selection rules derived in section 4.3.2. The dipole coupling part of the Hamiltonian now takes the form

$$H_I = \hbar g \left(\hat{\Sigma}_0^\dagger \hat{a} + \hat{\Sigma}_0 \hat{a}^\dagger \right) + \hbar g \left[\left(\frac{\hat{\Sigma}_{-1}^\dagger + \hat{\Sigma}_{+1}^\dagger}{\sqrt{2}} \right) \hat{b} + \left(\frac{\hat{\Sigma}_{-1} + \hat{\Sigma}_{+1}}{\sqrt{2}} \right) \hat{b}^\dagger \right]. \tag{4.36}$$

The modified atomic raising and lowering operators $\hat{\Sigma}_{0,\pm 1}$ (the so-called *atomic dipole transition operators*) have expansions in terms of atomic states and Clebsch-Gordan coefficients. In

particular, the atomic lowering operators are given by[1]

$$\hat{\Sigma}_q = \sum_{m_F=-F}^{F} \left\langle F, 1; m_F, q \middle| F, 1; F', m'_F \right\rangle |F, m_F\rangle \left\langle F', m_F + q \right| . \tag{4.37}$$

We see that the matrix elements of the dipole operator are equal to the Clebsch-Gordan coefficients for adding spin 1 to spin F to reach total spin F'. Such coefficients can be evaluated by way of several known formulae; many such formulae are provided by Edmonds [23]. The Clebsch-Gordan coefficients are closely related to Wigner's 3-j symbol, and can also be evaluated in this fashion. Several computer algebra packages, such as *Sage* [25], implement Clebsch-Gordan coefficient calculators.

In the cavity QED experiment we are modelling, the atomic transition is an $F = 3$ to $F' = 4$ transition. In this case the atomic lowering operators are given by:

$$\begin{aligned}\hat{\Sigma}_{-1} = {} & |g-3\rangle\langle e-4| + \sqrt{\frac{3}{4}}|g,-2\rangle\langle e,-3| + \sqrt{\frac{15}{28}}|g,-1\rangle\langle e,-2| + \sqrt{\frac{5}{14}}|g,0\rangle\langle e,-1| \\ & + \sqrt{\frac{3}{14}}|g,1\rangle\langle e,0| + \sqrt{\frac{3}{28}}|g,2\rangle\langle e,1| + \sqrt{\frac{1}{28}}|g,3\rangle\langle e,2| ,\end{aligned} \tag{4.38a}$$

$$\begin{aligned}\hat{\Sigma}_{0} = {} & \sqrt{\frac{1}{4}}|g,-3\rangle\langle e,-3| + \sqrt{\frac{3}{7}}|g,-2\rangle\langle e,-2| + \sqrt{\frac{15}{28}}|g,-1\rangle\langle e,-1| + \sqrt{\frac{4}{7}}|g,0\rangle\langle e,0| \\ & + \sqrt{\frac{15}{28}}|g,1\rangle\langle e,1| + \sqrt{\frac{3}{7}}|g,2\rangle\langle e,2| + \sqrt{\frac{1}{4}}|g,3\rangle\langle e,3| ,\end{aligned} \tag{4.38b}$$

$$\begin{aligned}\hat{\Sigma}_{+1} = {} & \sqrt{\frac{1}{28}}|g,-3\rangle\langle e,-2| + \sqrt{\frac{3}{28}}|g,-2\rangle\langle e,-1| + \sqrt{\frac{3}{14}}|g,-1\rangle\langle e,0| + \sqrt{\frac{5}{14}}|g,0\rangle\langle e,1| \\ & + \sqrt{\frac{15}{28}}|g,1\rangle\langle e,2| + \sqrt{\frac{3}{4}}|g,2\rangle\langle e,3| + |g,3\rangle\langle e,4| .\end{aligned} \tag{4.38c}$$

The raising operators can of course be found by taking the Hermitian adjoint of the lowering operators.

4.3.4 The Zeeman energy shift

We now consider stronger magnetic fields, for which the energy level splitting due to the Zeeman effect needs to be taken into account. The Zeeman shift manifests itself as a detuning of the atomic energy levels within the ground and excited manifolds. Our task is to evaluate, to first order, the magnitude of this detuning, so that it can be included phenomenologically in the atomic Hamiltonian.

The interaction between the electrons in the atom and the nuclear spin **I** gives rise to the

[1] This expression can be obtained by making an expansion of the **r** operator in terms of matrix elements in the Hilbert space spanned by $\{|F, m_F\rangle\}$, along the lines of the expansion we made in section 3.1.3 for the two-state atom.

hyperfine structure. The hyperfine interaction Hamiltonian has the form [26]

$$H_{HFS} = A\mathbf{I}\cdot\mathbf{J}\,, \tag{4.39}$$

where $\mathbf{J} = \mathbf{L} + \mathbf{S}$ is the resultant of the total orbital and spin momenta of the electrons, and A is the hyperfine structure constant. The interaction energy of the magnetic moment $\boldsymbol{\mu}$ of the atom with an applied magnetic field $\mathbf{B}$ is given by $H_{\rm mag} = -\boldsymbol{\mu}\cdot\mathbf{B}$. The total atomic magnetic moment is the sum of the electronic and nuclear moments [27],

$$\boldsymbol{\mu} = -g_J\frac{\mu_B}{\hbar}\mathbf{J} + g_I\frac{\mu_N}{\hbar}\mathbf{I} \approx -g_J\mu_B\mathbf{J} \tag{4.40}$$

where g_J is the Landé g-factor, g_I is the nuclear g-factor, and μ_B and μ_N are the Bohr and nuclear magnetons. Since $\mu_N \ll \mu_B$ we can neglect the nuclear contribution for all but the most precise measurements. Thus, we obtain

$$H_{\rm mag} = g_J\frac{\mu_B}{\hbar}\mathbf{J}\cdot\mathbf{B}\,. \tag{4.41}$$

When the interaction with the external magnetic field is much weaker than the hyperfine interaction, that is to say $H_{\rm mag} \ll H_{HFS}$, the magnetic interaction $H_{\rm mag}$ can be considered to be a perturbation. If this is the case, the vectors $\mathbf{J}$ and $\mathbf{I}$ move rapidly around their resultant $\mathbf{F}$, while $\mathbf{F}$ precesses more slowly about the magnetic field. In this regime F and m_F are good quantum numbers, while m_J and m_I are not. Thus the unperturbed eigenstates are simultaneous eigenstates of $\mathbf{F}^2$, $\mathbf{J}^2$, $\mathbf{I}^2$ and F_z, labelled $|FJIm_F\rangle$. To evaluate the first-order energy shift, we need to take the projection of the magnetic moment along $\mathbf{F}$, and evaluate its interaction with $\mathbf{B}$:

$$H_{\rm mag} = g_J\frac{\mu_B}{\hbar}\frac{\langle\mathbf{J}\cdot\mathbf{F}\rangle}{F(F+1)}\mathbf{F}\cdot\mathbf{B} = g_F\frac{\mu_B}{\hbar}\mathbf{F}\cdot\mathbf{B}\,, \tag{4.42}$$

with

$$g_F \approx \frac{F(F+1)+J(J+1)-I(I+1)}{2F(F+1)}g_J\,, \tag{4.43}$$

where the approximation sign indicates that we have neglected a nuclear contribution, consistent with our earlier approximation. For Rubidium-85, $I = 5/2$. The Landé g-factor is given by [28]

$$g_J = 1 + \frac{J(J+1)+S(S+1)-L(L+1)}{2J(J+1)}\,. \tag{4.44}$$

Choosing the magnetic field to be applied along the z-axis, $\mathbf{B} = B\mathbf{e}_z$, we obtain the interaction energy

$$H_{\rm mag} = g_F\frac{\mu_B}{\hbar}BF_z\,. \tag{4.45}$$

The Zeeman energy shift is therefore given by the first-order energy shift

$$\begin{aligned}\Delta E &= \left\langle FJIm_F\middle|H_{\text{mag}}\middle|FJIm_F\right\rangle \\ &= \frac{1}{\hbar}\left\langle FJIm_F\middle|g_F\mu_B BF_z\middle|FJIm_F\right\rangle \\ &= g_F\mu_B m_F B\,, \end{aligned} \tag{4.46}$$

where we have used $F_z\left|FJIm_F\right\rangle = \hbar m_F\left|FJIm_F\right\rangle$.

The degeneracy of the magnetic sublevels of the atom is now lifted, and we obtain a Hamiltonian which includes detunings due to the Zeeman effect,

$$H_A = \sum_{m_F=-F}^{F} E_{g,m_F}\left|g,m_F\right\rangle\left\langle g,m_F\right| + \sum_{m'_F=-F'}^{F'} E_{e,m'_F}\left|e,m'_F\right\rangle\left\langle e,m'_F\right|\,, \tag{4.47}$$

with

$$\begin{aligned} E_{g,m_F} &= E_{g,0} + g_F\mu_B m_F B\,, \\ E_{e,m'_F} &= E_{e,0} + g'_F\mu_B m'_F B\,, \end{aligned}$$

where $E_{g,0}$ and $E_{e,0}$ are the unperturbed ground and excited state energies, and g_F and g'_F are the different g-factors for the ground and excited states respectively.

4.3.5 The complete system Hamiltonian for two-mode cavity QED

We can now combine the various parts of the Hamiltonian derived in the above sections, to obtain the complete Hamiltonian for a two-mode cavity QED system. We define the frequency of the central $m_F = 0 \leftrightarrow m'_F = 0$ transition to be ω_A, giving

$$E_{g,0} = -\frac{1}{2}\hbar\omega_A \quad \text{and} \quad E_{e,0} = \frac{1}{2}\hbar\omega_A\,. \tag{4.49}$$

In the experiment we are modelling the cavity (rather than the atom) is driven by a periodic classical field. Thus, the driving term in the Hamiltonian will take the form (3.46). Finally, in the Schrödinger picture, the Hamiltonian for a two-mode cavity QED system, in which the atom is resonant with both cavity modes ($\omega \equiv \omega_A = \omega_F$), is

$$\begin{aligned} H_S =& \hbar\mathcal{E}\left(\hat{a}^\dagger \mathrm{e}^{-\mathrm{i}\omega_L t} + \hat{a}\mathrm{e}^{\mathrm{i}\omega_L t}\right) + \hbar\omega\left(\hat{a}^\dagger\hat{a} + \hat{b}^\dagger\hat{b}\right) \\ &+ \sum_{m_F=-F}^{F}\left(-\frac{1}{2}\hbar\omega + g_F\mu_B m_F B\right)\left|g,m_F\right\rangle\left\langle g,m_F\right| \\ &+ \sum_{m'_F=-F'}^{F'}\left(\frac{1}{2}\hbar\omega + g'_F\mu_B m'_F B\right)\left|e,m'_F\right\rangle\left\langle e,m'_F\right| \\ &+ \hbar g\left(\hat{\Sigma}_0^\dagger\hat{a} + \hat{\Sigma}_0\hat{a}^\dagger\right) + \hbar g\left[\left(\frac{\hat{\Sigma}_{-1}^\dagger + \hat{\Sigma}_{+1}^\dagger}{\sqrt{2}}\right)\hat{b} + \left(\frac{\hat{\Sigma}_{-1} + \hat{\Sigma}_{+1}}{\sqrt{2}}\right)\hat{b}^\dagger\right]. \end{aligned} \tag{4.50}$$

Transforming to the rotating frame gives

$$\begin{aligned} H_S =& \hbar\mathcal{E}\left(\hat{a}^\dagger + \hat{a}\right) + \hbar\Delta\omega\left(\hat{a}^\dagger\hat{a} + \hat{b}^\dagger\hat{b}\right) \\ &+ \sum_{m_F=-F}^{F}\left(-\frac{1}{2}\hbar\Delta\omega + g_F\mu_B m_F B\right)|g, m_F\rangle\langle g, m_F| \\ &+ \sum_{m'_F=-F'}^{F'}\left(\frac{1}{2}\hbar\Delta\omega + g'_F\mu_B m'_F B\right)|e, m'_F\rangle\langle e, m'_F| \\ &+ \hbar g\left(\hat{\Sigma}_0^\dagger\hat{a} + \hat{\Sigma}_0\hat{a}^\dagger\right) + \hbar g\left[\left(\frac{\hat{\Sigma}_{-1}^\dagger + \hat{\Sigma}_{+1}^\dagger}{\sqrt{2}}\right)\hat{b} + \left(\frac{\hat{\Sigma}_{-1} + \hat{\Sigma}_{+1}}{\sqrt{2}}\right)\hat{b}^\dagger\right]. \end{aligned} \tag{4.51}$$

It is in fact the case, for the experiment we are modelling, that the cavity QED system is driven on-resonance, that is $\omega_L = \omega$. Thus, the Hamiltonian takes on a simpler form,

$$\begin{aligned} H_S =& \hbar\mathcal{E}\left(\hat{a}^\dagger + \hat{a}\right) \\ &+ \sum_{m_F=-F}^{F}\left(g_F\mu_B m_F B\right)|g, m_F\rangle\langle g, m_F| + \sum_{m'_F=-F'}^{F'}\left(g'_F\mu_B m'_F B\right)|e, m'_F\rangle\langle e, m'_F| \\ &+ \hbar g\left(\hat{\Sigma}_0^\dagger\hat{a} + \hat{\Sigma}_0\hat{a}^\dagger\right) + \hbar g\left[\left(\frac{\hat{\Sigma}_{-1}^\dagger + \hat{\Sigma}_{+1}^\dagger}{\sqrt{2}}\right)\hat{b} + \left(\frac{\hat{\Sigma}_{-1} + \hat{\Sigma}_{+1}}{\sqrt{2}}\right)\hat{b}^\dagger\right]. \end{aligned} \tag{4.52}$$

This is the form we will use throughout our two-mode cavity QED calculations, as it is the only one relevant to the experimental set-up in question [1–3].

There are several things that have been left out of this model, which could potentially be included in future work. For example, we have neglected any birefringence of the cavity mirrors.

4.4 Master equation for the two-mode cavity QED system

If we refer back to section 4.3.1, we have a starting point for the construction of a master equation for the complete two-mode cavity QED system. We have already seen that the dissipator $2\kappa(\mathcal{D}[\hat{a}]\rho + \mathcal{D}[\hat{b}]\rho)$ accounts for light of both orthogonal modes leaking out of the cavity. When we include the magnetic substructure of the atomic levels in our model, we also have to take into account the polarisation of the light that exits out the side of the cavity. Atomic dipole transitions with different Δm_F refer to light with different polarisation[2] and couple to statistically independent reservoirs. Thus, in addition to the two decay channels for each of the two cavity modes, we have an additional three decay channels corresponding to spontaneous emission events of the atom, that is, one for each of the $\Delta m_F = 0, \pm 1$ transitions. The dissipation term which will be added to the master equation to account for spontaneous emission is the sum over these three decay channels,

$$\sum_q \gamma\mathcal{D}[\hat{\Sigma}_q]\rho\,. \tag{4.53}$$

[2] $\Delta m_F = 0$ refers to linearly polarised light, or π photons. $\Delta m_F = \pm 1$ refers to $\sigma^\pm$ photons, with σ^+ corresponding to left circular polarisation, and σ^- corresponding to right circular polarisation [29]. The b mode is linearly polarised, corresponding to an equal combination of σ^+ and σ^- photons.

The atomic decay rate γ represents only the emission of a photon of the resonant frequency in a direction other than that of the cavity mode. The rate is in reality determined by several factors, but other processes, such as the atom decaying to other levels, represent a breakdown of the two-level atom approximation we are using, and will thus not be considered.

Thus, we obtain the master equation for the two-level atom with magnetic substructure, two-mode cavity QED system,

$$\dot{\rho} = \frac{1}{\mathrm{i}\hbar}[H_S, \rho] + 2\kappa\left(\mathcal{D}[\hat{a}]\rho + \mathcal{D}[\hat{b}]\rho\right) + \sum_q \gamma\mathcal{D}[\hat{\Sigma}_q]\rho\,, \tag{4.54}$$

where H_S is given by (4.52). Recall that κ and γ denote the cavity mode and atomic decay rates respectively.

References

[1] M. L. Terraciano, R. Olson Knell, D. L. Freimund, L. A. Orozco, J. P. Clemens, and P. R. Rice. Enhanced spontaneous emission into the mode of a cavity qed system. *Optics Letters*, 32:982–984, 2007.

[2] M. L. Terraciano, R. Olson Knell, D. G. Norris, J. Jing, A. Fernández, and L. A. Orozco. Photon burst detection of single atoms in an optical cavity. *Nature Physics*, 5:480–484, 2009.

[3] D. G. Norris, L. A. Orozco, P. Barberis-Blostein, and H. J. Carmichael. Observation of ground-state quantum beats in atomic spontaneous emission. To be published in *Physical Review Letters*, 2010.

[4] M. Kronenwett. *Photon Correlations in Two-Mode Cavity Quantum Electrodynamics*. Master's thesis, The University of Auckland, 2007.

[5] E. C. Viveros. *Photon correlations in two mode cavity QED in an external magnetic field*. PGDipSci dissertation, The University of Auckland, 2008.

[6] S. J. Whalen. *Photon correlation functions and photon blockade in two-mode cavity QED*. BSc (Honours) dissertation, The University of Auckland, 2008.

[7] R. Hanbury Brown and R. Q. Twiss. Correlation between photons in two coherent beams of light. *Nature*, 177:27–29, 1956.

[8] R. Loudon. *The quantum theory of light*, section 3.7. Oxford University Press, third edition, 2000.

[9] A. M. Fox. *Quantum Optics*, section 8.5. Oxford University Press, 2006.

[10] R. Loudon. *The quantum theory of light*, section 4.12. Oxford University Press, third edition, 2000.

[11] R. Loudon. *The quantum theory of light*, sections 6.4 & 6.5. Oxford University Press, third edition, 2000.

[12] A. M. Fox. *Quantum Optics*, chapter 6. Oxford University Press, 2006.

[13] R. Loudon. *The quantum theory of light*, section 4.8. Oxford University Press, third edition, 2000.

[14] E. A. Power and S. Zienau. Coulomb gauge in non-relativistic quantum electro-dynamics

and the shape of spectral lines. *Philosophical Transactions of the Royal Society of London. Series A, Mathematical and Physical Sciences*, 251:427–454, 1959.

[15] R. G. Woolley. Molecular quantum electrodynamics. *Proceedings of the Royal Society of London. Series A, Mathematical and Physical Sciences*, 321:557–572, 1971.

[16] J. D. Jackson. *Classical Electrodynamics*, chapter 4. Wiley, third edition, 1999.

[17] F. Mandl. *Quantum Mechanics*, section 2.5.2. Wiley, 1992.

[18] C. J. Foot. *Atomic Physics*, section 4.3. Oxford University Press, 2005.

[19] A. M. Fox. *Quantum Optics*, section 4.3. Oxford University Press, 2006.

[20] J. J. Sakurai. *Modern Quantum Mechanics*, pages 238–242. Addison-Wesley, revised edition, 1994.

[21] F. Mandl. *Quantum Mechanics*, section 6.2. Wiley, 1992.

[22] J. J. Sakurai. *Modern Quantum Mechanics*, pages 210–215. Addison-Wesley, revised edition, 1994.

[23] A. R. Edmonds. *Angular Momentum in Quantum Mechanics*. Princeton University Press, 1957.

[24] C. J. Foot. *Atomic Physics*, section 5.4. Oxford University Press, 2005.

[25] W. A. Stein et al. *Sage Mathematics Software*. The Sage Development Team, 2009. `http://www.sagemath.org`.

[26] C. J. Foot. *Atomic Physics*, section 6.1. Oxford University Press, 2005.

[27] C. J. Foot. *Atomic Physics*, section 6.3. Oxford University Press, 2005.

[28] F. Mandl. *Quantum Mechanics*, section 7.5. Wiley, 1992.

[29] A. M. Fox. *Quantum Optics*, sections 2.1.4 & 4.3. Oxford University Press, 2006.

5

Two-mode cavity QED II: results

In this chapter we apply the theory developed in chapter 4, performing two specific calculations. We compute second-order photon correlation functions for the non-driven mode of the cavity, and investigate interference effects known as *quantum beats* which appear in these. We also simulate the strong driving behaviour of the system and explain the results obtained by way of an analogy to a simpler model.

5.1 Numerical solution of the master equation

In general, a quantum master equation may be difficult or impossible to solve analytically. Therefore numerical solutions of the master equation are necessary to model the behaviour of the system. In this section we detail some of the considerations necessary when doing this type of modelling.

All the numerical results presented in the following sections, and indeed in later chapters of this thesis, were computed using programs written in the *Python* programming language [1]. Much use was made of the Python libraries *NumPy* [2, 3] and *SciPy* [4]: the former adds support for large, multi-dimensional arrays and matrices to the Python language, while the latter contains many algorithms and mathematical tools, in particular sparse matrix data structures and numerical integration tools. Several of the Python programs written were based on the methods used by Sze Tan's *quantum optics toolbox* for the *Matlab* programming language [5].

5.1.1 Dimensionless master equation

The floating point numbers used in computing have a mantissa of limited precision, and their magnitude is limited, due to the limited number of bits available. These limitations inevitably lead to accuracy problems (rounding errors, for example), particularly when adding two numbers that differ by many orders of magnitude. To avoid this problem, we rewrite the master equation so that all its terms are of a similar order of magnitude. We can construct a dimensionless master equation which satisfies these conditions by scaling (4.54) by the reciprocal of some parameter of the system which has the dimensions of a rate, that is, inverse seconds. Choosing to scale by $1/\gamma$, (4.54) gives

$$\frac{\mathrm{d}}{\mathrm{d}(\gamma t)}\rho = -\mathrm{i}\left[\frac{H_S}{\hbar\gamma}, \rho\right] + \frac{2\kappa}{\gamma}(\mathcal{D}[\hat{a}]\rho + \mathcal{D}[\hat{b}]\rho) + \sum_q \mathcal{D}[\hat{\Sigma}_q]\rho\,, \tag{5.1}$$

with

$$\frac{H_S}{\hbar\gamma} = \frac{\mathcal{E}}{\gamma}\left(\hat{a}^\dagger + \hat{a}\right) + \frac{g}{\gamma}\left(\hat{\Sigma}_0^\dagger \hat{a} + \hat{\Sigma}_0 \hat{a}^\dagger\right) + \frac{g}{\gamma}\left[\left(\frac{\hat{\Sigma}_{-1}^\dagger + \hat{\Sigma}_{+1}^\dagger}{\sqrt{2}}\right)\hat{b} + \left(\frac{\hat{\Sigma}_{-1} + \hat{\Sigma}_{+1}}{\sqrt{2}}\right)\hat{b}^\dagger\right] + \sum_{m_F=-F}^{F}\left(g_F m_F \frac{\mathcal{B}}{\gamma}\right)|g, m_F\rangle\langle g, m_F| + \sum_{m'_F=-F'}^{F'}\left(g'_F m'_F \frac{\mathcal{B}}{\gamma}\right)|e, m'_F\rangle\langle e, m'_F|\,, \tag{5.2}$$

where we have defined $\mathcal{B} = \mu_B B/\hbar$.

Another advantage of scaling by $1/\gamma$ is that we have reduced the number of parameters that determine the dynamics of the system. We now have four dimensionless parameters to consider: $\mathcal{E}/\gamma$, $\mathcal{B}/\gamma$, g/γ and κ/γ.

5.1.2 Fock space truncation

For a given set of parameters and a given driving field strength, the number of photons in a given cavity mode μ is unlikely to exceed some maximum number N_μ. Therefore it is clearly a good approximation to neglect all Fock states with a photon number larger than N_μ. This is referred to as truncating the Fock space of the cavity mode μ.

If, in our two-mode calculation, N_a and N_b are the maximum allowed photon numbers in the driven and non-driven cavity modes respectively, and N_A is the number of atomic states considered, then the Hilbert space of the atom-cavity system, $\mathcal{H} = \mathcal{H}_A \otimes \mathcal{H}_a \otimes \mathcal{H}_b$, will be $N_A(N_a+1)(N_b+1)$-dimensional. As we will see in the following section, solving a master equation in a Hilbert space of this dimensionality requires the solution of a set of $[N_A(N_a+1)(N_b+1)]^2$ coupled ordinary differential equations. For small N_a and N_b it is a straightforward numerical task to solve these equations, but the results may be affected by the absence of some relevant Fock states. For large N_a and N_b this task can become too difficult numerically to be worth pursuing. Therefore we must try to choose small enough N_a and N_b that the solution of the master equation will be straightforward, but not so small that the results are affected by the approximation.

5.1.3 Numerical modelling in Liouville space

The Liouvillian super-operator is a linear operator on Liouville space. Provided the Hilbert space of the system is finite-dimensional, then the density matrix can be written as an $N \times N$ matrix, with N the dimension of the Hilbert space. If the density matrix is instead written as a vector in which each element corresponds to an element of the $N \times N$ matrix, then the Liouvillian super-operator can be expressed as a square $N^2 \times N^2$ matrix. As a result, the form of the master equation (2.23) is preserved; we repeat it here for convenience:

$$\frac{\mathrm{d}}{\mathrm{d}t}\rho(t) = \mathcal{L}\rho(t)\,. \tag{5.3}$$

Given an initial condition $\rho(0)$, we can integrate the master equation numerically.

The steady state of the system is of course defined by

$$\dot{\rho}(\infty) = \mathcal{L}\rho(\infty) = 0\,, \tag{5.4}$$

where $\rho(\infty)$ is the steady state density matrix of the system. Finding the null space of the Liouvillian matrix yields the solution of this equation. The null space of a matrix can be computed by several methods, such as the singular value decomposition (SVD). When the null space is only one-dimensional we can employ the inverse power method, or transform (5.4) into an inhomogeneous equation. The latter can be done because $\mathrm{tr}(\rho) = 1$ at all times, which reduces the dimensionality of the problem by one. This means that $\mathcal{L}$ can be transformed into an $(N^2-1)\times(N^2-1)$ matrix; the transformation results in an inhomogeneous equation when applied to both sides of (5.4), and the null space (assuming it is one-dimensional) can be found by solving the system of linear equations numerically.

5.1.4 Second-order photon correlation functions

Using the quantum regression formula (2.67), we can evaluate the second-order photon correlation function (4.8) as

$$g^{(2)}_{\mu\nu}(\tau) = \frac{\left\langle \hat{\mu}^\dagger(0)\hat{\nu}^\dagger(\tau)\hat{\nu}(\tau)\hat{\mu}(0)\right\rangle}{\langle\hat{\mu}^\dagger\hat{\mu}\rangle\langle\hat{\nu}^\dagger\hat{\nu}\rangle_\tau} = \frac{1}{\langle\hat{\nu}^\dagger\hat{\nu}\rangle_\tau}\mathrm{tr}\left\{\hat{\nu}^\dagger\hat{\nu}\exp(\mathcal{L}\tau)\left[\frac{\hat{\mu}\rho(t_0)\hat{\mu}^\dagger}{\langle\hat{\mu}^\dagger\hat{\mu}\rangle}\right]\right\}, \tag{5.5}$$

where all expectation values are taken with respect to the density operator at some time t_0, $\rho(t_0)$, except for $\langle\hat{\nu}^\dagger\hat{\nu}\rangle_\tau = \mathrm{tr}[\hat{\nu}^\dagger\hat{\nu}\rho(t_0+\tau)]$. If we let $t_0\to\infty$, we obtain the steady state second-order photon correlation function; in this case it is clear that $\rho(t_0+\tau) = \rho(t_0)$, so we can drop the subscript τ from $\langle\hat{\nu}^\dagger\hat{\nu}\rangle_\tau$ and evaluate it using the same steady-state density matrix as for all the other expectation values. The collapsed density matrix $\hat{\mu}\rho(t_0)\hat{\mu}^\dagger$ has been normalised by $\langle\hat{\mu}^\dagger\hat{\mu}\rangle$ so that it has unit trace: this has numerical advantages, in that it prevents matrix elements from becoming too small during computation, but is not strictly speaking necessary.

If we define

$$\rho_{\mu\mu^\dagger}(\tau) = \exp(\mathcal{L}\tau)\left[\frac{\hat{\mu}\rho(t_0)\hat{\mu}^\dagger}{\langle\hat{\mu}^\dagger\hat{\mu}\rangle}\right], \tag{5.6}$$

it is clear that

$$\rho_{\mu\mu^\dagger}(0) = \left[\frac{\hat{\mu}\rho(t_0)\hat{\mu}^\dagger}{\langle\hat{\mu}^\dagger\hat{\mu}\rangle}\right], \tag{5.7}$$

and

$$\frac{\mathrm{d}}{\mathrm{d}\tau}\rho_{\mu\mu^\dagger}(\tau) = \mathcal{L}\exp(\mathcal{L}\tau)\left[\frac{\hat{\mu}\rho(t_0)\hat{\mu}^\dagger}{\langle\hat{\mu}^\dagger\hat{\mu}\rangle}\right] = \mathcal{L}\rho_{\mu\mu^\dagger}(\tau)\,. \tag{5.8}$$

Thus, we have a first-order differential equation for $\rho_{\mu\mu^\dagger}$ with initial condition (5.7). This is used to compute the second-order photon correlation function using numerical integration.

From (5.5) and (5.6), the second-order photon correlation function is given in terms of $\rho_{\mu\mu^\dagger}$ by

$$g^{(2)}_{\mu\nu}(\tau) = \frac{1}{\langle \hat{v}^\dagger \hat{v} \rangle_\tau} \mathrm{tr}\left\{ \hat{v}^\dagger \hat{v} \rho_{\mu\mu^\dagger}(\tau) \right\} . \tag{5.9}$$

Note that all these results generalise quite simply to the case of a time-dependent generator (as introduced in section 2.2.3): (5.8) becomes

$$\frac{\mathrm{d}}{\mathrm{d}\tau} \rho_{\mu\mu^\dagger}(\tau) = \mathcal{L}(t_0 + \tau) \rho_{\mu\mu^\dagger}(\tau) . \tag{5.10}$$

The formula (5.9) makes the physical interpretation of the correlation function clear: if we refer to the detection of a photon of the μ mode at time t_0 as event E_1, and detection of a photon in the ν mode at time $t_0 + \tau$ as event E_2, then the correlation function is equivalent to $P(E_2|E_1)/P(E_2)$.

5.2 Atom-cavity coupling strength & choice of parameters

The relative strength of the atom-cavity coupling is characterised by three parameters: the cavity mode damping rate κ, the spontaneous emission rate γ, and the atom-cavity dipole coupling constant g. The interaction is said to be in the *strong coupling* regime when $g \gg (\kappa, \gamma)$, and in the *weak coupling* regime when $g \ll (\kappa, \gamma)$. In the case of strong coupling, where the atom-cavity coupling rate is larger than the decay rates, the interaction between the photons in the cavity mode and the atom is a reversible process: a photon emitted by the atom may be reabsorbed before it is lost from the cavity. On the other hand, in the case of weak coupling, the decay rates κ and γ dominate; photons are lost from the system (either by leakage through the cavity mirrors or by spontaneous emission) at a rate greater than the characteristic rate g of the atom-cavity interaction. A typical emission of light by the atom in the cavity is therefore irreversible.

The strong coupling regime is very interesting; it has been the subject of many theoretical investigations and experimental measurements. However, the experiment of Norris et al. [6], which we are in principle modelling, is not operated in the strong coupling regime, but in an intermediate regime where the characteristic parameters of the system are all of the same order of magnitude, $g \sim (\kappa, \gamma)$. We therefore choose for our simulations parameters based on, but not identical to, those used by Barberis-Blostein et al. in their recent work [7]. Our model is too simple to seek quantitative agreement with experiment: the primary deficiency is that we consider only a single atom, while the experiment deals with an atomic beam. Thus, we are not going to worry overly about choosing parameters that agree exactly with experimental values. The parameters we have chosen to use for all calculations in this chapter, unless stated otherwise, are given in table 5.1.

The parameters w and v in table 5.1 relate to later simulations, in which we will allow the atom to move through the cavity mode waist, resulting in a time-varying $g(t)$. The beam waist is $w = 56\,\mu\mathrm{m}$. The velocity of the atom is also given in metres, because we will be

Parameter	Description	Value
$\mathcal{B}/\gamma$	Magnetic field parameter	1
g/γ	Atom-cavity dipole coupling constant	1/4
κ/γ	Cavity mode damping rate	1/2
w	Cavity waist	56×10^{-6} m
v	Velocity of atom	$15\,\mathrm{ms}^{-1}/(2\pi \times 6 \times 10^6\,\mathrm{Hz})$

TABLE 5.1: Parameters used in calculations pertaining to the two-mode cavity QED system. Note that all rates are divided by γ, such that they become dimensionless (see section 5.1.1).

integrating with respect to the dimensionless "time" parameter γt: the velocity parameter is $v = 15\,\mathrm{ms}^{-1}/(2\pi \times 6\,\mathrm{MHz})$, which corresponds to an atom with spontaneous emission rate $\gamma = 2\pi \times 6\,\mathrm{MHz}$ moving at a velocity of $v = 15\,\mathrm{ms}^{-1}$. The parameter g is the *maximum* dipole coupling strength, taken with respect to the transitions with the largest Clebsch-Gordan coefficients in equations (4.37) and (4.38): the $m_F = -3 \leftrightarrow m'_F = -4$ and $m_F = 3 \leftrightarrow m'_F = 4$ transitions. The coupling strength for the central $m_F = 0 \leftrightarrow m'_F = 0$ transition will be $\sqrt{4/7}g$. The driving strength $\mathcal{E}/\gamma$ remains an adjustable parameter.

5.3 Semiclassical treatment of the driven mode

We have already noted that the a-mode of the cavity is driven by an external field; photons present in the b-mode, on the other hand, are due entirely to the interaction with the atom. In the case where the cavity is strongly driven and the damping rate κ of the cavity small in comparison with $\mathcal{E}$, the number of photons in the driven mode will be large. Also, with the parameters listed in table 5.1, we are not in the strong coupling regime where single photons have significant interactions with the atom. In light of these facts, we suspect that we can approximate the driven mode of the cavity as a coherent classical field.

We turn now to the details of this semiclassical approximation. We replace the cavity mode operators with mean field amplitudes,

$$\hat{a} \to \langle \hat{a} \rangle = \alpha\,, \quad \hat{a}^\dagger \to \langle \hat{a}^\dagger \rangle = \alpha^*\,. \tag{5.11}$$

From equations (5.1) and (5.2) we obtain the modified master equation

$$\frac{\mathrm{d}}{\mathrm{d}(\gamma t)}\rho = -\mathrm{i}\left[\frac{H_S}{\hbar\gamma}, \rho\right] + \frac{2\kappa}{\gamma}\mathcal{D}[\hat{b}]\rho + \sum_q \mathcal{D}[\hat{\Sigma}_q]\rho\,, \tag{5.12}$$

and Hamiltonian

$$\begin{aligned}\frac{H_S}{\hbar\gamma} =& \frac{g}{\gamma}\left(\alpha\hat{\Sigma}_0^\dagger + \alpha^*\hat{\Sigma}_0\right) + \frac{g}{\gamma}\left[\left(\frac{\hat{\Sigma}_{-1}^\dagger + \hat{\Sigma}_{+1}^\dagger}{\sqrt{2}}\right)\hat{b} + \left(\frac{\hat{\Sigma}_{-1} + \hat{\Sigma}_{+1}}{\sqrt{2}}\right)\hat{b}^\dagger\right] \\ &+ \sum_{m_F=-F}^{F}\left(g_F m_F \frac{\mathcal{B}}{\gamma}\right)|g, m_F\rangle\langle g, m_F| + \sum_{m'_F=-F'}^{F'}\left(g'_F m'_F \frac{\mathcal{B}}{\gamma}\right)|e, m'_F\rangle\langle e, m'_F|\,,\end{aligned} \tag{5.13}$$

in which the driven mode a is treated semiclassically. We also need to find an equation of

motion for α, including, in particular, its dependence on the driving strength $\mathcal{E}$, our sole adjustable parameter. In the absence of an atom in the cavity, the master equation is given by

$$\dot{\rho} \equiv \frac{\mathrm{d}}{\mathrm{d}(\gamma t)}\rho = -\mathrm{i}\left[\frac{\mathcal{E}}{\gamma}(\hat{a}^\dagger + \hat{a}), \rho\right] + \frac{2\kappa}{\gamma}\left(\hat{a}\rho\hat{a}^\dagger - \frac{1}{2}\hat{a}^\dagger\hat{a}\rho - \frac{1}{2}\rho\hat{a}^\dagger\hat{a}\right). \tag{5.14}$$

From this, we can obtain the equation of motion for the mean-field amplitude with no atom in the cavity,

$$\begin{aligned}\frac{\mathrm{d}}{\mathrm{d}(\gamma t)}\langle\hat{a}\rangle &= \mathrm{tr}(\hat{a}\dot{\rho}) \\ &= -\mathrm{i}\frac{\mathcal{E}}{\gamma}\mathrm{tr}\{\hat{a}[\hat{a}^\dagger + \hat{a}, \rho]\} + \frac{2\kappa}{\gamma}\mathrm{tr}\left[\hat{a}\left(\hat{a}\rho\hat{a}^\dagger - \frac{1}{2}\hat{a}^\dagger\hat{a}\rho - \frac{1}{2}\rho\hat{a}^\dagger\hat{a}\right)\right] \\ &= -\mathrm{i}\frac{\mathcal{E}}{\gamma} - \frac{\kappa}{\gamma}\mathrm{tr}(\hat{a}\rho)\,,\end{aligned} \tag{5.15}$$

where we have made ample use of the cyclic property of the trace. In order to take into account the back-action of the atom on the field, we use the full master equation (5.1) and Hamiltonian (5.2), instead of (5.14). The resulting equation of motion for the mean-field amplitude is

$$\frac{\mathrm{d}}{\mathrm{d}(\gamma t)}\langle\hat{a}\rangle = -\mathrm{i}\left[\frac{\mathcal{E}}{\gamma} + \frac{g}{\gamma}\mathrm{tr}(\hat{\Sigma}_0\rho)\right] - \frac{\kappa}{\gamma}\mathrm{tr}(\hat{a}\rho)\,, \tag{5.16}$$

giving the equation of motion for $\alpha = \langle\hat{a}\rangle$,

$$\dot{\alpha} = -\mathrm{i}\left(\frac{\mathcal{E}}{\gamma} + \frac{g}{\gamma}\left\langle\hat{\Sigma}_0\right\rangle\right) - \frac{\kappa}{\gamma}\alpha\,. \tag{5.17}$$

The equation of motion for α^* is the Hermitian conjugate of the above,

$$\dot{\alpha}^* = \mathrm{i}\left(\frac{\mathcal{E}}{\gamma} + \frac{g}{\gamma}\left\langle\hat{\Sigma}_0^\dagger\right\rangle\right) - \frac{\kappa}{\gamma}\alpha^*\,. \tag{5.18}$$

Now, suppose it is the case that the state of the system, and in particular the expectation value $\langle\hat{\Sigma}_0\rangle$, varies slowly compared with the damping rate κ/γ. If this is the case, α will follow the state of the system adiabatically, remaining in an instantaneous "steady state" which only depends on the state of the system by way of a dependence on $\langle\hat{\Sigma}_0\rangle$. In this case we have

$$\alpha = -\mathrm{i}\frac{\mathcal{E} + g\left\langle\hat{\Sigma}_0\right\rangle}{\kappa}\,. \tag{5.19}$$

Here we are basically neglecting the small amount time it takes for the mean-field amplitude α to relax towards the steady state following a change in the expectation value $\langle\hat{\Sigma}_0\rangle$.

We see that we now have three slightly different models of the system:

1. a full quantum model,

2. a model with a semiclassical driven mode,

3. a model in which the driving mode is semiclassical and adiabatically follows the state of the system.

In order to characterise the difference between the three different treatments, we will examine a quantity of interest calculated using each of the three different models. The quantity of interest is the second-order photon correlation function for the non-driven mode b.

The self-correlation of the non-driven mode is calculated in the manner given in section 5.1.4. We specialise the formula (5.5) to the case of the steady state, obtaining

$$\begin{aligned} g^{(2)}_{bb}(\tau) &= \frac{\left\langle \hat{b}^\dagger(0)\hat{b}^\dagger(\tau)\hat{b}(\tau)\hat{b}(0)\right\rangle_{\mathrm{ss}}}{\left\langle \hat{b}^\dagger\hat{b}\right\rangle_{\mathrm{ss}}\left\langle \hat{b}^\dagger\hat{b}\right\rangle_{\mathrm{ss}}} \\ &= \frac{1}{\left\langle \hat{b}^\dagger\hat{b}\right\rangle_{\mathrm{ss}}}\mathrm{tr}\left\{\hat{b}^\dagger\hat{b}\exp(\mathcal{L}\tau)\left[\frac{\hat{b}\rho_{\mathrm{ss}}\hat{b}^\dagger}{\left\langle \hat{b}^\dagger\hat{b}\right\rangle_{\mathrm{ss}}}\right]\right\}. \end{aligned} \tag{5.20}$$

The steady state density matrix used in this calculation could be obtained, for the case of the full quantum treatment, by finding the kernel of the Liouvillian matrix. However this method is not as suitable when we also have to take into account a semiclassical cavity mode, which depends on some expectation value such as $\langle\hat{\Sigma}_0\rangle$. Consider how we might deal with the numerical issues surrounding case 2 in the list above. The equations of motion for α and α^* are still linear, so we could write down a matrix which would generate the evolution of α and α^* as well as the matrix elements of ρ, but we have not chosen this method. Instead, we have chosen the simple and effective, if somewhat inelegant, method of simply integrating the coupled equations of motion for α, α^*, and ρ for a long period of time, until an approximately steady state has been reached. The same technique is used for case 3.

In order to compare the three variations of our model detailed above more directly, we have integrated all three in similar fashion. For cases 1 and 2, we have used the common fourth-order Runge-Kutta (RK4) numerical integration algorithm. For case 3, in which the Liouvillian $\mathcal{L}$ for the quantum part of the system is a function of the mean-field amplitudes, we have used a modified RK4 scheme in which $\mathcal{L}(\alpha,\alpha^*)$ is only computed once per time-step (at the beginning of each time-step); this is justified by the assumption underlying the adiabatic approximation: α varies slowly. In all three cases we integrate the master equation over a time period $t_f - t_i = 50\gamma^{-1}$. The results are shown in Figs. 5.1 and 5.2.

5.4 Quantum beats

All the correlation functions shown in Fig. 5.2 show prominent oscillations, which are due to *quantum beats*. In order to elucidate, qualitatively, the cause of these oscillations, we consider, following Barberis-Blostein et al. [7], a subset of the allowed electric dipole transitions for the $F = 3$ to $F' = 4$ transition we are modelling.[1] The transitions we are going to consider are shown in Fig. 5.3a: they are the transitions which couple the six central hyperfine levels, with magnetic quantum numbers $m_F = 0, \pm 1$. As is shown in the figure, the applied magnetic field

[1] Refer back to section 4.3.2, in particular Fig. 4.2, for information about these transitions.

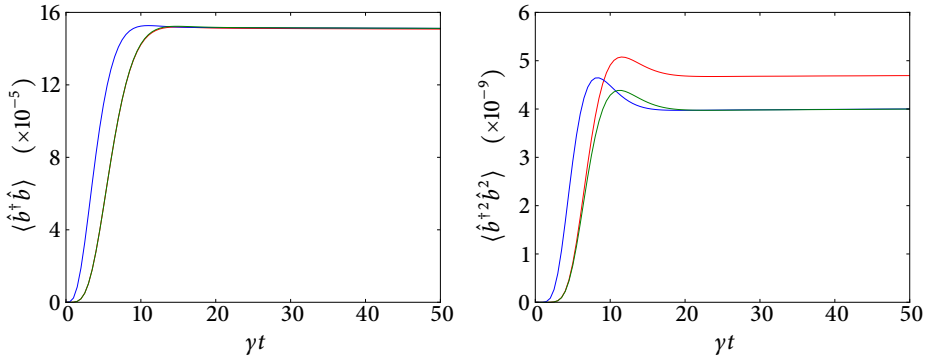

FIGURE 5.1: Comparison of quantum (red), semiclassical (green) and semiclassical with adiabatic following (blue) models. These results were obtained using the parameters in table 5.1, with $\mathcal{E}/\gamma = 0.1$.

creates ground and excited state frequency detunings, $\pm\delta_g$ and $\pm\delta_e$ respectively, between the $m_F = \pm 1$ and $m_F = 0$ magnetic sublevels. From our consideration of the Zeeman energy shift, these detunings are given by

$$\delta_g = g_F \mu_B B\,, \quad \delta_e = g'_F \mu_B B\,. \tag{5.21}$$

We will consider two principle processes by which the atom may emit a photon into the non-driven cavity mode. These processes are illustrated in Figs. 5.3b and 5.3c, and will be explained in further detail below.[2]

We consider an initial condition in which optical pumping has prepared the atom in the state $|g, 0\rangle$. The interaction with the driven cavity mode then excites the atom to the $|e, 0\rangle$ state. From the excited state, the atom may decay back to the ground state through the emission of a π, σ^+ or σ_- photon. If a π photon is emitted, it is added to the driven mode and we are not terribly interested. If, on the other hand, a σ_+ or σ_- photon is emitted, it will populate the non-driven b-mode. When this photon is detected,[3] the atom ends up in the superposition state

$$c_{g,-1}\,|g, -1\rangle + c_{g,1}\,|g, 1\rangle\ . \tag{5.22}$$

This is because photons are detected in the "x-y basis" (corresponding to the linear polarisation of the b-mode), so the measurement does not tell us anything about the helicity of the photon that has been detected. It is not necessary for the purposes of this discussion to evaluate the coefficients $c_{g,\pm 1}$, but they are of course subject to the constraint $|c_{g,-1}|^2 + |c_{g,1}|^2 = 1$. This process is illustrated in Fig. 5.3b.

After the emission of the first σ-polarised photon described above, the atom continues to interact with the driven mode of the cavity. The atom once again becomes excited by way of its interaction with the driven mode, and, starting from the prepared ground state superposition

[2]The following argument is adapted from the work of Barberis-Blostein et al. [7].

[3]With the cavity decay rate κ comparable to the atom-cavity coupling g, it is probable that the photon will leak from the cavity and be detected before it can be reabsorbed by the atom.

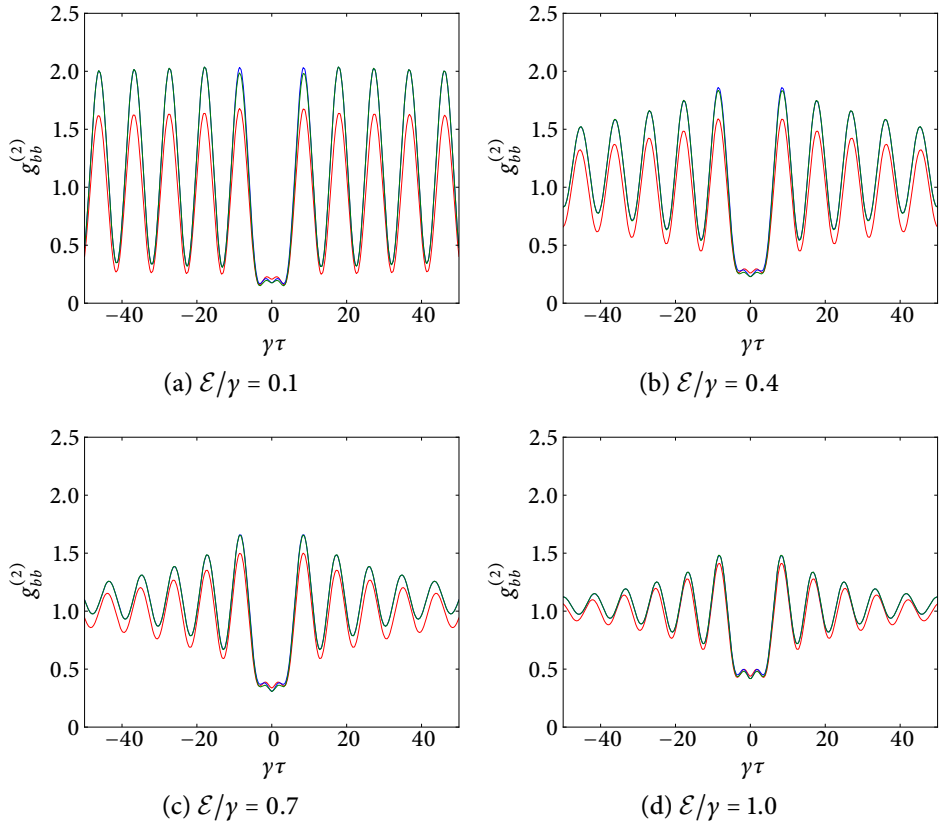

(a) $\mathcal{E}/\gamma = 0.1$ (b) $\mathcal{E}/\gamma = 0.4$

(c) $\mathcal{E}/\gamma = 0.7$ (d) $\mathcal{E}/\gamma = 1.0$

FIGURE 5.2: Comparison of second-order photon correlation functions obtained using quantum (red), semiclassical (green) and semiclassical with adiabatic following (blue) models. These results were obtained using the parameters in table 5.1, for various different driving field strengths. Here the atom is held to be stationary in the centre of the cavity, and the master equation is integrated over a time period $t_f - t_i = 50\gamma^{-1}$. For the quantum simulation, the driven a-mode is truncated at the 10-photon level; for all three simulations, the non-driven b-mode is truncated at the 3-photon level.

(5.22), ends up in the excited state superposition

$$c_{e,-1}\,|e,-1\rangle + c_{e,1}\,|e,1\rangle\ . \tag{5.23}$$

From here, the atom can return to its original state $|g,0\rangle$ by emitting a second photon into the non-driven b-mode. This process is illustrated in Fig. 5.3c.

The conditional detection of both the non-driven photons emitted in the processes described above is equivalent to a measurement of the second-order photon correlation function $g^{(2)}_{bb}$. The two photons necessary for this measurement may be emitted into the non-driven mode by either of two indistinguishable paths: $|g,0\rangle \to |e,0\rangle \to |g,-1\rangle \to |e,-1\rangle \to |g,0\rangle$, and $|g,0\rangle \to |e,0\rangle \to |g,1\rangle \to |e,1\rangle \to |g,0\rangle$. We denote the phase factor along the former path ϕ_{-1}, while the phase factor gained along the latter path is denoted ϕ_{+1}. Due to the detunings δ_g and δ_e created by the applied magnetic field, the phase change along each of the two paths is different ($\phi_{-1} \neq \phi_{+1}$). Interference between the two paths therefore results in oscillations in $g^{(2)}_{bb}$: quantum beats.

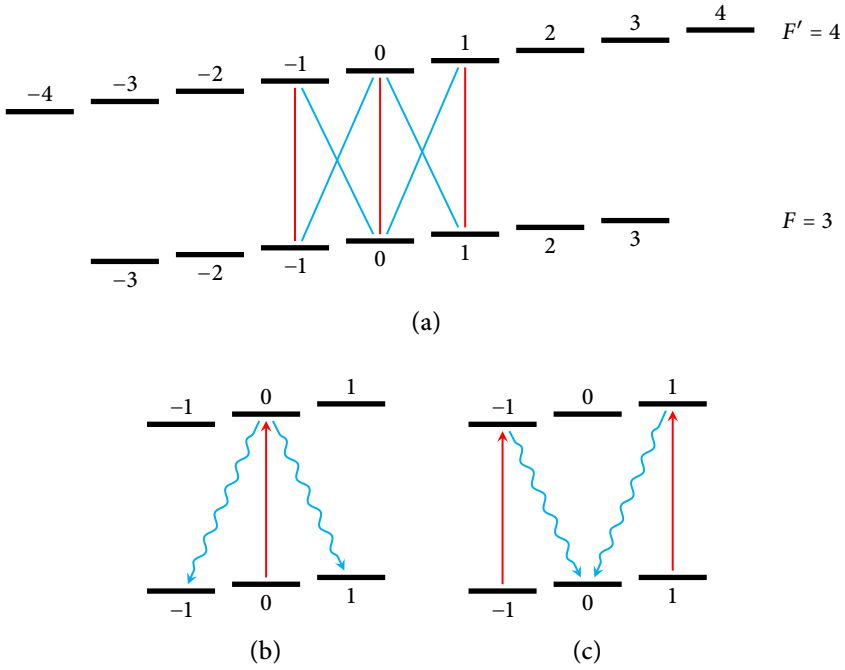

FIGURE 5.3: (a) Atomic energy level structure, with π transitions shown in red, and σ transitions shown in blue. The applied magnetic field creates ground and excited state frequency detunings, $\pm\delta_g$ and $\pm\delta_e$ respectively, between the $m_F = \pm 1$ and $m_F = 0$ magnetic sublevels. (b) & (c) Two processes by which a photon may be emitted by the atom into the non-driven cavity mode.

The difference between the phase factors gained along each of the two paths can also be seen as a consequence of the atom's Larmor precession [8, 9] in the applied magnetic field. Note that, as we can see in Fig. 5.2, the quantum beats are suppressed around $\gamma\tau = 0$. This is due to the photon antibunching of single-atom resonance fluorescence [10–12].

Of course, the qualitative explanation of the origin of quantum beats presented in this section, in which we considered only six atomic states out of a total of sixteen, does not describe the whole picture. It does, however, capture the essential physics. All the calculations relating to the two-mode cavity QED system presented in this chapter take into account the full atomic level structure.

5.4.1 Quantum beats with a moving atom

Our model of the two-mode cavity QED system can be modified to take into account the motion of the single atom through the cavity. When we derived the Hamiltonian for the interaction between the atom and the radiation field in section 3.1.3, we noted that the dipole coupling constant in reality depends on the position of the atom. When considering a stationary atom (as one does, for example, in the Jaynes-Cummings model), one suppresses this dependence, but here we wish to restore it. The master equation (5.1) remains the same, while the only change to the Hamiltonian (5.2) is that we replace the stationary g with $g(\mathbf{R})$, which includes the position dependence.

The position dependence we are to include is fairly simple. Say the cavity axis is oriented

in the z direction. The field within the cavity has a Gaussian profile, so its amplitude falls off radially from the centre of the beam, going as $\exp(-r^2/w^2)$. The atom traverses the cavity radially (perpendicular to the z direction), at an antinode of the cavity mode standing wave, so we have a position-dependent atom-cavity coupling,

$$g(r) = g_0 \exp\left(-\frac{r^2}{w^2}\right), \tag{5.24}$$

where r is the radial distance from the optic axis of the cavity, and w is the cavity waist, given in table 5.1 as $w = 56\,\mu$m. The parameter g_0 is the maximum atom-cavity coupling strength; its value is equal to that given for the coupling strength in table 5.1: $g_0/\gamma = 1/4$. The radial location r of the atom is time-dependent, and $\dot{r} = v$. Thus the coupling strength may be considered to depend on time,

$$g(t) = g_0 \exp\left(-\frac{r(t)^2}{w^2}\right). \tag{5.25}$$

This result is substituted into (5.2) in place of g, yielding a time-dependent Hamiltonian, and thus a time-dependent Liouvillian $\mathcal{L}(t)$.

In the case of a time-dependent coupling, we can still treat the driven mode semiclassically, substituting (5.25) into (5.13). In view of our previous success with the approximation of allowing the mean field amplitude α to adiabatically follow the state of the system, we use this technique here, obtaining

$$\alpha = -\mathrm{i}\frac{\mathcal{E} + g(t)\left\langle\hat{\Sigma}_0\right\rangle}{\kappa}. \tag{5.26}$$

We integrate the resulting equation of motion for a time period $t_i \le t \le t_f$, where $t_f - t_i = 2d/v$. The position of the atom is given by $r(t) = -d + vt$; thus the atom moves, over the period of the integration, from $r = -d$ to $r = d$. Ideally we would let $d \to \infty$, but this is numerically impossible. Instead, we choose $d = 2w$, so that $g(r = \pm d)$ is very small.

During the aforementioned integration we take a number, N, of regularly-spaced samples of the system state. For each of these sampled states, we compute an unnormalised second-order photon correlation function,

$$G^{(2)}_{bb}(t_{0,i}, \tau) = \left\langle \hat{b}^\dagger(t_{0,i})\hat{b}^\dagger(t_{0,i}+\tau)\hat{b}(t_{0,i}+\tau)\hat{b}(t_{0,i})\right\rangle, \tag{5.27}$$

where $t_{0,i}$ is the time at which the particular sample was taken. Then by applying the quantum regression formula, we find that we can compute the unnormalised correlation function using

$$G^{(2)}_{bb}(t_{0,i}, \tau) = \mathrm{tr}\{\hat{b}^\dagger\hat{b}\bar{\rho}_{bb^\dagger,i}(\tau)\}, \tag{5.28}$$

where $\bar{\rho}_{bb^\dagger,i}(\tau)$ has the equation of motion

$$\frac{\mathrm{d}}{\mathrm{d}\tau}\bar{\rho}_{bb^\dagger,i}(\tau) = \mathcal{L}(t_{0,i}+\tau)\bar{\rho}_{bb^\dagger,i}(\tau)\,, \tag{5.29}$$

with initial condition

$$\bar{\rho}_{bb^\dagger,i}(0) = \hat{b}\rho(t_{0,i})\hat{b}^\dagger\,. \tag{5.30}$$

We also define the quantities

$$\overline{G^{(2)}_{bb}(\tau)} \equiv \frac{1}{N}\sum_i G^{(2)}_{bb}(t_{0,i},\tau) \approx \frac{1}{t_f - t_i}\int_{t_i}^{t_f}\mathrm{d}t\, G^{(2)}_{bb}(t,\tau)\,, \tag{5.31}$$

and

$$\overline{\left\langle\hat{b}^\dagger\hat{b}\right\rangle} \equiv \frac{1}{N}\sum_i \left\langle\hat{b}^\dagger\hat{b}(t_{0,i})\right\rangle \approx \frac{1}{t_f - t_i}\int_{t_i}^{t_f}\mathrm{d}t\,\left\langle\hat{b}^\dagger\hat{b}(t)\right\rangle\,, \tag{5.32}$$

where N is the number of samples taken.

Suppose we consider our atom to be just one of many atoms which are to pass through the cavity. This is physically sensible given that real-world experiments of this type are performed using atomic beams. In the steady state, the normalised second-order correlation function $g^{(2)}_{bb}$ will be given by

$$\begin{aligned} g^{(2)}_{bb}(\tau) &= 1 + \frac{\int_{t_i}^{t_f}\mathrm{d}t\, G^{(2)}_{bb}(t,\tau)}{\left(\int_{t_i}^{t_f}\mathrm{d}t\,\left\langle\hat{b}^\dagger\hat{b}(t)\right\rangle\right)^2} \\ &= 1 + \overline{G^{(2)}_{bb}(\tau)}\Big/\left(\overline{\left\langle\hat{b}^\dagger\hat{b}\right\rangle}\right)^2\,. \end{aligned} \tag{5.33}$$

We have added 1 in the above expressions to ensure that $g^{(2)}_{bb}(\tau)$ tends to unity as $\tau\to\infty$. It would not do so otherwise, as eventually the atom leaves the cavity, but in an atomic beam experiment it would be replaced by another atom after some extended time period. When we add unity, we are adding the contribution from uncorrelated joint counts where the first count comes while one atom is in the interaction volume, and the second comes when the first atom has left and a second, independent atom is in the interaction volume. This approximation is valid assuming a sufficiently dilute atomic beam, so that there are never two or more atoms in the interaction volume simultaneously.

We have implicitly assumed throughout our derivation that multi-atom effects (arising from the real-world atomic beam mentioned above) can be neglected. This assumption requires the mean number of atoms in the cavity $\bar{N}_A$ to be much less than one (the appearance of an atom in the interaction volume is a Poisson process). In a simulation of a dilute atomic beam, such as that of Barberis-Blostein et al. [7], the amplitude of the fringes which appear in the normalised second-order photon correlation function due to quantum beating is scaled by

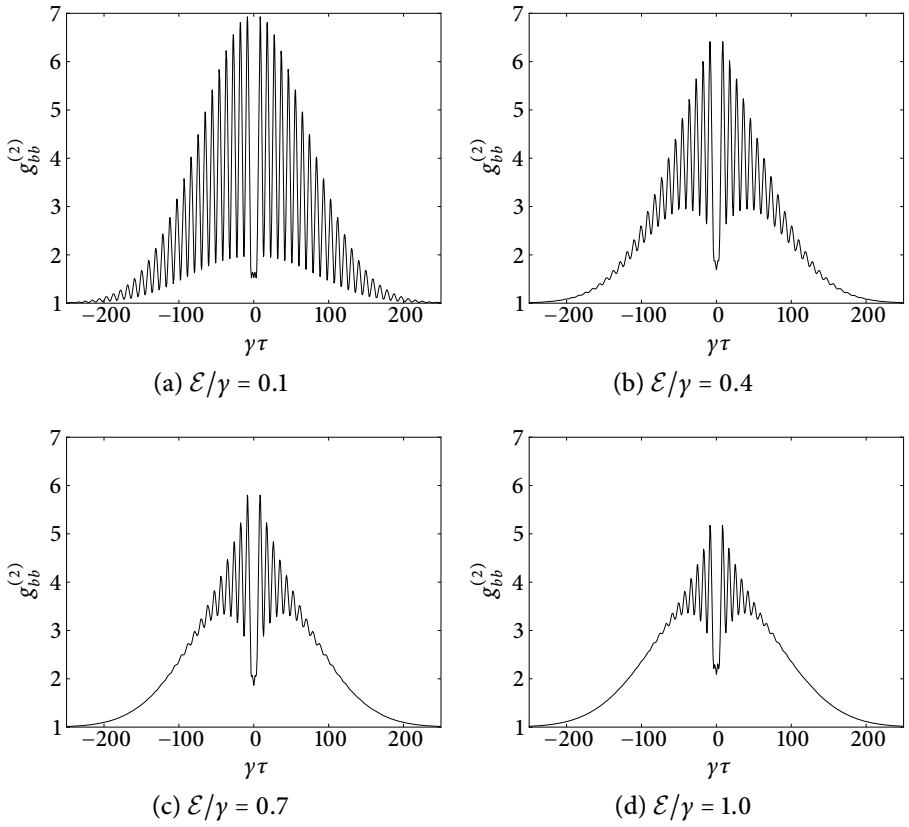

(a) $\mathcal{E}/\gamma = 0.1$ (b) $\mathcal{E}/\gamma = 0.4$

(c) $\mathcal{E}/\gamma = 0.7$ (d) $\mathcal{E}/\gamma = 1.0$

FIGURE 5.4: Second-order photon correlation functions, computed using the semiclassical approximation with adiabatic following. These results were obtained using the parameters in table 5.1, for various different driving field strengths. Here the atom moves through the cavity in the manner described in section 5.4.1. The non-driven b-mode is truncated at the 3-photon level.

$1/\bar{N}_A$. This scaling is neglected for the purposes of our single-atom simulation.

Second-order photon correlation functions obtained using (5.33) are displayed in Fig. 5.4. For each of the calculations shown, we have taken $N = 100$ samples of the system state.

5.5 Strong driving in two-mode cavity QED

In this section we investigate the dependence of the non-driven mode photon number, $\hat{b}^\dagger\hat{b}$, on the strength of the classical driving field $\mathcal{E}$.

In order to evaluate the mean photon number $\langle\hat{b}^\dagger\hat{b}\rangle$, we use the model in which the driven mode is treated semiclassically, defined by equations (5.12), (5.13) and (5.19). We use the parameters given in table 5.1, except we have $\mathcal{B}/\gamma = 0$, and the atom is held stationary in the centre of the cavity. For each driving field strength $\mathcal{E}$, we wish to compute the mean photon number in the steady state. As in the case of Fig. 5.2, we integrate the master equation over a time period $t_f - t_i = 50\gamma^{-1}$ to yield a pseudo-steady state which we use to evaluate $\langle\hat{b}^\dagger\hat{b}\rangle$. Figure 5.5 is the result of this calculation.

The main interesting feature of the dependence of the mean photon number on driving

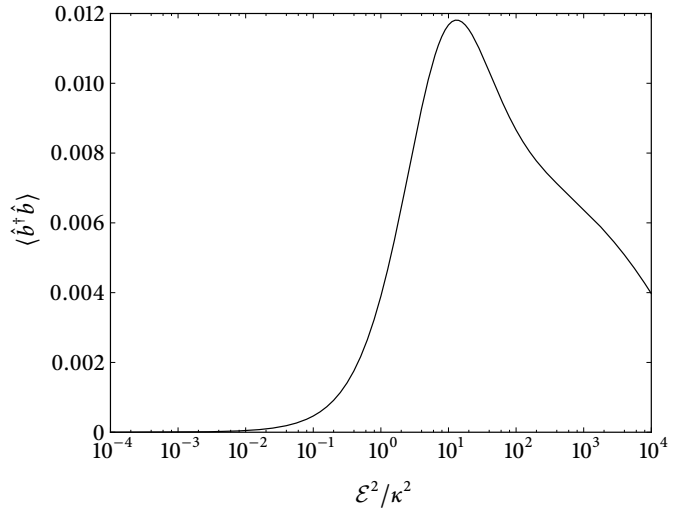

FIGURE 5.5: Mean photon number in the non-driven mode against $\mathcal{E}^2/\kappa^2$. These results were obtained using the parameters in table 5.1, except with $\mathcal{B}/\gamma = 0$. Here the atom is held stationary in the centre of the cavity, and the master equation is integrated over a time period $t_f - t_i = 50\gamma^{-1}$. The non-driven b-mode is truncated at the 3-photon level.

field strength, as shown in the figure, is how $\langle \hat{b}^\dagger \hat{b} \rangle$ peaks in the vicinity of $\mathcal{E}^2/\kappa^2 = 10^1$, and then turns over and decreases. This feature is what we now seek to explain.

5.5.1 Simplified model

The additional atomic energy levels involved in our model of the two-mode cavity QED system may obscure the essential physics involved in the strong driving behaviour of the mean photon number in the non-driven mode. In order to investigate this phenomenon in a less complicated context, we use a simple model derived from the Jaynes-Cummings model:

$$H = \hbar\mathcal{E}_\alpha(\hat{\sigma}_+ + \hat{\sigma}_-) + \hbar g_b(\hat{\sigma}_+\hat{b} + \hat{\sigma}_-\hat{b}^\dagger)\,, \tag{5.34}$$

with master equation

$$\dot{\rho} = \frac{1}{\mathrm{i}\hbar}[H, \rho] + 2\kappa\mathcal{D}[\hat{b}]\rho + \gamma\mathcal{D}[\hat{\sigma}_-]\rho\,. \tag{5.35}$$

$\mathcal{E}_\alpha$ is a real constant.

Similarly to the two-mode QED model, we have an atom – in this case a two-level atom – which is driven by a classical field. The atom interacts with an optical cavity mode, and photons may be lost from the system by way of spontaneous emission, or by leaking from the cavity.

The mean photon numbers for different values of $\mathcal{E}_\alpha$ are obtained by finding the kernel of the Liouvillian by direct numerical calculation; the resulting steady state density matrix yields the expectation values. The parameters used are similar to those in table 5.1: $g_b/\gamma = 1/4$ and $\kappa/\gamma = 1/2$. The resulting curve showing $\langle \hat{b}^\dagger \hat{b} \rangle$ against driving field strength is presented in Fig. 5.6. It is clear that this model also exhibits the reduction in mean photon number at high driving field strength observed in Fig. 5.5. Explaining this phenomenon in the context of the

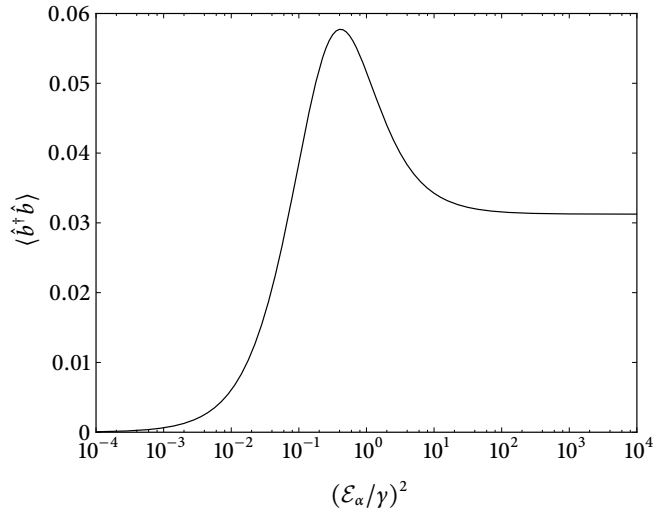

FIGURE 5.6: Steady state mean photon number in the non-driven mode against $(\mathcal{E}_\alpha/\gamma)^2$, for the simplified model. These results were obtained using the parameters: $g_b/\gamma = 1/4$, $\kappa/\gamma = 1/2$. The cavity mode is truncated at the 3-photon level. The steady state has been computed by direct numerical calculation.

simplified model may lead us to an explanation in the context of two-mode cavity QED.

5.5.2 Explanation of the strong driving behaviour

Consider a two-level atom which is driven by a periodic classical field, such as the atom described by (5.34) with the coupling to the cavity (and the spontaneous emission) neglected. The state vector describing the two-level atom can be written

$$|\psi\rangle = c_g\,|g\rangle + c_e\,|e\rangle\ . \tag{5.36}$$

We are interested in the effect of the driving Hamiltonian $H_{\mathcal{E}} = \hbar\mathcal{E}_\alpha(\hat{\sigma}_+ + \hat{\sigma}_-)$ on this state, so from the time-dependent Schrödinger equation,

$$\mathrm{i}\hbar\frac{\mathrm{d}}{\mathrm{d}t}\,|\psi\rangle = H_{\mathcal{E}}\,|\psi\rangle\ , \tag{5.37}$$

we obtain

$$\dot{c}_g(t) = -\mathrm{i}\mathcal{E}_\alpha c_e(t)\,, \tag{5.38a}$$
$$\dot{c}_e(t) = -\mathrm{i}\mathcal{E}_\alpha c_g(t)\,. \tag{5.38b}$$

If the atom is in the ground state at time $t = 0$, so that $c_g(0) = 1$ and $c_e(0) = 0$, the solutions of the above equations are

$$c_g(t) = \cos(\mathcal{E}_\alpha t)\,, \tag{5.39a}$$
$$c_e(t) = -\mathrm{i}\sin(\mathcal{E}_\alpha t)\,. \tag{5.39b}$$

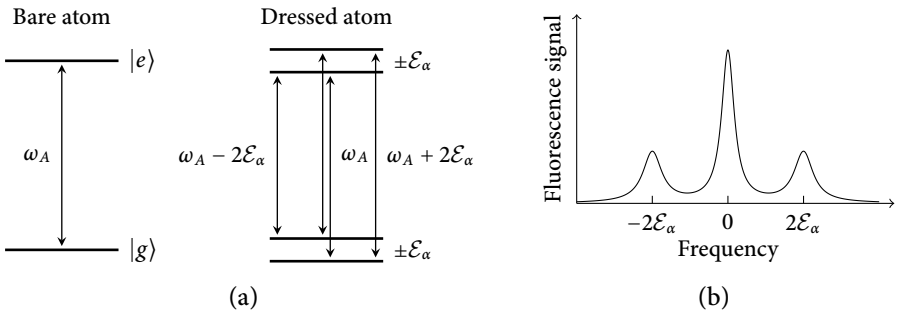

FIGURE 5.7: (a) When a two-level atom interacts with an intense resonant light field, the AC Stark effect splits the bare atom states into doublets separated by the Rabi frequency $2\mathcal{E}_\alpha$. This results in three emission lines, at frequencies ω_A, $\omega_A \pm 2\mathcal{E}_\alpha$. (b) The Mollow triplet spectrum which results from the dressing of the atom states.

These equations describe Rabi oscillations[4] with Rabi frequency $\Omega_R = 2\mathcal{E}_\alpha$. These oscillations can be interpreted in terms of dressed atoms [14, 15]: in the presence of an intense resonant light field, the AC Stark effect splits the bare atom states into doublets separated by the Rabi frequency, as shown in Fig. 5.7a. Transitions between the dressed atom states lead to three emission lines at frequencies ω_A, $\omega_A \pm 2\mathcal{E}_\alpha$. The fluorescence spectrum[5] of an atom driven in this way is of course the well-known Mollow triplet [16, 17], in which the coherent oscillations of the atomic state beat with the fundamental transition frequency to produce side bands in the emission spectrum at $\omega_A \pm \Omega_R$.

When $\mathcal{E}_\alpha$ is sufficiently large, the side bands in the Mollow triplet spectrum will lie outside the cavity linewidth. Consider a driven cavity, described by the master equation

$$\dot{\rho} = \frac{1}{\mathrm{i}\hbar}\left[\mathcal{E}_c(\hat{b}^\dagger + \hat{b}) + \delta\hat{b}^\dagger\hat{b}, \rho\right] + 2\kappa\mathcal{D}[\hat{b}]\rho\,, \tag{5.40}$$

where δ represents a detuning of the driving laser from resonance with the cavity. This master equation yields the steady state expectation values

$$\langle\hat{b}\rangle_{\mathrm{ss}} = -\mathrm{i}\frac{\mathcal{E}_c}{\kappa + \mathrm{i}\delta}\,, \quad \langle\hat{b}^\dagger\rangle_{\mathrm{ss}} = \mathrm{i}\frac{\mathcal{E}_c}{\kappa - \mathrm{i}\delta}\,, \tag{5.41}$$

and

$$\left\langle\hat{b}^\dagger\hat{b}\right\rangle_{\mathrm{ss}} = -\mathrm{i}\frac{\mathcal{E}_c}{2\kappa}\left(\langle\hat{b}^\dagger\rangle_{\mathrm{ss}} - \langle\hat{b}\rangle_{\mathrm{ss}}\right) = \frac{{\mathcal{E}_c}^2}{\kappa^2 + \delta^2}\,, \tag{5.42}$$

illustrating a Lorentzian dependence on detuning.

Referring to the Mollow triplet spectrum shown in Fig. 5.7b, we see that the detuning of the side bands from resonance with the cavity will depend on $2\mathcal{E}_\alpha$. Thus, as $\mathcal{E}_\alpha$ increases, we except a Lorentzian drop-off, going approximately as $(\kappa^2 + 4{\mathcal{E}_\alpha}^2)^{-1}$, in the steady state mean

[4] See Fox [13] and references therein for an overview.

[5] When we introduced the Rabi oscillations, we neglected the atomic decay terms in the master equation for simplicity's sake; however, when speaking of transitions and fluorescence we must of course consider the decay terms, and the coupling of the atom to the cavity mode.

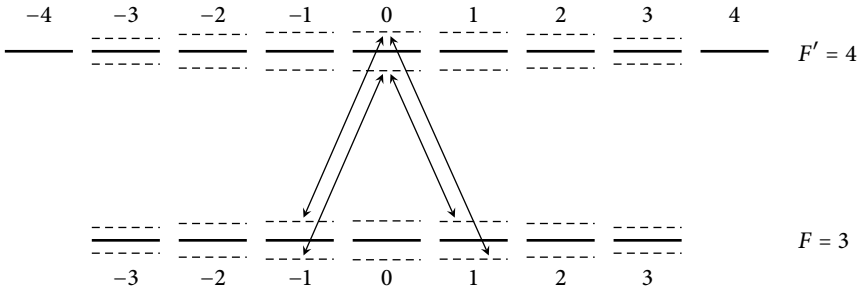

FIGURE 5.8: Atomic level structure for an $F = 3$ to $F' = 4$ transition, with splitting due to the AC Stark effect shown as dashed lines. The driven cavity mode interacts with the atom via π ($\Delta m_F = 0$) transitions, and the non-driven mode via σ ($\Delta m_F = \pm 1$) transitions. Example σ transitions between the dressed states are shown. The variation in the splittings is due to the various Clebsch-Gordan coefficients, written out in (4.38), which characterise the strength of the coupling between the atom and the driven mode.

photon number $\langle \hat{b}^\dagger \hat{b} \rangle_{\text{ss}}$. The central peak of the Mollow triplet will always remain within the cavity linewidth, and thus the steady state mean photon number will fall off to some fraction of its peak value as we increase $\mathcal{E}_\alpha$, but it will not get all the way to zero. This is approximately what is observed in Fig. 5.6.

The results obtained from the simplified model can be generalised to the two-mode cavity QED system, as shown in Fig. 5.8. The two rightmost σ transitions shown in the diagram lie outside the cavity linewidth, and contribute to sidebands analogous to those of the Mollow triplet. The various magnetic sublevels of the atom complicate the situation, but we can see the qualitative similarity between the two-mode cavity QED system and the simplified system of section 5.5.1. The transitions which lie outside the cavity linewidth are the primary cause of the strong driving behaviour that we observe in Fig. 5.5 – the decrease in mean photon number above a certain driving strength.

At very high driving strengths, the mean photon number shown in Fig. 5.5 continues to decrease (and will eventually reach zero), while the mean photon number in Fig. 5.6 settles down to a non-zero value. This is due to the variation in the splittings between the different m_F and m'_F states, caused by the differing Clebsch-Gordan coefficients in the atomic dipole transition operator $\hat{\Sigma}_0$. For a large enough driving field strength, the differing splittings will cause all possible σ transitions (such as those shown in Fig. 5.8) to lie outside the cavity linewidth, and the mean photon number in the non-driven mode will fall off to zero.

References

[1] G. van Rossum et al. Python Programming Language. `http://www.python.org`.

[2] T. E. Oliphant. Python for scientific computing. *Computing in Science and Engineering*, 9: 10–20, 2007.

[3] D. Ascher, P. F. Dubois, K. Hinsen, J. Hugunin, and T. Oliphant. Numerical Python. Technical Report UCRL-MA-128569, Lawrence Livermore National Laboratory, 2001. `http://numpy.scipy.org`.

[4] E. Jones, T. Oliphant, P. Peterson, et al. SciPy: Open source scientific tools for Python, 2001–. `http://www.scipy.org`.

[5] S. M. Tan. A computational toolbox for quantum and atomic optics. *Journal of Optics B: Quantum and Semiclassical Optics*, 1:424–432, 1999.

[6] D. G. Norris, L. A. Orozco, P. Barberis-Blostein, and H. J. Carmichael. Observation of ground-state quantum beats in atomic spontaneous emission. To be published in *Physical Review Letters*, 2010.

[7] P. Barberis-Blostein, D. G. Norris, L. A. Orozco, and H. J. Carmichael. From quantum feedback to probabilistic error correction: manipulation of quantum beats in cavity QED. *New Journal of Physics*, 12:023002, 2010.

[8] C. J. Foot. *Atomic Physics*, section 1.8. Oxford University Press, 2005.

[9] A. M. Fox. *Quantum Optics*, appendix E. Oxford University Press, 2006.

[10] H. J. Carmichael and D. F. Walls. Proposal for the measurement of the resonant Stark effect by photon correlation techniques. *Journal of Physics B*, 9:L43–L46, 1976.

[11] H. J. Carmichael and D. F. Walls. A quantum-mechanical master equation treatment of the dynamical Stark effect. *Journal of Physics B*, 9:1199–1219, 1976.

[12] L. Tian and H. J. Carmichael. Quantum trajectory simulations of two-state behavior in an optical cavity containing one atom. *Physical Review A*, 46:R6801–R6804, 1992.

[13] A. M. Fox. *Quantum Optics*, section 9.5. Oxford University Press, 2006.

[14] C. Cohen-Tannoudji. Atoms in strong resonant fields. In R. Balian, S. Haroche, and S. Liberman, editors, *Frontiers in laser spectroscopy*, volume 1, pages 3–104. Les Houches (session XXVII, 1975), North-Holland, 1977.

[15] C. Cohen-Tannoudji and S. Reynaud. Dressed-atom description of resonance fluorescence and absorption spectra of a multi-level atom in an intense laser beam. *Journal of Physics B*, 10:345–363, 1977.

[16] B. R. Mollow. Power spectrum of light scattered by two-level systems. *Physical Review*, 188:1969–1975, 1969.

[17] R. E. Grove, F. Y. Wu, and S. Ezekiel. Measurement of the spectrum of resonance fluorescence from a two-level atom in an intense monochromatic field. *Physical Review A*, 15:227–233, 1976.

6

Circuit QED I: review

6.1 Introduction to circuit quantum electrodynamics

Circuit quantum electrodynamics [1] is an implementation of a cavity QED system in a superconducting circuit, originally designed as an architecture for quantum computation [2]. In a circuit QED system, a superconducting Josephson junction qubit plays the role of an artificial atom. To complete the analogy with cavity QED, the qubit must be coupled to a quantised harmonic oscillator. In an electrical circuit, photons can be understood as the quantised excitations of any electromagnetic resonator, including the simple combination of an inductor and a capacitor (see appendix A). A solid-state electromagnetic resonator can therefore play the role of the cavity in the circuit QED system. Strong coupling (see section 5.2) was first achieved in circuit QED in 2004 [3, 4].

One particular implementation of circuit QED makes use of a *transmission line resonator*, which consists of a superconducting wire placed between two ground plates. Photons are confined in one dimension along the transmission line, and gaps in the wire, placed an integer number of half-wavelengths apart, are the "mirrors" used to form a microwave cavity. The rate at which photons enter and leave the cavity depends on the size and shape of the gaps. To form a circuit QED system, the electric fields of the transmission line resonator are coupled to a superconducting charge qubit, one of several different types of superconducting qubit which we will consider below.

In the past couple of years, two notable experiments have made use of the particular type of system described above [5, 6]. Both experiments involved the measurement of the characteristic $\sqrt{n}$ scaling of the spacing of the Jaynes-Cummings energy ladder (see Fig. 3.1). It has been pointed out that an observation of this scaling is sufficient to prove that the system is quantum mechanical in nature [7].

Consider the first "rung" of the Jaynes-Cummings ladder, depicted in Fig. 6.1a, which comprises two dressed states separated by an energy $2\hbar g$. Strong coupling, where the coupling g greatly exceeds the dissipation rates, allows transitions from the ground state to each of these dressed states to be resolved, resulting in the splitting of the cavity transmission peak into a doublet. This is known as vacuum Rabi splitting; the type of doublet spectrum which might be observed is illustrated in Fig. 6.1b. The vacuum Rabi spectrum for a single trapped atom in an optical Fabry-Pérot cavity has been observed by Boca et al. [8], with a separation between the peaks of less than ten peak linewidths. The analogous measurement of Bishop et al. [6] has a vacuum Rabi splitting, g/π, exceeding 260 linewidths. Another vacuum Rabi

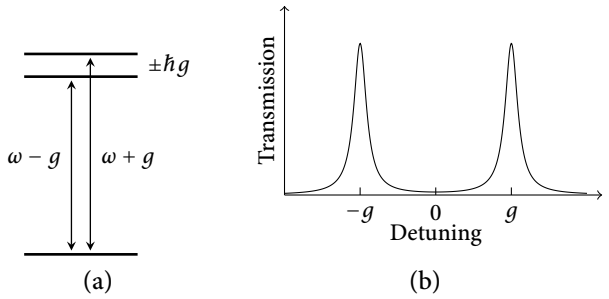

FIGURE 6.1: Vacuum Rabi splitting. (a) Transitions from the ground state to the first "rung" of the Jaynes-Cummings ladder. (b) The vacuum Rabi spectrum which is observed in the regime of strong coupling: the cavity transmission peak is split into a doublet.

spectrum result is given by Schoelkopf and Girvin [1], in which the coupling g approaches the fine-structure limit for cavity QED, which gives the maximum strength of the electric dipole coupling between an atom and a cavity [9].

The experiment of Bishop et al. furthermore observed the supersplitting of each vacuum Rabi peak into a doublet, as predicted by Carmichael and co-workers [10]. The excellent agreement between theory and experiment obtained by these authors provides the impetus for our theoretical consideration of circuit quantum electrodynamics.

6.2 Superconducting quantum bits

There exist several different types of superconducting quantum bit, but there are three main types, classified according to the variables by which they are controlled and excited: the flux qubit, the phase qubit, and the charge qubit. Here we will consider the prototypical form of each type. For an excellent and thorough review of the various superconducting qubits, see Clarke and Wilhelm [11].

6.2.1 The RF SQUID

The prototypical flux qubit is the RF SQUID (radio frequency superconducting quantum interference device), consisting of a superconducting ring interrupted by a single Josephson junction as shown in Fig. 6.2a [12]. The junction has capacitance C_J, the superconducting loop has self-inductance L, and an externally applied magnetic flux Φ_x biases the system. Taking into account contributions from the charging energy, magnetic energy, and Josephson coupling, we obtain the Hamiltonian[1]

$$H = \frac{Q^2}{2C_J} + \frac{(\Phi - \Phi_x)^2}{2L} - E_J \cos\left(2\pi \frac{\Phi}{\Phi_0}\right). \tag{6.1}$$

[1]The phase difference across the Josephson junction γ is related to the flux in the loop by $\gamma/2\pi = \Phi/\Phi_0 + \text{integer}$. Recall that $\Phi_0 = h/2e$ is the flux quantum.

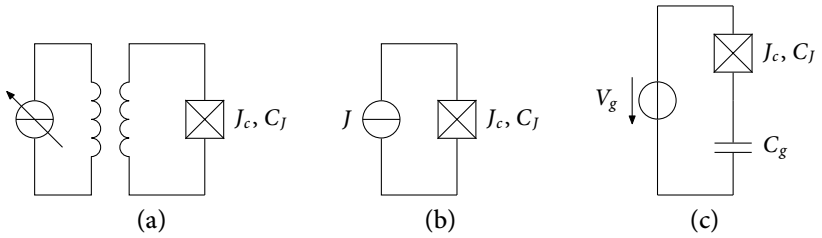

FIGURE 6.2: Schematic depictions of various types of superconducting quantum bit. (a) An RF SQUID qubit. (b) A current-biased Josephson junction qubit. (c) A Cooper pair box qubit. The superconducting charge island, or "box" lies between the capacitively shunted junction and the gate capacitor.

The dynamics described by this Hamiltonian are analogous to the dynamics of a particle[2] with "mass" C_J moving in a one-dimensional potential given by the sum of the magnetic energy of the loop and the Josephson coupling energy of the junction. For appropriate parameters,[3] the two central minima of the aforementioned potential form a double well separated by a barrier whose height depends on the Josephson coupling energy E_J; see Fig. 6.3a.

The left and right potential wells correspond to the quantum states $|0\rangle$ and $|1\rangle$ respectively. When the qubit is in state $|0\rangle$, there is a current present in the loop which tends to cancel Φ_x; when the qubit is in state $|1\rangle$ the current tends to augment Φ_x. These circulating supercurrents are equal and opposite, with magnitude J_q. The system can coherently tunnel between these two states.

At the degeneracy point where $\Phi_x = \Phi_0/2$, the magnetic energy of the loop contributes a constant, which can be neglected. In the spirit of the tight-binding approximation [13], we can write the Hamiltonian for the qubit at the degeneracy point as $H = -\Delta/2\,(|0\rangle\langle 1| + |1\rangle\langle 0|)$, where Δ is a coupling parameter known as the tunnel splitting [12]. Away from the degeneracy point we must add a term to take into account the circulating supercurrents. From the relation for the energy stored in an inductor, we obtain

$$H = \frac{1}{2}\varepsilon\sigma_z - \frac{1}{2}\Delta\sigma_x\,, \tag{6.2}$$

where $\varepsilon = 2J_q\,(\Phi_x - \frac{1}{2}\Phi_0)$. The energy eigenvalues of (6.2) are $\pm\frac{1}{2}\sqrt{\Delta^2 + \varepsilon^2}$. When $\Phi_x = \Phi_0/2$, the ground and excited states are the antisymmetric and symmetric combinations $(|0\rangle \mp |1\rangle)/\sqrt{2}$ respectively.

Of course, several other flux qubit configurations have been proposed. For example, three-junction SQUID rings are common [14]. Flux qubits play no further role in this thesis, so we will not consider any other configurations here. For more information, see Makhlin et al. [15].

[2]Due to the identification $Q = -i\hbar\partial/\partial\Phi$, the Hamiltonian can be written entirely in terms of the variable Φ.
[3]See, for example, the experimental parameters used by Friedman et al. [12].

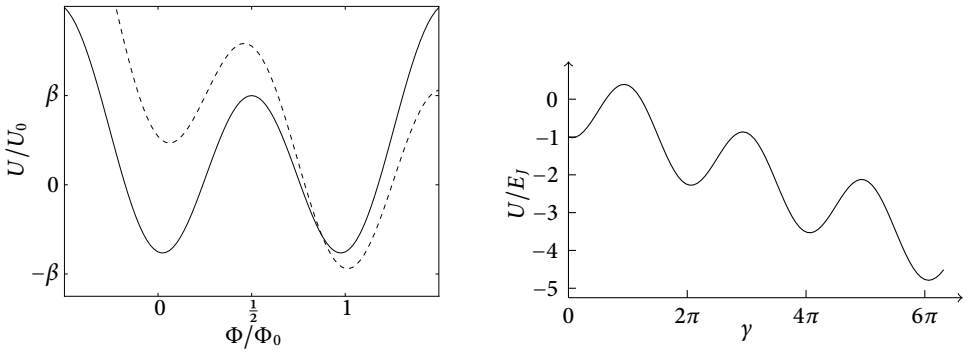

FIGURE 6.3: (a) Flux qubit potentials. The solid line shows the symmetric potential obtained when $\Phi_x = \Phi_0/2$. The dashed line shows the tilted potential obtained when $\Phi_x \neq \Phi_0/2$; in this case $\Phi_x/\Phi_0 = 1.25$. (b) The tilted-washboard potential, with $J/J_c = 0.2$. Reproduced from appendix B.

6.2.2 The current-biased junction

The prototypical phase qubit is the current-biased Josephson junction [16, 17], consisting of a single Josephson junction connected to a current source. A schematic depiction of the current-biased junction is shown in Fig. 6.2b. Referring to sections B.4.3 and B.4.4 of appendix B, we see that the dynamics of the phase difference between the sides of the junction are analogous to the dynamics of a particle moving in a potential $U(\gamma)$, given by (B.41). This potential has the form of a "tilted washboard", and is depicted in Fig. 6.3b. See Clarke et al. [18] for further reading.

When the external bias current J is less than the critical current of the junction, that is $J < J_c$, U has local minima in which the motion of the coordinate γ (which we can alternatively think of in terms of our fictitious particle) can be localised. When the bias current is equal to the critical current, the local minima become points of inflection, so for $J \gtrsim J_c$ no bound states exist. The local potential wells are approximately cubic [16], and as such anharmonic; the energy level spacing becomes smaller as the quantum number n increases. The qubit involves transitions between the ground state $|0\rangle$ of one of these potential wells, and first excited state $|1\rangle$.

6.2.3 The Cooper pair box

The prototypical charge qubit is the Cooper pair box [2, 15, 19]. This type of qubit plays a major role in the theory of circuit quantum electrodynamics presented in the following chapter, so we will not consider it in great detail here. Chapter 7 will contain a more comprehensive treatment.

The Cooper pair box is depicted schematically in Fig. 6.2c. It consists of a superconducting island ("box") connected by a Josephson junction (with Josephson coupling energy E_J and capacitance C_J) to a superconducting electrode. A gate voltage V_g is coupled to the system via a gate capacitor C_g. The number of excess Cooper pairs on the charge island is a quantised, integer operator $\hat{n}$. If the circuit is operated in a suitable parameter regime, Cooper pair number

states with $n > 1$ may be neglected. In this case, the Cooper pair box Hamiltonian reduces to that of a qubit.

The *transmon* is a charge-insensitive qubit design derived from the Cooper pair box [20]. While it behaves in many ways more similarly to an anharmonic oscillator than a qubit, it has seen use in recent circuit QED experiments [5, 6], and as such will be considered in detail in the following chapter.

References

[1] R. J. Schoelkopf and S. M. Girvin. Wiring up quantum systems. *Nature*, 451:664–669, 2008.

[2] A. Blais, R.-S. Huang, A. Wallraff, S. M. Girvin, and R. J. Schoelkopf. Cavity quantum electrodynamics for superconducting electrical circuits: An architecture for quantum computation. *Physical Review A*, 69:062320, 2004.

[3] I. Chiorescu, P. Bertet, K. Semba, Y. Nakamura, C. J. P. M. Harmans, and J. E. Mooij. Coherent dynamics of a flux qubit coupled to a harmonic oscillator. *Nature*, 431:159–162, 2004.

[4] A. Wallraff, D. I. Schuster, A. Blais, L. Frunzio, R.-S. Huang, J. Majer, S. Kumar, S. M. Girvin, and R. J. Schoelkopf. Strong coupling of a single photon to a superconducting qubit using circuit quantum electrodynamics. *Nature*, 431:162–167, 2004.

[5] J. M. Fink, M. Göppl, M. Baur, R. Bianchetti, P. J. Leek, A. Blais, and A. Wallraff. Climbing the Jaynes-Cummings ladder and observing its $\sqrt{n}$ nonlinearity in a cavity QED system. *Nature*, 454:315–318, 2008.

[6] L. S. Bishop, J. M. Chow, J. Koch, A. A. Houck, M. H. Devoret, E. Thuneberg, S. M. Girvin, and R. J. Schoelkopf. Nonlinear response of the vacuum Rabi resonance. *Nature Physics*, 5:105–109, 2009.

[7] H. J. Carmichael, P. Kochan, and B. C. Sanders. Photon correlation spectroscopy. *Physical Review Letters*, 77:631–634, 1996.

[8] A. Boca, R. Miller, K. M. Birnbaum, A. D. Boozer, J. McKeever, and H. J. Kimble. Observation of the vacuum Rabi spectrum for one trapped atom. *Physical Review Letters*, 93:233603, 2004.

[9] M. H. Devoret, S. Girvin, and R. Schoelkopf. Circuit-QED: How strong can the coupling between a Josephson junction atom and a transmission line resonator be? *Annalen der Physik*, 16:767–779, 2007.

[10] L. Tian and H. J. Carmichael. Quantum trajectory simulations of two-state behavior in an optical cavity containing one atom. *Physical Review A*, 46:R6801–R6804, 1992.

[11] J. Clarke and F. K. Wilhelm. Superconducting quantum bits. *Nature*, 453:1031–1042, 2008.

[12] J. R. Friedman, V. Patel, W. Chen, S. K. Tolpygo, and J. E. Lukens. Quantum superposition of distinct macroscopic states. *Nature*, 406:43–46, 2000.

[13] J. J. Sakurai. *Modern Quantum Mechanics*, section 4.3. Addison-Wesley, revised edition, 1994.

[14] C. H. van der Wal, A. C. J. ter Haar, F. K. Wilhelm, R. N. Schouten, C. J. P. M. Harmans, T. P. Orlando, S. Lloyd, and J. E. Mooij. Quantum superposition of macroscopic persistent-current states. *Science*, 290:773–777, 2000.

[15] Y. Makhlin, G. Schön, and A. Shnirman. Quantum-state engineering with Josephson-junction devices. *Reviews of Modern Physics*, 73:357–400, 2001.

[16] J. M. Martinis, S. Nam, and J. Aumentado. Rabi oscillations in a large Josephson-junction qubit. *Physical Review Letters*, 89:117901, 2002.

[17] K. B. Cooper, M. Steffen, R. McDermott, R. W. Simmonds, S. Oh, D. A. Hite, D. P. Pappas, and J. M. Martinis. Observation of quantum oscillations between a Josephson phase qubit and a microscopic resonator using fast readout. *Physical Review Letters*, 93:180401, 2004.

[18] J. Clarke, A. N. Cleland, M. H. Devoret, D. Esteve, and J. M. Martinis. Quantum mechanics of a macroscopic variable: The phase difference of a Josephson junction. *Science*, 239:992–997, 1988.

[19] D. I. Schuster. *Circuit quantum electrodynamics*, section 3.2. PhD thesis, Yale University, 2007.

[20] J. Koch, T. M. Yu, J. Gambetta, A. A. Houck, D. I. Schuster, J. Majer, A. Blais, M. H. Devoret, S. M. Girvin, and R. J. Schoelkopf. Charge-insensitive qubit design derived from the Cooper pair box. *Physical Review A*, 76:042319, 2007.

7

Circuit QED II: theory

Recent experiments in circuit quantum electrodynamics [1, 2] have used a *transmon* qubit [3] as an artificial atom, coupled to a transmission-line resonator to realise a cavity QED system. In this chapter we develop a model of each of the elements of such a system, as well as the coupling between them, and explore connections to the Jaynes-Cummings model. We also construct the Lindblad master equation which models the damping of the circuit QED system.

7.1 The artificial atom

7.1.1 The Cooper pair box

In section 6.2.3 we introduced the Cooper pair box qubit, which is depicted schematically in Fig. 6.2c. Here we consider the physics of this qubit in greater detail.

Firstly, we will derive the Hamiltonian for the electrostatic energy of the charge island. The island has total capacitance $C_\Sigma = C_J + C_g$, where C_J is the geometric capacitance of the Josephson junction, and C_g is the gate capacitance. The Cooper pair charging energy of the island – the electrostatic charging energy to add a single Cooper pair to the superconducting island – is given by $E_c = (2e)^2/2C_\Sigma$. The dimensionless gate charge $n_g \equiv C_g V_g/2e$ accounts for the effect of the gate voltage V_g, and can be thought of as the preferred number of excess Cooper pairs on the superconducting island (although it is a continuous variable). The actual excess charge is a quantised, integer operator $\hat{n}$. The Hamiltonian for the electrostatic component of the junction is given by

$$H_c = E_c \left(\hat{n} - n_g\right)^2 = \frac{1}{2}\frac{\left(\hat{Q} - 2en_g\right)^2}{C_\Sigma}\,. \tag{7.1}$$

To take into account the coherent tunnelling of Cooper pairs across the junction, we must add an interaction term to the Hamiltonian. Using eigenstates of the Cooper pair number operator $\hat{n}$, we obtain

$$H = \sum_n \left[E_c \left(n - n_g\right)^2 |n\rangle\langle n| - \frac{1}{2}E_J \left(|n\rangle\langle n+1| + |n+1\rangle\langle n|\right)\right]. \tag{7.2}$$

Figure 7.1 shows the effect of the Josephson coupling on the energy levels of a charge qubit. In the so-called *charge regime*, where $E_c \gg E_J$, and in the vicinity of the degeneracy points where $n_g = \frac{1}{2}, \frac{3}{2}, \ldots$, the energy difference between the $n = 1$ and $n = 2$ (and higher) Cooper pair number states is very large, so we can neglect number states with $n > 1$. Making this

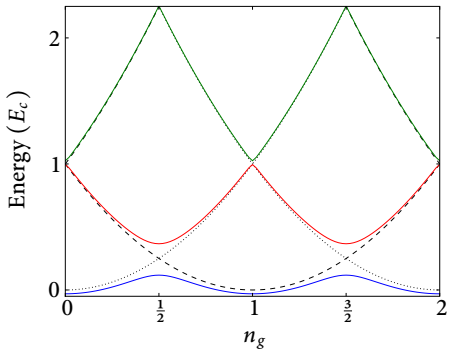

FIGURE 7.1: Charge qubit energy levels. Dotted and dashed black lines show the electrostatic energy of the superconducting island for various even and odd numbers of Cooper pairs present on the island, respectively. Near the degeneracy points, the Josephson coupling mixes the charge states and modifies the energy of the eigenstates: blue, red and green solid lines show the ground, first excited, and second excited state energy levels with $E_J/E_c = 0.25$, obtained via numerical diagonalisation of the Hamiltonian (7.2).

approximation, the Hamiltonian becomes

$$H \approx E_c n_g^2 \left|0\right\rangle \left\langle 0\right| + E_c \left(1 - n_g\right)^2 \left|1\right\rangle \left\langle 1\right| - \frac{1}{2} E_J \left(\left|0\right\rangle \left\langle 1\right| + \left|1\right\rangle \left\langle 0\right|\right) . \tag{7.3}$$

Subtracting the mean of the unperturbed energies of the states $|0\rangle$ and $|1\rangle$, given by $\frac{1}{2}E_c(1 - 2n_g + 2n_g^2)$, and thus shifting the zero of energy gives

$$H = \frac{1}{2} E_c \left(1 - 2n_g\right) \left(\left|1\right\rangle \left\langle 1\right| - \left|0\right\rangle \left\langle 0\right|\right) - \frac{1}{2} E_J \left(\left|0\right\rangle \left\langle 1\right| + \left|1\right\rangle \left\langle 0\right|\right) . \tag{7.4}$$

If we make the identifications

$$\left|0\right\rangle \doteq \begin{pmatrix} 0 \\ 1 \end{pmatrix} \quad \text{and} \quad \left|1\right\rangle \doteq \begin{pmatrix} 1 \\ 0 \end{pmatrix} , \tag{7.5}$$

the Hamiltonian (7.4) can be written in terms of the Pauli matrices σ_x and σ_z as

$$H = \frac{1}{2} E_c \left(1 - 2n_g\right) \sigma_z - \frac{1}{2} E_J \sigma_x . \tag{7.6}$$

At the charge degeneracy point where $n_g = \frac{1}{2}$ (we restrict our attention to the gate charge range $n_g \in [0, 1]$, as we can see from Fig. 7.1 that the energy level structure repeats periodically as we scan across n_g) the Hamiltonian (7.6) simplifies to

$$H = -\frac{1}{2} E_J \sigma_x . \tag{7.7}$$

This Hamiltonian is diagonal in the basis $\{\left|+\right\rangle, \left|-\right\rangle\}$, where

$$\left|\pm\right\rangle = \frac{1}{\sqrt{2}} \left(\left|0\right\rangle \mp \left|1\right\rangle\right) \doteq \frac{1}{\sqrt{2}} \begin{pmatrix} \mp 1 \\ 1 \end{pmatrix} ; \tag{7.8}$$

the energy eigenvalues are thus given by

$$H|+\rangle = \frac{1}{2}E_J|+\rangle \quad \text{and} \quad H|-\rangle = -\frac{1}{2}E_J|-\rangle\,, \tag{7.9}$$

allowing us to write the Hamiltonian transformed into the $|\pm\rangle$ basis as

$$H = \frac{1}{2}E_J\sigma_z\,. \tag{7.10}$$

It is also possible to express the Hamiltonian (7.2) in terms of the phase γ of the superconducting order parameter of the charge island, which is the canonical conjugate to Cooper pair number n [4]. The eigenstates of number and phase are related to one another by[1]

$$|\gamma\rangle = \sum_{n=-\infty}^{\infty} \mathrm{e}^{\mathrm{i}\gamma n}|n\rangle\,, \tag{7.11a}$$

$$|n\rangle = \int_0^{2\pi} \mathrm{d}\gamma\, \mathrm{e}^{-\mathrm{i}\gamma n}|\gamma\rangle\,. \tag{7.11b}$$

In the phase basis, the Cooper pair number operator is given by

$$\hat{n} = -\mathrm{i}\frac{\partial}{\partial\gamma}\,, \tag{7.12}$$

and so in the phase representation [6] the Hamiltonian (7.2) becomes

$$H = E_c\left(-\mathrm{i}\frac{\partial}{\partial\gamma} - n_g\right)^2 - E_J\cos\hat{\gamma}\,. \tag{7.13}$$

The time-independent Schrödinger equation derived from this Hamiltonian is a form of Mathieu's differential equation, and has analytic solutions [7]. We will not make use of these solutions in this thesis, but a brief derivation is presented in appendix C.

Using (7.13), we can evaluate the current passing through the Josephson junction. The current in the Cooper pair box circuit is given by

$$\hat{J} = -2e\dot{\hat{n}}\,, \tag{7.14}$$

the charge of a Cooper pair multiplied by the rate at which the pairs tunnel off the charge island.

[1] For information about phase operators, see Loudon [5].

We can thus evaluate the current,

$$\begin{aligned}\hat{J} &= -2e\frac{1}{\mathrm{i}\hbar}\left[\hat{n}, H\right] \\ &= -2e\frac{1}{\mathrm{i}\hbar}\left[\hat{n}, -E_J\cos\hat{\gamma}\right] \\ &= -2e\frac{1}{\mathrm{i}\hbar}\left[-\mathrm{i}\frac{\partial(-E_J\cos\hat{\gamma})}{\partial\hat{\gamma}}\right] \\ &= \frac{2eE_J}{\hbar}\sin\hat{\gamma} \\ &= J_c\sin\hat{\gamma}\,, \end{aligned} \tag{7.15}$$

where we have used the fact that $E_J = J_c\Phi_0/2\pi$, and that $\Phi_0 = h/2e$. We see that the phenomenological Josephson coupling Hamiltonian first introduced in (7.2) eventually leads to the correct Josephson current-phase relation.[2]

7.1.2 Island potential

From (B.35), the potential difference across the junction of two superconducting electrodes in a quantum circuit is related to the phase difference between the electrodes by

$$\hat{V} = \frac{\Phi_0}{2\pi}\frac{\mathrm{d}\hat{\gamma}}{\mathrm{d}t}\,. \tag{7.16}$$

Because the phase difference γ and the Cooper pair number n are conjugate variables, in the Heisenberg picture we can write [8, 9]

$$\frac{\mathrm{d}\hat{A}}{\mathrm{d}t} = \frac{1}{\mathrm{i}\hbar}\left[\hat{A}, H\right], \tag{7.17}$$

and

$$\frac{\partial\hat{A}}{\partial\hat{\gamma}} = \frac{1}{\mathrm{i}}\left[\hat{A}, \hat{n}\right], \tag{7.18a}$$

$$\frac{\partial\hat{A}}{\partial\hat{n}} = -\frac{1}{\mathrm{i}}\left[\hat{A}, \hat{\gamma}\right], \tag{7.18b}$$

where $\hat{A}$ is any operator.

Using the above relations, we can write the potential difference across a Josephson junction – and thus the potential of the Cooper pair box charge island – as

$$\hat{V} = \frac{1}{\mathrm{i}\hbar}\frac{\Phi_0}{2e}\left[\hat{\gamma}, H\right] = \frac{1}{2e}\frac{\partial H}{\partial\hat{n}}\,. \tag{7.19}$$

Because the electrostatic component of the Cooper pair box Hamiltonian (7.1) is a function

[2] See sections (B.4.1) and (B.4.2).

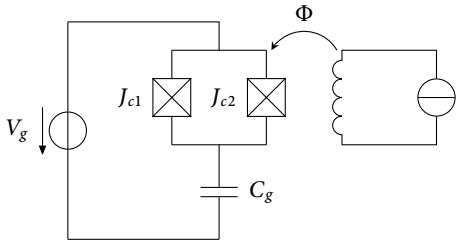

FIGURE 7.2: Split Cooper pair box.

only of $(\hat{n} - n_g)$, we have

$$\hat{V} = -\frac{1}{2e}\frac{\partial H_c}{\partial n_g}\,, \tag{7.20}$$

which yields

$$\hat{V} = \frac{2e}{C_\Sigma}\left(\hat{n} - n_g\right)\,. \tag{7.21}$$

7.1.3 The split Cooper pair box

The electrostatic component of the Cooper pair box Hamiltonian (7.2) can be tuned by varying the gate voltage V_g. Splitting the Josephson junction as shown in Fig. 7.2 provides the ability to tune the tunnelling portion of the Hamiltonian as well.

When the Josephson junction coupling the superconducting electrode to the charge island is split into two, the Josephson component of the qubit Hamiltonian becomes the sum of the contributions of the two junctions,

$$H_J = -E_{J1}\cos\gamma_1 - E_{J2}\cos\gamma_2\,, \tag{7.22}$$

which is equivalent to

$$H_J = -\frac{1}{2}\sum_{n_1} E_{J1}\left(|n_1\rangle\langle n_1+1| + |n_1+1\rangle\langle n_1|\right) - \frac{1}{2}\sum_{n_2} E_{J2}\left(|n_2\rangle\langle n_2+1| + |n_2+1\rangle\langle n_2|\right)\,. \tag{7.23}$$

Our discussion of the DC SQUID device in section B.5.1 includes the result that the difference between the phase differences across the two junctions can be written $\gamma_1 - \gamma_2 = 2\pi\Phi/\Phi_0 \pmod{2\pi}$; see equation (B.49). Substituting this relation into (7.22), and making use of some trigonometric identities, we find that (7.22) becomes

$$H_J = -\left(E_{J1} + E_{J2}\right)\cos\left(\pi\frac{\Phi}{\Phi_0}\right)\cos\gamma - \left(-E_{J1} + E_{J2}\right)\sin\left(\pi\frac{\Phi}{\Phi_0}\right)\sin\gamma\,, \tag{7.24}$$

where we have defined $\gamma \equiv (\gamma_1 + \gamma_2)/2$. In the case where the junctions are symmetric (having

the same critical currents and thus the same coupling energies), or when there is no external flux present in the DC SQUID loop, the Hamiltonian (7.22) reduces to an effective single-junction Hamiltonian, with a flux-tunable Josephson coupling energy

$$H_J = -E_J^{\text{eff}}(\Phi)\cos\gamma\,. \tag{7.25}$$

In order to consider cases where the above conditions do not hold, we define the variables

$$E_{J\Sigma} = E_{J1} + E_{J2}\,, \tag{7.26}$$

$$d = \frac{E_{J1} - E_{J2}}{E_{J\Sigma}}\,. \tag{7.27}$$

Using the transformation between the phase and charge bases introduced in §7.1.1, we can now write the split Cooper pair box Hamiltonian as

$$H_J = -\frac{1}{2}E_{J\Sigma}\sum_n \left[\cos\left(\pi\frac{\Phi}{\Phi_0}\right)\left(|n\rangle\langle n+1| + |n+1\rangle\langle n|\right) + \mathrm{i}d\sin\left(\pi\frac{\Phi}{\Phi_0}\right)\left(|n\rangle\langle n+1| - |n+1\rangle\langle n|\right)\right]. \tag{7.28}$$

In the two-state approximation, the complete Hamiltonian for the split Cooper pair box is

$$H = E_c\left(1-2n_g\right)\sigma_z - \frac{1}{2}E_{J\Sigma}\left[\cos\left(\pi\frac{\Phi}{\Phi_0}\right)\sigma_x + d\sin\left(\pi\frac{\Phi}{\Phi_0}\right)\sigma_y\right]. \tag{7.29}$$

See Cottet [10], Schuster [11] for further information about the split Cooper pair box.

7.1.4 The transmon

The *transmon* [3] is a charge qubit, similar in design to the split Cooper pair box. The chief difference from the split Cooper pair box is, as we can see from Fig. 7.3,[3] an additional large capacitance C_B. This additional capacitance means that the total capacitance to ground of the charge island $C_\Sigma = C_J + C_g + C_B$ (where C_g is the total capacitance of the split junction) is larger than in the case of the Cooper pair box, and so the electrostatic charging energy of the island, $E_c = (2e)^2/C_\Sigma$, is comparatively small. Indeed, the transmon is, in contrast to both types of Cooper pair box, operated in a regime where $E_c \ll E_J$. The reason for this will become clear below.

We now consider the Josephson tunnelling component of the transmon Hamiltonian. This Hamiltonian is identical to the relevant component of the split Cooper pair box Hamiltonian, so the reader can refer back to section 7.1.3 for details, but we reproduce it here for convenience:

[3] Figure 7.3 does not depict the full capacitance network for the transmon device; an effective network is presented here as it is sufficient for our purposes. A complete analysis of the full network is presented in Koch et al. [3].

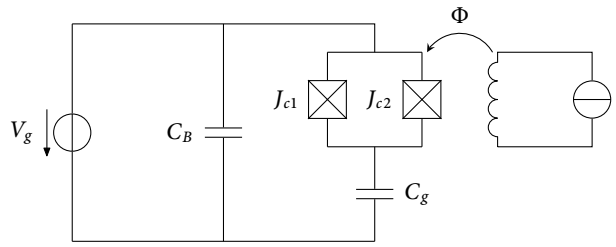

FIGURE 7.3: Schematic diagram of a transmon charge qubit. The split Josephson junction, which forms a DC SQUID loop, has total capacitance C_J.

$$H_J = -E_{J\Sigma}\left[\cos\left(\pi\frac{\Phi}{\Phi_0}\right)\cos\hat{\gamma} + d\sin\left(\pi\frac{\Phi}{\Phi_0}\right)\sin\hat{\gamma}\right]. \tag{7.30}$$

This Hamiltonian can be rewritten [3]

$$H_J = -E_{J\Sigma}\cos\left(\pi\frac{\Phi}{\Phi_0}\right)\sqrt{1+d^2\tan^2\left(\pi\frac{\Phi}{\Phi_0}\right)}\cos\left(\hat{\gamma}-\gamma_0\right), \tag{7.31}$$

where the phase γ_0 is determined by $\tan\gamma_0 = d\tan(\pi\Phi/\Phi_0)$. When the magnetic flux through the DC SQUID loop is constant, this phase can be eliminated by a shift of variables [3], and the split Josephson junction can be taken to have an effective single-junction coupling energy,

$$E_J^{\text{eff}} = E_{J\Sigma}\cos\left(\pi\frac{\Phi}{\Phi_0}\right)\sqrt{1+d^2\tan^2\left(\pi\frac{\Phi}{\Phi_0}\right)}. \tag{7.32}$$

As such, we may as well take the two junctions to be symmetrical from here onwards, writing

$$H_J = -E_J\cos\hat{\gamma} \tag{7.33}$$

for the Josephson component of the transmon Hamiltonian. The full result for asymmetrical junctions can always be recovered by letting $E_J \to E_J^{\text{eff}}$.

If we now take into account the charging component of the Hamiltonian, including the new capacitance C_B mentioned above, we obtain the full phenomenological Hamiltonian for the transmon device,

$$H = E_c\left(\hat{n}-n_g\right)^2 - E_J\cos\hat{\gamma}. \tag{7.34}$$

This Hamiltonian is *identical* to that of the basic Cooper pair box charge qubit, which we have already considered in section 7.1.1.

We see, therefore, that the only fundamental difference between the Cooper pair box and the transmon is the regime in which it is operated: the Cooper pair box is operated with $E_J/E_c \ll 1$ in order that it might behave as a qubit, whereas the transmon is operated with $E_J/E_c \gg 1$. As is clear from Fig. 7.4, when the ratio E_J/E_c is increased, the anharmonicity of the transmon energy levels decreases substantially. However, the so-called *charge dispersion* – the

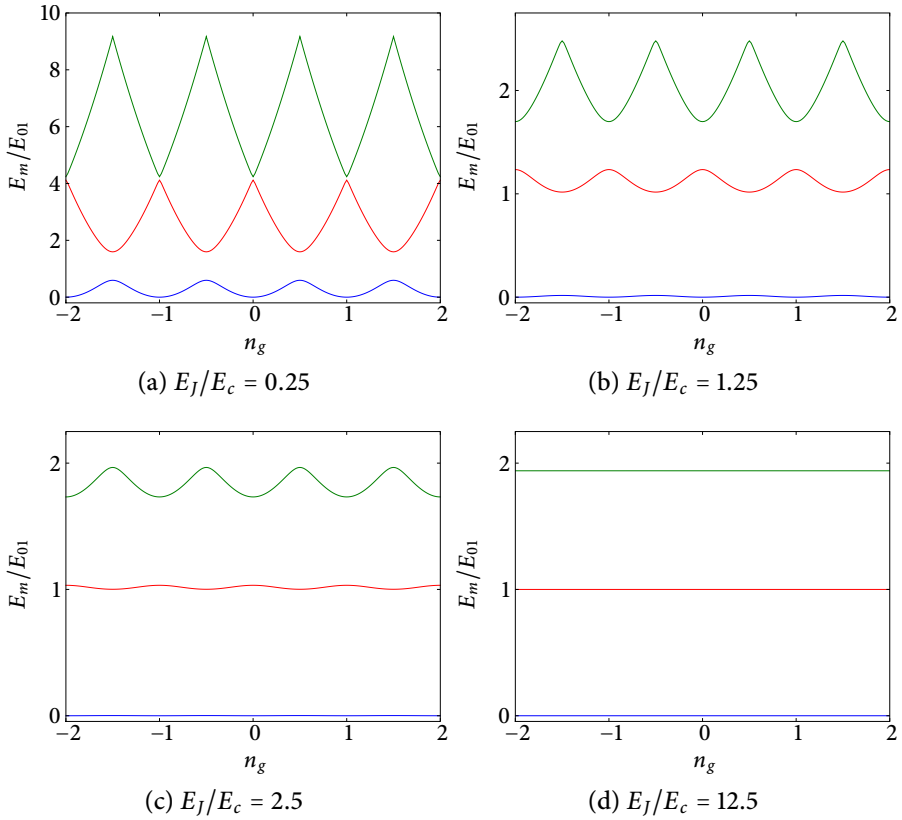

(a) $E_J/E_c = 0.25$ (b) $E_J/E_c = 1.25$

(c) $E_J/E_c = 2.5$ (d) $E_J/E_c = 12.5$

FIGURE 7.4: Eigenenergies E_m of the transmon Hamiltonian (7.34) as a function of effective gate charge n_g, obtained by numerical diagonalisation. The minimum difference between the energies of the ground state and the first excited state is denoted E_{01}.

peak-to-peak variation of each eigenenergy as we sweep across n_g – also decreases. Specifically, the charge dispersion of the m^{th} transmon energy level, which has energy E_m, is given by

$$\epsilon_m = E_m\left(n_g = \tfrac{1}{2}\right) - E_m\left(n_g = 0\right). \tag{7.35}$$

This decrease in the charge dispersion also decreases the sensitivity of the transmon to charge noise, which is of experimental value. It is shown by Koch et al. [3] that an increase of the ratio E_J/E_c results in an *exponential* decrease in the charge dispersion, with only a polynomial decrease in the anharmonicity of the energy levels.

In order to further understand these results, and the transmon itself, we need to search for analytic and perturbative expressions for the energy levels of the transmon.

7.1.5 Transmon: perturbation theory

In the large E_J/E_c limit, the transmon behaves like an anharmonic oscillator. The quantisation of this oscillator follows the treatment of the quantised LC oscillator presented in appendix A, but with the inductor replaced by a Josephson junction.[4]

[4]Here we follow the treatments in Schuster [12] and Koch et al. [3].

We have already seen that the Cooper pair box Hamiltonian – and thus the transmon Hamiltonian – can be expressed in the phase basis using equations (7.11). and . The transmon Hamiltonian in the phase basis, given by (7.13), is repeated here for convenience:

$$H = E_c \left(-\mathrm{i}\frac{\partial}{\partial \gamma} - n_g \right)^2 - E_J \cos \hat{\gamma} \,. \tag{7.36}$$

This is the Hamiltonian for a rigid pendulum or rotor, with a strong gravitational force $-E_J \cos \hat{\gamma}$ restricting the motion of the rotor to a small range of angles. Thus, we expand out the cosine (Josephson) term in the transmon Hamiltonian, keeping terms up to fourth order,

$$H \approx E_c \left(-\mathrm{i}\frac{\partial}{\partial \gamma} \right)^2 - E_J \left(1 - \frac{\hat{\gamma}^2}{2!} + \frac{\hat{\gamma}^4}{4!} \right) , \tag{7.37}$$

where the gate charge n_g, which plays the role of a "vector potential", has been eliminated by a gauge transformation. This Hamiltonian consists of a harmonic oscillator part, and a quartic perturbation:

$$H \approx \left[E_c \left(-\mathrm{i}\frac{\partial}{\partial \gamma} \right)^2 + \frac{1}{2} E_J \hat{\gamma}^2 \right] - E_J - \frac{1}{24} E_J \hat{\gamma}^4 \,. \tag{7.38}$$

We introduce the annihilation operator for the harmonic oscillator which approximates the transmon,

$$\hat{b} = \sqrt{\frac{m_p \omega_p}{2}} \left(\hat{\gamma} + \mathrm{i}\frac{\hat{n}}{m_p \omega_p} \right) , \tag{7.39}$$

with $m_p = \hbar / 2E_c$ and $\omega_p = \sqrt{2E_c E_J}/\hbar$. Thus, we can write the phase operator as

$$\hat{\gamma} = \frac{\hat{b} + \hat{b}^\dagger}{\sqrt{2}} \left(\frac{2E_c}{E_J} \right)^{1/4} . \tag{7.40}$$

And so the transmon Hamiltonian can be written as

$$H \approx \sqrt{2E_c E_J} \left(\hat{b}^\dagger \hat{b} + \frac{1}{2} \right) - E_J - \frac{1}{48} E_c \left(\hat{b} + \hat{b}^\dagger \right)^4 . \tag{7.41}$$

The first-order energy correction to the j^{th} state is given by

$$-\frac{1}{48} E_c \left\langle j \middle| \left(\hat{b} + \hat{b}^\dagger \right)^4 \middle| j \right\rangle = -\frac{1}{48} E_c \left(6j^2 + 6j + 3 \right) , \tag{7.42}$$

which means that the energy of the j^{th} level is given by

$$E_j \approx \hbar \omega_p j - \frac{E_c}{48} \left(6j^2 + 6j + 3 \right) . \tag{7.43}$$

To put this another way, when $\omega_c \ll \omega_p$, as is the case for the transmon, we can neglect those

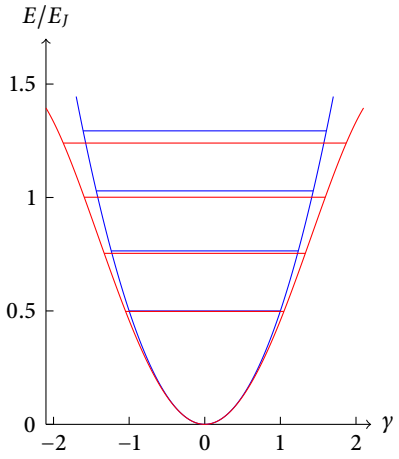

FIGURE 7.5: The transmon as an anharmonic oscillator. The blue lines represent the potential and energy levels of a harmonic oscillator. The red lines show the effect adding a quartic perturbation to the harmonic potential has on the energy eigenvalues. The relative sizes of the energy corrections are correct to first order in perturbation theory, as the energy levels are given by the result (7.43). Parameters are arbitrary.

terms in the expansion of $(\hat{b} + \hat{b}^\dagger)^4$ which provide no first-order perturbative correction to the Hamiltonian, obtaining

$$H = \hbar\omega_p \hat{b}^\dagger \hat{b} - \frac{1}{8}\hbar\omega_c \left[\hat{b}^\dagger \hat{b} + \left(\hat{b}^\dagger \hat{b}\right)^2\right], \tag{7.44}$$

where $\hbar\omega_c = E_c$. Because the transmon will be coupled to some sort of cavity which is resonant with the ground–first excited state transition (the "qubit" transition), we wish to write the Hamiltonian in terms of this resonant frequency, $\omega \equiv \omega_p - \omega_c/4$. When we do this, we obtain

$$\begin{aligned} H &= \hbar\omega \hat{b}^\dagger \hat{b} + \frac{1}{8}\hbar\omega_c \left[\hat{b}^\dagger \hat{b} - \left(\hat{b}^\dagger \hat{b}\right)^2\right] \\ &= \hbar\omega \hat{b}^\dagger \hat{b} - \frac{1}{8}\hbar\omega_c \hat{b}^\dagger \hat{b}^\dagger \hat{b}\hat{b}\,. \end{aligned} \tag{7.45}$$

We have obtained a simple Hamiltonian for the transmon: a charge qubit "reimagined" as an anharmonic oscillator. Figure 7.5 shows qualitatively the effect of the quartic perturbation, and of the first-order energy correction (7.42).

7.2 The transmission-line resonator

A cavity quantum electrodynamics experiment involves an atom coupled to a cavity or other electromagnetic resonator. In circuit QED, a superconducting qubit, or a transmon as described above, can be used as an artificial atom. The "cavity" used in recent experiments [1, 2] is a quasi-one-dimensional superconducting transmission line resonator, also sometimes referred to as a *stripline resonator*. This is essentially just a superconducting wire placed between two ground plates. Gaps in the wire, placed an integer number of half-wavelengths apart, play the role of "mirrors", forming a microwave cavity analogous to the Fabry-Pérot geometry used in

optics. The rate at which photons enter and leave the cavity depends on the size and shape of the gaps.

For relatively low frequencies, when the cross-sectional dimension of the resonator is much less than the wavelength of the transmitted signal, the transmission line can be described by a one-dimensional model: an infinite series of inductors with each node capacitively connected to ground. The classical Lagrangian density for such an LC oscillator is

$$\mathscr{L} = \frac{l}{2} j^2 + \frac{1}{2c} q^2 , \tag{7.46}$$

where l and c are respectively the inductance and capacitance per unit length, and $j(x,t)$ and $q(x,t)$ are the local current and the local charge density. We follow Blais et al. [13] in quantising the oscillator in the usual way. First, we define

$$\theta(x,t) \equiv \int_{-M/2}^{x} \mathrm{d}x' q(x',t) , \tag{7.47}$$

where the resonator has length M. This allows us to write the Lagrangian as

$$L = \int_{-M/2}^{M/2} \mathrm{d}x \left(\frac{l}{2} \dot{\theta}^2 - \frac{1}{2c} (\nabla\theta)^2 \right) . \tag{7.48}$$

The corresponding Euler-Lagrange equation is a wave equation $\ddot{\theta} = v^2 \nabla^2 \theta$ with speed $v = 1/\sqrt{lc}$. The overall charge neutrality of the resonator imposes Dirichlet boundary conditions

$$\theta(-M/2, t) = \theta(M/2, t) = 0 . \tag{7.49}$$

The general solution for $\theta(x,t)$ thus becomes[5]

$$\theta(x,t) = \sqrt{\frac{2}{M}} \sum_{k \text{ odd}} \phi_k(t) \cos\left(\frac{\pi k x}{M}\right) + \sqrt{\frac{2}{M}} \sum_{k \text{ even}} \phi_k(t) \sin\left(\frac{\pi k x}{M}\right) . \tag{7.50}$$

This normal mode expansion allows us to write the Lagrangian (7.48), after spatial integration, as

$$L = \sum_k \left[\frac{1}{2l} {\pi_k}^2 - \frac{l\omega_k^2}{2} {\phi_k}^2 \right] , \tag{7.51}$$

with $\pi_k = l\dot{\phi}_k$ and $\omega_k = \pi k v / M$.

The Hamiltonian obtained from the Lagrangian (7.51) is in the typical form of a set of

[5]Note that there will exist some k above which the assumption that the resonator can be considered to be one-dimensional will no longer apply.

harmonic oscillators, and thus we define boson annihilation and creation operators,

$$\hat{a}_k(t) = \sqrt{\frac{l\omega_k}{2\hbar}}\left(\hat{\phi}_k(t) + \mathrm{i}\frac{\hat{\pi}_k(t)}{l\omega_k}\right), \tag{7.52a}$$

$$\hat{a}_k^\dagger(t) = \sqrt{\frac{l\omega_k}{2\hbar}}\left(\hat{\phi}_k(t) - \mathrm{i}\frac{\hat{\pi}_k(t)}{l\omega_k}\right), \tag{7.52b}$$

which satisfy

$$\left[\hat{a}_k, \hat{a}_{k'}^\dagger\right] = \delta_{kk'}\,. \tag{7.53}$$

The Hamiltonian for the cavity, therefore, is

$$H = \sum_k \hbar\omega_k\left(\hat{a}_k^\dagger\hat{a}_k + \frac{1}{2}\right), \tag{7.54}$$

as expected.

7.3 Coupling of qubit to cavity

The voltage on the resonator is given by

$$\begin{aligned}\hat{V}(x,t) &= \frac{1}{c}\frac{\partial\theta}{\partial x}\\ &= -\sum_{k\,\mathrm{odd}}\sqrt{\frac{\hbar\omega_k}{cM}}\sin\left(\frac{\pi k x}{M}\right)\left[\hat{a}_k(t) + \hat{a}_k^\dagger(t)\right]\\ &\quad + \sum_{k\,\mathrm{even}}\sqrt{\frac{\hbar\omega_k}{cM}}\cos\left(\frac{\pi k x}{M}\right)\left[\hat{a}_k(t) + \hat{a}_k^\dagger(t)\right].\end{aligned} \tag{7.55}$$

If the qubit is coupled to a certain mode k of the resonator, and the combined system is driven at or close to the resonant frequency, other modes can be neglected. Here, the qubit is placed at the centre of the resonator ($x = 0$), and coupled to the $k = 2$ mode. Thus, the potential that the qubit feels is given by

$$\hat{V}(t) = V_0\left[\hat{a}(t) + \hat{a}^\dagger(t)\right], \tag{7.56}$$

with $V_0 = \sqrt{\hbar\omega_2/cM}$. We have dropped the mode index on the resonator operators for simplicity of notation.

Recall that the electrostatic part of the Cooper pair box (or transmon) Hamiltonian is given by

$$H_c = E_c\left(\hat{n} - n_g\right)^2, \tag{7.57}$$

where

$$n_g = \frac{C_g V_g}{2e}, \tag{7.58}$$

V_g being the classical bias voltage coupled to the Josephson junction. Inside the transmission line cavity, the total voltage that the qubit feels is the sum of the classical gate voltage and the quantum voltage due to the photons in the resonator,

$$\begin{aligned}\hat{V}_{\text{tot}} &= V_g + \hat{V} \\ &= V_g + V_0\left(\hat{a} + \hat{a}^\dagger\right).\end{aligned} \tag{7.59}$$

Replacing V_g with $\hat{V}_{\text{tot}}$ and expanding out the electrostatic Hamiltonian gives

$$H_c = E_c\left(\hat{n} - n_g\right)^2 + \frac{C_g}{e} n_g \hat{V} + \frac{{C_g}^2}{4e^2}\hat{V}^2 - \frac{C_g}{e}\hat{V}\hat{n}. \tag{7.60}$$

The first term is the electrostatic Hamiltonian with classical bias, which we have already taken into account. The middle two terms are the extra energy stored in the geometric capacitance of the Josephson junction; as they do not depend on the qubit state, they do not affect the qubit-cavity interaction and can be neglected (by way of shifting the zero of energy). The last term is our interaction term, which we will write as

$$H_I = 2\hbar g\left(\hat{a} + \hat{a}^\dagger\right)\hat{n}, \tag{7.61}$$

with

$$g = \frac{eV_0}{\hbar}\beta, \tag{7.62}$$

where $\beta = C_g/C_\Sigma$ accounts for division of voltage within the qubit.

Recall that earlier, when we were deriving (7.4), we shifted the zero of energy, making the substitution $\hat{n} \to (|1\rangle\langle 1| - |0\rangle\langle 0|)/2$. In the qubit basis $\{|+\rangle, |-\rangle\}$ this becomes $\hat{n} = -\sigma_x/2$, giving

$$H_I = -\hbar g\left(\hat{a} + \hat{a}^\dagger\right)\sigma_x. \tag{7.63}$$

If we make the rotating wave approximation,[6] neglecting terms like $\hat{a}\sigma_-$ and $\hat{a}^\dagger\sigma_+$ which do not conserve energy to first order, and absorb a phase into the definitions of σ_+ and σ_-, we obtain

$$H_I = \hbar g\left(\hat{a}\sigma_+ + \hat{a}^\dagger\sigma_-\right), \tag{7.64}$$

the usual Jaynes-Cummings coupling.

In the case of the transmon, the Cooper pair number operator can be related to the transmon

[6] Recall section 3.1.4.

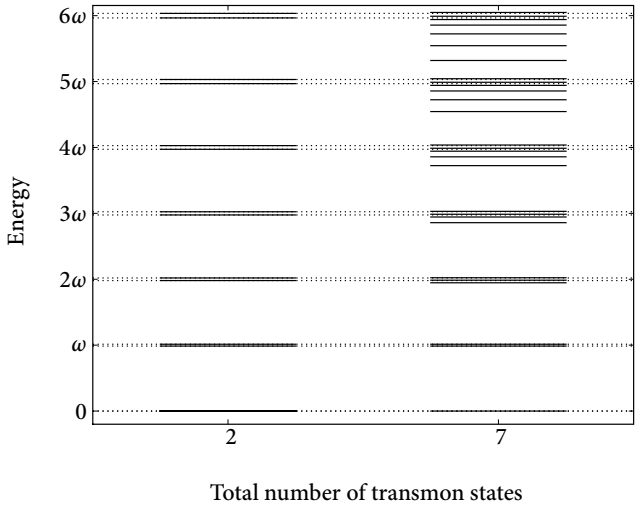

FIGURE 7.6: Energy eigenvalues of the coupled transmon-resonator Hamiltonian (7.69), obtained by numerical diagonalisation. The "ladder" on the left, with only two transmon states, is equivalent to the Jaynes-Cummings ladder.

ladder operators using (7.39),

$$\hat{n} = -\mathrm{i}\frac{1}{\sqrt{2}}\left(\frac{E_J}{2E_c}\right)^{\frac{1}{4}}\left(\hat{b} - \hat{b}^\dagger\right). \tag{7.65}$$

We may absorb a phase into the definition of $\hat{b}$, giving

$$\hat{n} = \frac{1}{\sqrt{2}}\left(\frac{E_J}{2E_c}\right)^{\frac{1}{4}}\left(\hat{b} + \hat{b}^\dagger\right), \tag{7.66}$$

which in the rotating wave approximation gives a similar result [1–3],

$$H_I = \hbar g\left(\hat{a}\hat{b}^\dagger + \hat{a}^\dagger\hat{b}\right), \tag{7.67}$$

with different coupling strength g.

Combining the contributions from the cavity, the qubit, and the interaction, we obtain the full Hamiltonian for a Cooper pair box qubit coupled to a transmission line resonator,

$$H = \hbar\omega\hat{a}^\dagger\hat{a} + \frac{1}{2}\hbar\omega\sigma_z + \hbar g\left(\hat{a}\sigma_+ + \hat{a}^\dagger\sigma_-\right), \tag{7.68}$$

the usual Jaynes-Cummings Hamiltonian.

The complete Hamiltonian for a transmon coupled to a resonator becomes

$$H = \hbar\omega_a\hat{a}^\dagger\hat{a} + \hbar\omega_b\hat{b}^\dagger\hat{b} - \frac{1}{8}\hbar\omega_c\hat{b}^\dagger\hat{b}^\dagger\hat{b}\hat{b} + \hbar g\left(\hat{a}\hat{b}^\dagger + \hat{a}^\dagger\hat{b}\right). \tag{7.69}$$

An example calculation of the energy eigenvalues of the coupled transmon-resonator Hamiltonian is shown in Fig. 7.6.

In order to help evaluate the resonator-transmon coupling strength g, we re-write the

Hamiltonian in the basis of uncoupled transmon states $|i\rangle$, obtaining [3]

$$H = \hbar \sum_j \omega_j |j\rangle\langle j| + \hbar\omega_a \hat{a}^\dagger \hat{a} + \hbar \sum_i \sum_j g_{ij} |i\rangle\langle j| \left(\hat{a} + \hat{a}^\dagger\right), \tag{7.70}$$

with coupling energies

$$\hbar g_{ij} = \hbar g_{ji}^* = 2e\beta V_0 \langle i|\hat{n}|j\rangle \ . \tag{7.71}$$

The matrix element $\langle i|\hat{n}|j\rangle$ is easily evaluated using (7.66). We find that

$$\langle j+1|\hat{n}|j\rangle = \frac{1}{\sqrt{2}} \left(\frac{E_J}{2E_c}\right)^{\frac{1}{4}} \sqrt{j+1}, \tag{7.72}$$

and $\langle j|\hat{n}|j+1\rangle = \langle j+1|\hat{n}|j\rangle$ are the only non-zero matrix elements of this type. Of course, we have made many approximations in deriving the form of $\hat{n}$ used to evaluate the matrix elements above, so the other matrix elements will in reality be very small but non-zero. See Koch et al. [3] for a discussion of how these matrix elements behave. In the rotating-wave approximation the coupling takes on the form

$$\hbar \sum_j g_j \left(|j+1\rangle\langle j| \, \hat{a} + \text{h.c.}\right) , \tag{7.73}$$

where $g_j \equiv g_{j+1,j}$. We now know that

$$g_j \sim g_0 \sqrt{j+1}, \tag{7.74}$$

where g_0 is some reference coupling strength. This is in line with what we already know from (7.69), given that $\hat{b} = \sum_j \sqrt{j+1}\,|j\rangle\langle j+1|$.

7.4 Master equation for the circuit QED system

To model a driven transmon-resonator system, we add a driving term to the Hamiltonian (7.69),

$$H = \hbar\omega_a \hat{a}^\dagger \hat{a} + \hbar\omega_b \hat{b}^\dagger \hat{b} - \frac{1}{8}\hbar\omega_c \hat{b}^\dagger \hat{b}^\dagger \hat{b}\hat{b} + \hbar g \left(\hat{a}\hat{b}^\dagger + \hat{a}^\dagger \hat{b}\right) + \hbar\mathcal{E}\left(\hat{a}e^{i\omega_L t} + \hat{a}^\dagger e^{-i\omega_L t}\right) . \tag{7.75}$$

Transforming the above into a frame rotating at the driving field frequency, to remove the time-dependence, we obtain

$$H = \hbar\Delta\omega_a \hat{a}^\dagger \hat{a} + \hbar\Delta\omega_b \hat{b}^\dagger \hat{b} - \frac{1}{8}\hbar\omega_c \hat{b}^\dagger \hat{b}^\dagger \hat{b}\hat{b} + \hbar g \left(\hat{a}\hat{b}^\dagger + \hat{a}^\dagger \hat{b}\right) + \hbar\mathcal{E}\left(\hat{a} + \hat{a}^\dagger\right) , \tag{7.76}$$

where $\Delta\omega_a \equiv \omega_a - \omega_L$ and $\Delta\omega_b \equiv \omega_b - \omega_L$.

Interactions with the environment are modelled by way of the Lindblad master equation

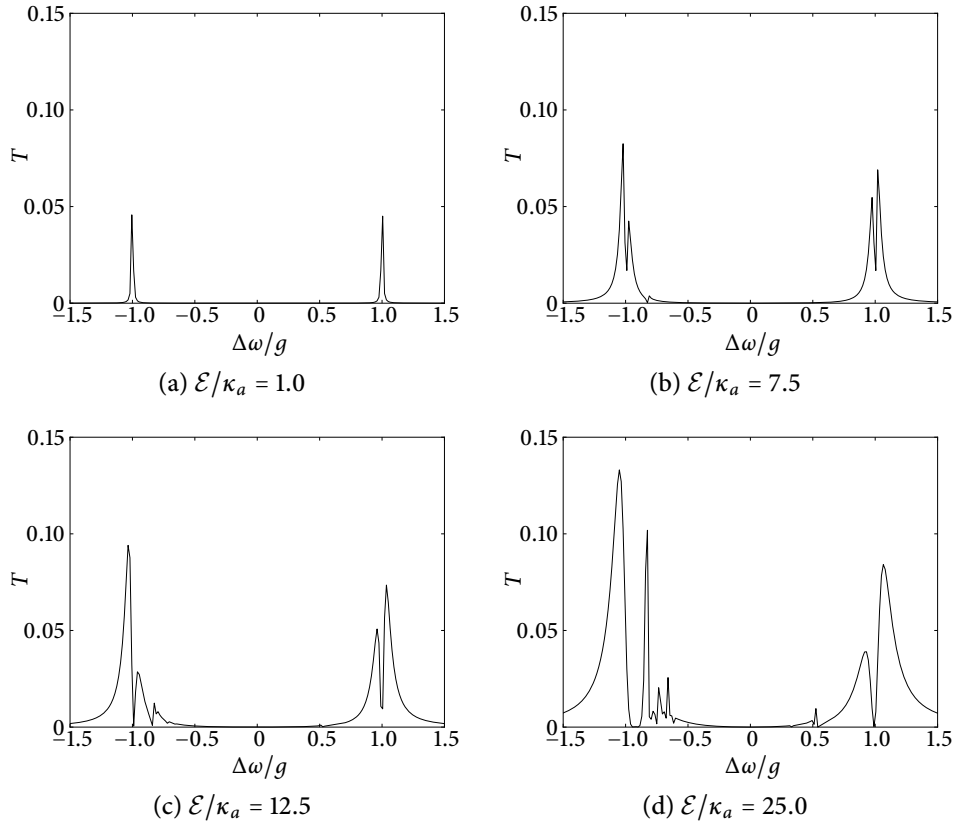

(a) $\mathcal{E}/\kappa_a = 1.0$ (b) $\mathcal{E}/\kappa_a = 7.5$

(c) $\mathcal{E}/\kappa_a = 12.5$ (d) $\mathcal{E}/\kappa_a = 25.0$

FIGURE 7.7: Coherent spectra $T = |\langle \hat{a} \rangle|^2$ of the light transmitted by a transmission line resonator coupled to a transmon. Obtained numerically by solving for the steady state of the master equation, with parameters $g/\kappa_a = 350$, $\omega_c/\kappa_a = 4500$, and $\kappa_b/\kappa_a = 1$. Following Bishop et al. [2], the Hilbert space for these calculations is truncated to a subspace with maximum number of excitations $N = 7$, using the projector $P_N = \sum_{0 \leq n+j \leq N} |n, j\rangle \langle n, j|$.

for the density operator ρ,

$$\dot{\rho} = \mathcal{L}\rho = \frac{1}{i\hbar}[H, \rho] + \kappa_a \mathcal{D}[\hat{a}]\rho + \kappa_b \mathcal{D}[\hat{b}]\rho \,. \tag{7.77}$$

There are two decay channels, taking into account loss of cavity photons and relaxation of transmon excitations respectively. The rate of loss of photons from the cavity is given by κ_a, while the relaxation rate of the transmon excitations is given by κ_b. Following Bishop et al. [2], we have assumed that the relaxation of higher transmon levels arises due to a coupling of environmental degrees of freedom to the charge on the superconducting island. Thus, the relative strengths of the relaxation of the levels $|j\rangle$ are taken to go as g_j/g_0. This yields the expected dissipation term,

$$\kappa_b \mathcal{D}\left[\sum_j \frac{g_j}{g_0} |j\rangle \langle j+1|\right] = \kappa_b \mathcal{D}\left[\sum_j \sqrt{j+1}\, |j\rangle \langle j+1|\right] = \kappa_b \mathcal{D}[\hat{b}] \,. \tag{7.78}$$

It is noted by Bishop et al. that another damping term, taking into account pure dephasing of transmon state superpositions, ought to be present. However, transmon manufacturing has

advanced to the point that the dephasing rate can be set to zero [2].

As an example calculation using the model we have developed, several plots of the coherent spectrum of the light transmitted by the resonator, in the case where the transmon's lowest excited state is resonant with the transmission line, $\Delta\omega \equiv \Delta\omega_a = \Delta\omega_b$, are shown in Fig. 7.7. Note that for weak driving ($\mathcal{E}/\kappa_a = 1.0$) the transmission spectrum of the transmon-cavity system is essentially the vacuum Rabi spectrum; at higher driving field strengths, additional peaks arise due to multi-photon transitions. Also visible is the supersplitting of each vacuum Rabi peak into a doublet, predicted by Tian and Carmichael [14].

References

[1] J. M. Fink, M. Göppl, M. Baur, R. Bianchetti, P. J. Leek, A. Blais, and A. Wallraff. Climbing the Jaynes-Cummings ladder and observing its $\sqrt{n}$ nonlinearity in a cavity QED system. *Nature*, 454:315–318, 2008.

[2] L. S. Bishop, J. M. Chow, J. Koch, A. A. Houck, M. H. Devoret, E. Thuneberg, S. M. Girvin, and R. J. Schoelkopf. Nonlinear response of the vacuum Rabi resonance. *Nature Physics*, 5:105–109, 2009.

[3] J. Koch, T. M. Yu, J. Gambetta, A. A. Houck, D. I. Schuster, J. Majer, A. Blais, M. H. Devoret, S. M. Girvin, and R. J. Schoelkopf. Charge-insensitive qubit design derived from the Cooper pair box. *Physical Review A*, 76:042319, 2007.

[4] Y. Makhlin, G. Schön, and A. Shnirman. Quantum-state engineering with Josephson-junction devices. *Reviews of Modern Physics*, 73:357–400, 2001.

[5] R. Loudon. *The quantum theory of light*, pages 140–143. Oxford University Press, first edition, 1973.

[6] M. H. Devoret. Quantum fluctuations in electrical circuits. In S. Reynaud, E. Giacobino, and J. Zinn-Justin, editors, *Quantum Fluctuations*, pages 351–386. Les Houches (session LXIII, 1995), Elsevier, 1997.

[7] A. Cottet. *Implementation of a quantum bit in a superconducting circuit*, section 1.1.3. PhD thesis, l'Université Paris VI, 2002.

[8] J. J. Sakurai. *Modern Quantum Mechanics*, section 2.2. Addison-Wesley, revised edition, 1994.

[9] A. Cottet. *Implementation of a quantum bit in a superconducting circuit*, section 1.1.4 & 1-A-2. PhD thesis, l'Université Paris VI, 2002.

[10] A. Cottet. *Implementation of a quantum bit in a superconducting circuit*. PhD thesis, l'Université Paris VI, 2002.

[11] D. I. Schuster. *Circuit quantum electrodynamics*, section 3.2.3. PhD thesis, Yale University, 2007.

[12] D. I. Schuster. *Circuit quantum electrodynamics*, section 4.3.3. PhD thesis, Yale University, 2007.

[13] A. Blais, R.-S. Huang, A. Wallraff, S. M. Girvin, and R. J. Schoelkopf. Cavity quantum electrodynamics for superconducting electrical circuits: An architecture for quantum computation. *Physical Review A*, 69:062320, 2004.

[14] L. Tian and H. J. Carmichael. Quantum trajectory simulations of two-state behavior in an optical cavity containing one atom. *Physical Review A*, 46:R6801–R6804, 1992.

8

Circuit QED III: dispersive optical bistability

A system is said to display *optical bistability* if for a single intensity of the light input to the system, there exist two stable output intensities, one large and one small [1]. Optical bistability due to the presence of a single atom (or artificial atom) in a cavity is mentioned by Schoelkopf and Girvin [2] as being a phenomenon which may appear in the new regimes of quantum optics opened up by circuit QED technology. In this chapter, we investigate optical bistability in the circuit QED system comprising a transmon coupled to a transmission line resonator.

Drummond and Walls [3] (and, following them, Walls and Milburn [4]) give a treatment of optical bistability in a system comprising a nonlinear dispersive medium inside a single-mode optical cavity. They consider a cubic nonlinearity in the polarisation (or *Kerr nonlinearity*), which leads to a quartic term of the form $\hat{a}^{\dagger 2}\hat{a}^2$ in the electric field in the Hamiltonian. Referring back to the Hamiltonian for the transmon qubit (7.45), we see that the transmon also has a term of this quartic form which describes the nonlinearity of its energy levels, so we suspect that the physics might be similar. Bistability due to the presence of a purely dispersive medium (with no absorption or gain) is referred to as *dispersive optical bistability*.

The master equation for the driven transmon-resonator circuit QED system is given by

$$\dot{\rho} = \mathcal{L}\rho = \frac{1}{\mathrm{i}\hbar}[H,\rho] + \kappa_a \mathcal{D}[\hat{a}]\rho + \kappa_b \mathcal{D}[\hat{b}]\rho\,, \tag{8.1}$$

where the Hamiltonian H is given by (7.75); in the interaction picture, the Hamiltonian becomes that given in (7.76). In order to obtain a dimensionless master equation we divide (8.1) through by κ_a, obtaining

$$\frac{\mathrm{d}}{\mathrm{d}(\kappa_a t)}\rho = -\mathrm{i}\left[\frac{H}{\hbar\kappa_a},\rho\right] + \mathcal{D}[\hat{a}]\rho + \xi\mathcal{D}[\hat{b}]\rho\,, \tag{8.2}$$

with

$$\frac{H}{\hbar\kappa_a} = \frac{\Delta\omega}{\kappa_a}\hat{a}^\dagger\hat{a} + \frac{\Delta\omega - \Delta\omega_{ab}}{\kappa_a}\hat{b}^\dagger\hat{b} - \frac{1}{8}\frac{\omega_c}{\kappa_a}\hat{b}^\dagger\hat{b}^\dagger\hat{b}\hat{b} + \frac{g}{\kappa_a}\left(\hat{a}\hat{b}^\dagger + \hat{a}^\dagger\hat{b}\right) + \frac{\mathcal{E}}{\kappa_a}\left(\hat{a} + \hat{a}^\dagger\right)\,, \tag{8.3}$$

where we have defined the ratio $\xi \equiv \kappa_b/\kappa_a$, and the detunings $\Delta\omega \equiv \Delta\omega_a$ and $\Delta\omega_{ab} \equiv \Delta\omega_a - \Delta\omega_b$.

8.1 Semiclassical analysis

From (8.2) and (8.3), and using

$$\frac{\partial}{\partial t}\left\langle \hat{A}\right\rangle = \mathrm{tr}\left(\hat{A}\dot{\rho}\right), \tag{8.4}$$

we have

$$\frac{\partial}{\partial t}\langle\hat{a}\rangle = -\mathrm{i}\mathcal{E} - \mathrm{i}\Delta\omega\langle\hat{a}\rangle - \mathrm{i}g\langle\hat{b}\rangle - \frac{1}{2}\langle\hat{a}\rangle, \tag{8.5a}$$

$$\frac{\partial}{\partial t}\langle\hat{a}^\dagger\rangle = \mathrm{i}\mathcal{E} + \mathrm{i}\Delta\omega\langle\hat{a}^\dagger\rangle + \mathrm{i}g\langle\hat{b}^\dagger\rangle - \frac{1}{2}\langle\hat{a}^\dagger\rangle, \tag{8.5b}$$

$$\frac{\partial}{\partial t}\langle\hat{b}\rangle = -\mathrm{i}(\Delta\omega - \Delta\omega_{ab})\langle\hat{b}\rangle + \frac{\mathrm{i}}{4}\omega_c\langle\hat{b}^\dagger\hat{b}\hat{b}\rangle - \mathrm{i}g\langle\hat{a}\rangle - \frac{1}{2}\xi\langle\hat{b}\rangle, \tag{8.5c}$$

$$\frac{\partial}{\partial t}\langle\hat{b}^\dagger\rangle = \mathrm{i}(\Delta\omega - \Delta\omega_{ab})\langle\hat{b}^\dagger\rangle - \frac{\mathrm{i}}{4}\omega_c\langle\hat{b}^\dagger\hat{b}^\dagger\hat{b}\rangle + \mathrm{i}g\langle\hat{a}^\dagger\rangle - \frac{1}{2}\xi\langle\hat{b}^\dagger\rangle, \tag{8.5d}$$

where we have written the parameters $\Delta\omega$, $\Delta\omega_{ab}$, g, and ω_c in units of κ_a, and t in units of ${\kappa_a}^{-1}$ (we do this simply to avoid the notation becoming too unwieldy).

Following Drummond and Walls [3], we define the mean-field amplitudes,

$$\alpha = \langle\hat{a}\rangle, \quad \alpha^* = \left\langle\hat{a}^\dagger\right\rangle, \quad \beta = \left\langle\hat{b}\right\rangle, \quad \beta^* = \left\langle\hat{b}^\dagger\right\rangle. \tag{8.6}$$

In the semiclassical approximation, the correlation functions factorise, and we obtain the equations of motion,

$$\frac{\partial}{\partial t}\begin{bmatrix}\alpha\\ \alpha^*\\ \beta\\ \beta^*\end{bmatrix} = \begin{bmatrix}-\mathrm{i}\mathcal{E} - \mathrm{i}\Delta\omega\alpha - \mathrm{i}g\beta - \frac{1}{2}\alpha\\ \mathrm{i}\mathcal{E} + \mathrm{i}\Delta\omega\alpha^* + \mathrm{i}g\beta^* - \frac{1}{2}\alpha^*\\ -\mathrm{i}(\Delta\omega - \Delta\omega_{ab})\beta + \mathrm{i}\frac{1}{4}\omega_c\beta^*\beta\beta - \mathrm{i}g\alpha - \frac{1}{2}\xi\beta\\ \mathrm{i}(\Delta\omega - \Delta\omega_{ab})\beta^* - \mathrm{i}\frac{1}{4}\omega_c\beta^*\beta^*\beta + \mathrm{i}g\alpha^* - \frac{1}{2}\xi\beta^*\end{bmatrix}. \tag{8.7}$$

The steady state mean-field amplitudes can be obtained by setting the derivatives on the left-hand side of (8.7) equal to zero. In the case of zero relative detuning between the transmon and cavity, that is when $\Delta\omega_{ab} = 0$, computing these steady states yields

$$g^2|\alpha|^2 = |\beta|^2\left[\frac{1}{4}\xi^2 + \left(\frac{1}{4}\omega_c|\beta|^2 - \Delta\omega\right)^2\right], \tag{8.8}$$

and

$$\mathcal{E}^2 = |\beta|^2\left[\left(\frac{\Delta\omega}{2g} + \frac{\xi\Delta\omega}{2g} - \frac{\omega_c}{8g}|\beta|^2\right)^2 + \left(\frac{\Delta\omega^2}{g} - \frac{\omega_c\Delta\omega}{4g}|\beta|^2 - \frac{\xi}{4g} - g\right)^2\right]. \tag{8.9}$$

Using the above relations we can solve for, and plot examples of, the mean-field amplitudes $|\alpha|$ and $|\beta|$, as seen in Fig. 8.1. The "s-shaped" curves suggest dispersive optical bistability [3], but a linearised stability analysis around the steady state will be necessary to confirm this.

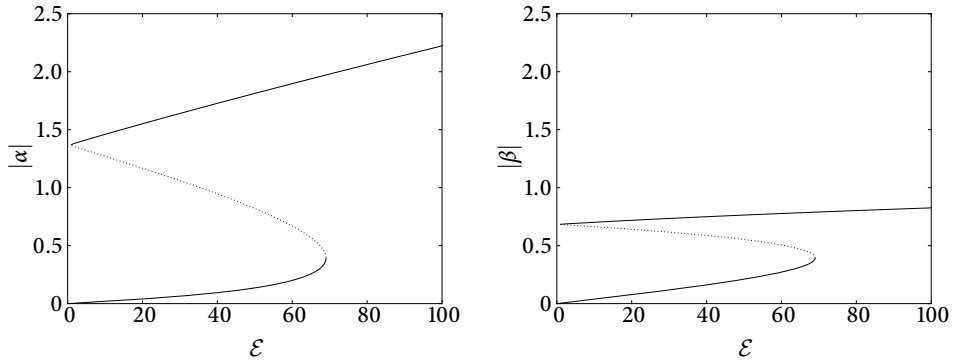

FIGURE 8.1: Steady state mean-field amplitudes as a function of $\mathcal{E}$, with parameters $g/\kappa_a = 350$, $\omega_c/\kappa_a = 4500$, $\Delta\omega = -g/2$, $\Delta\omega_{ab} = 0$, and $\xi = 1$. The full curves show steady states with stable eigenvalues, while the dotted curves show steady states with unstable eigenvalues.

Suppose we have an equation of the form

$$\frac{\partial \mathbf{x}}{\partial t} = \mathbf{F}(\mathbf{x}, t)\,, \tag{8.10}$$

which has a stationary point at $\mathbf{x}_0$, such that

$$F(\mathbf{x}_0, t) = 0\,. \tag{8.11}$$

The best linear approximation to the equation (8.10) at the point $\mathbf{x}_0$ is given by

$$\frac{\partial \mathbf{x}}{\partial t} = J_{\mathbf{F}}(\mathbf{x}_0, t)(\mathbf{x} - \mathbf{x}_0)\,, \tag{8.12}$$

where $J_{\mathbf{F}}$ is the Jacobian of $\mathbf{F}$ evaluated at $\mathbf{x}_0$. Here, we consider the stationary points given by the steady-state solutions of the equations of motion (8.7),

$$\mathbf{x}_0 = (\alpha, \alpha^*, \beta, \beta^*)_{\rm ss}{}^T\,. \tag{8.13}$$

The equations of motion for the mean-field amplitudes (8.7) lead to the Jacobian

$$J_{\mathbf{F}} = \begin{bmatrix} -\mathrm{i}\Delta\omega - \frac{1}{2} & 0 & -\mathrm{i}g & 0 \\ 0 & \mathrm{i}\Delta\omega - \frac{1}{2} & 0 & \mathrm{i}g \\ -\mathrm{i}g & 0 & -\mathrm{i}\Delta\omega + \mathrm{i}\frac{1}{2}\omega_c\beta^*\beta - \frac{1}{2}\xi & \mathrm{i}\frac{1}{4}\omega_c\beta^2 \\ 0 & \mathrm{i}g & -\mathrm{i}\frac{1}{4}\omega_c\beta^{*2} & \mathrm{i}\Delta\omega - \mathrm{i}\frac{1}{2}\omega_c\beta^*\beta - \frac{1}{2}\xi \end{bmatrix}. \tag{8.14}$$

For the steady state solutions to be stable, all eigenvalues of $J_{\mathbf{F}}$ must be negative [5]. We know that the determinant and trace of a matrix A can be written in terms of its eigenvalues λ_i as

$$\mathrm{tr}(A) = \sum_i \lambda_i\,, \quad \text{and} \quad \det(A) = \prod_i \lambda_i\,, \tag{8.15}$$

respectively. Therefore to have stable eigenvalues we must have

$$\mathrm{tr}(J_{\mathbf{F}}) < 0\,, \tag{8.16a}$$

$$\det(J_{\mathbf{F}}) > 0\,. \tag{8.16b}$$

The relation for the trace is always satisfied, as $\xi > 0$. It turns out that the determinant of the Jacobian is a function of $|\beta|^2$, so we can calculate it numerically without too much trouble. Figure 8.1 indicates which solutions for $|\alpha|$ and $|\beta|$ are stable or unstable according to this eigenvalue analysis.

8.1.1 Scaled equations of motion

In order to reduce the size of the parameter space we have to consider, we make a transformation of the equations of motion (8.7). We define the scaling parameter

$$n_s \equiv \frac{g}{\chi}\,, \tag{8.17}$$

where $\chi \equiv \omega_c/4$, and the scaled variables:

$$\tilde{\mathcal{E}} \equiv {n_s}^{-\frac{1}{2}}\mathcal{E}\,, \quad \tilde{\alpha} \equiv {n_s}^{-\frac{1}{2}}\alpha\,, \quad \tilde{\beta} \equiv {n_s}^{-\frac{1}{2}}\beta\,. \tag{8.18}$$

Carmichael [6, 7] refers to this type of transformation as a "system size transformation", but here we make no attempt to prove that the parameter n_s represents the size of the system. In similar fashion to (8.7), we obtain the equations of motion for the scaled variables

$$\frac{\partial}{\partial t}\begin{bmatrix}\tilde{\alpha}\\ \tilde{\alpha}^*\\ \tilde{\beta}\\ \tilde{\beta}^*\end{bmatrix} = \begin{bmatrix}-\mathrm{i}\tilde{\mathcal{E}} - \mathrm{i}\Delta\omega\tilde{\alpha} - \mathrm{i}\tilde{\beta} - \kappa\tilde{\alpha}\\ \mathrm{i}\tilde{\mathcal{E}} + \mathrm{i}\Delta\omega\tilde{\alpha}^* + \mathrm{i}\tilde{\beta}^* - \kappa\tilde{\alpha}^*\\ -\mathrm{i}(\Delta\omega - \Delta\omega_{ab})\tilde{\beta} - \mathrm{i}\tilde{\alpha} + \mathrm{i}\tilde{\beta}^*\tilde{\beta}\tilde{\beta} - \xi\kappa\tilde{\beta}\\ \mathrm{i}(\Delta\omega - \Delta\omega_{ab})\tilde{\beta}^* + \mathrm{i}\tilde{\alpha}^* - \mathrm{i}\tilde{\beta}^*\tilde{\beta}^*\tilde{\beta} - \xi\kappa\tilde{\beta}^*\end{bmatrix}, \tag{8.19}$$

where $\kappa \equiv \kappa_a/2$ and $\xi \equiv \kappa_b/\kappa_a$, and where we have written $\tilde{\mathcal{E}}$, $\Delta\omega$, $\Delta\omega_{ab}$ and κ in units of g, and t in units of g^{-1}. Setting the time-derivatives in (8.19) equal to zero, we obtain the steady state results

$$|\tilde{\alpha}|^2 = |\tilde{\beta}|^2\left[\xi^2\kappa^2 + \left((\Delta\omega - \Delta\omega_{ab}) - |\tilde{\beta}|^2\right)^2\right], \tag{8.20}$$

and

$$|\tilde{\mathcal{E}}|^2 = |\tilde{\beta}|^2\left[\left(\Delta\omega(\Delta\omega - \Delta\omega_{ab}) - \Delta\omega\,|\tilde{\beta}|^2 - \xi\kappa^2 - 1\right)^2 + \left(\kappa(\Delta\omega - \Delta\omega_{ab}) + \xi\kappa\Delta\omega - \kappa\,|\tilde{\beta}|^2\right)^2\right]. \tag{8.21}$$

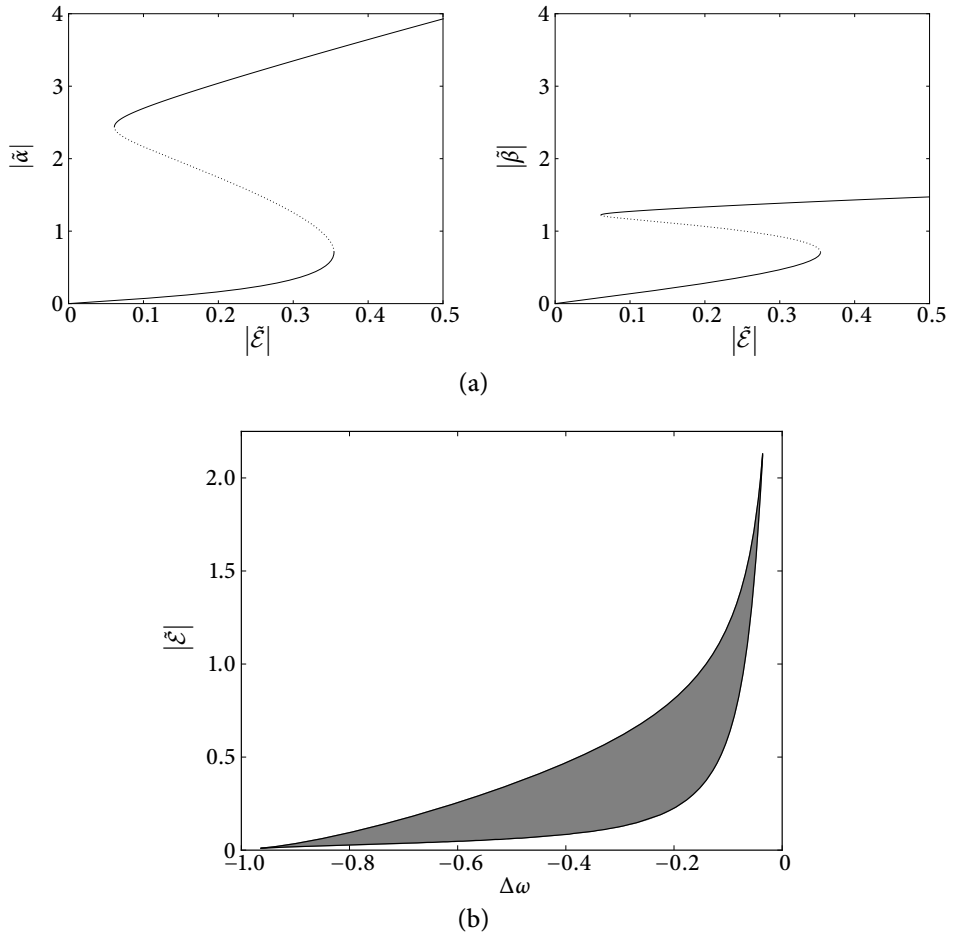

FIGURE 8.2: (a) Steady state mean-field amplitudes as a function of $|\tilde{\mathcal{E}}|$, with parameters, $\Delta\omega/g = -1/2$, $\Delta\omega_{ab} = 0$, $\kappa/g = 1/50$, and $\xi = 1$. The full curves show steady states with stable eigenvalues, while the dotted curves show steady states with unstable eigenvalues. (b) Within the shaded region, our linearised stability analysis yields unstable eigenvalues: this is the "bistable" region. Outside the shaded region, the mean-field amplitudes as functions of $|\tilde{\mathcal{E}}|$ and $\Delta\omega$ are single-valued. Parameters are $\kappa = 1/25$, and $\xi = 1$. In both figures, all parameters are written in units of g.

The equations of motion (8.19) furthermore lead to the Jacobian

$$J_{\mathbf{F}} = \begin{bmatrix} -\mathrm{i}\Delta\omega - \kappa & 0 & -\mathrm{i} & 0 \\ 0 & \mathrm{i}\Delta\omega - \kappa & 0 & \mathrm{i} \\ -\mathrm{i} & 0 & -\mathrm{i}(\Delta\omega - \Delta\omega_{ab}) + 2\mathrm{i}\tilde{\beta}^*\tilde{\beta} - \xi\kappa & \mathrm{i}\tilde{\beta}^2 \\ 0 & \mathrm{i} & -\mathrm{i}\tilde{\beta}^{*2} & \mathrm{i}(\Delta\omega - \Delta\omega_{ab}) - 2\mathrm{i}\tilde{\beta}^*\tilde{\beta} - \xi\kappa \end{bmatrix}, \tag{8.22}$$

which we use to performed a linearised stability analysis for the scaled system. As $\kappa > 0$ and $\xi > 0$, (8.16a) is satisfied, so we can search for stable solutions satisfying (8.16b) numerically. Example calculations are shown in Fig. 8.2a. We also use our linearised stability analysis to plot a region in parameter space in which bistability occurs; this is shown in Fig. 8.2b.

Parameter	Value
g/κ_a	25
$\Delta\omega/\kappa_a$	$-g/2$
$\Delta\omega_{ab}$	0
ω_c/κ_a	100
ξ	1

TABLE 8.1: Parameters used in various quantum-mechanical calculations relating to the circuit QED system.

8.2 Quantum treatment

In the semiclassical approximation, the circuit QED system displays dispersive optical bistability. The question now is whether or not the quantum fluctuations in the system will be large enough to destroy the bimodality by causing transitions between the two stable branches. To answer this question, we must investigate the full quantum dynamics of the system.

The parameters $\Delta\omega/g = -1/2$, $\Delta\omega_{ab} = 0$, $\kappa/g = 1/50$, and $\xi = 1$ used in Fig. 8.2a, along with the choice of scaling parameter $n_s = g/\chi = 1$, correspond to the parameters in table 8.1. These parameters will be used for several quantum-mechanical calculations relating to bistability in the circuit QED system.

The steady state solution of the master equation (8.2) can be found in a straightforward manner using the technique we have employed for many calculations throughout this thesis: finding the kernel of the Liouvillian super-operator. This allows us to compute steady-state properties of the system, such as the field amplitudes shown in Fig. 8.3. The stable branches yielded by the semiclassical analysis do not carry over into the quantum treatment: they are now only *metastable* due to quantum fluctuations. Solving for the steady state of the master equation yields the true steady state in the presence of quantum fluctuations, which is why there is no suggestion in Fig. 8.3 of the two stable branches seen in Figs. 8.1 and 8.2a.

The Q-function [8] is defined as

$$Q(\alpha) = \frac{1}{\pi} \langle \alpha | \rho | \alpha \rangle \ , \tag{8.23}$$

where $|\alpha\rangle$ is a coherent state; the Q-function is thus the diagonal matrix elements of the density operator in a pure coherent state. The Q-function is a quasi-probability distribution which can be used to visualise a quantum state. It is well-behaved: because the density operator ρ is a positive operator, the Q-function is always positive; it is also bounded, $Q(\alpha) < 1/\pi$.

The Q-function is used, in Fig. 8.4, to visualise the steady state solutions of the master equation (8.2), for four different values of the driving field strength. The Q-functions at $\mathcal{E}/\kappa_a = 5.0$ and $\mathcal{E}/\kappa_a = 9.0$ possess a single peak, corresponding to a single stable state. However at intermediate driving strengths, $\mathcal{E}/\kappa_a = 6.5$ and $\mathcal{E}/\kappa_a = 7.5$, a bimodality arises in the quasi-probability distribution, indicating two metastable states as we would expect from our semiclassical analysis.

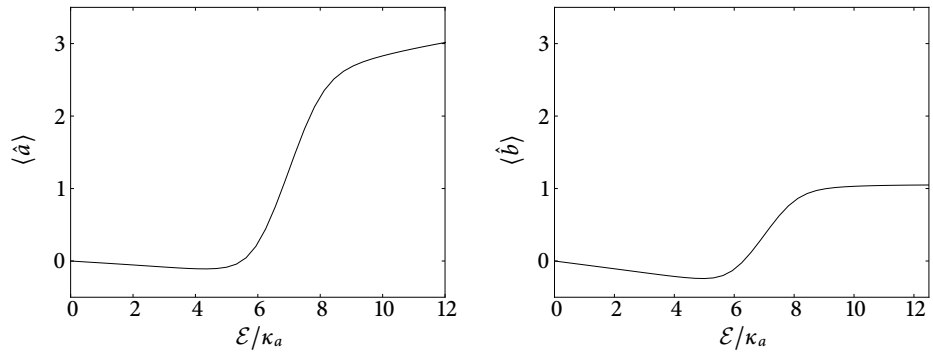

FIGURE 8.3: Steady state field amplitudes as a function of $\mathcal{E}$, with dimensionless parameters listed in table 8.1. The cavity mode Fock space is truncated at the 29-photon level, while the transmon is truncated at the 4-excitation level; the overall Hilbert space is 150-dimensional.

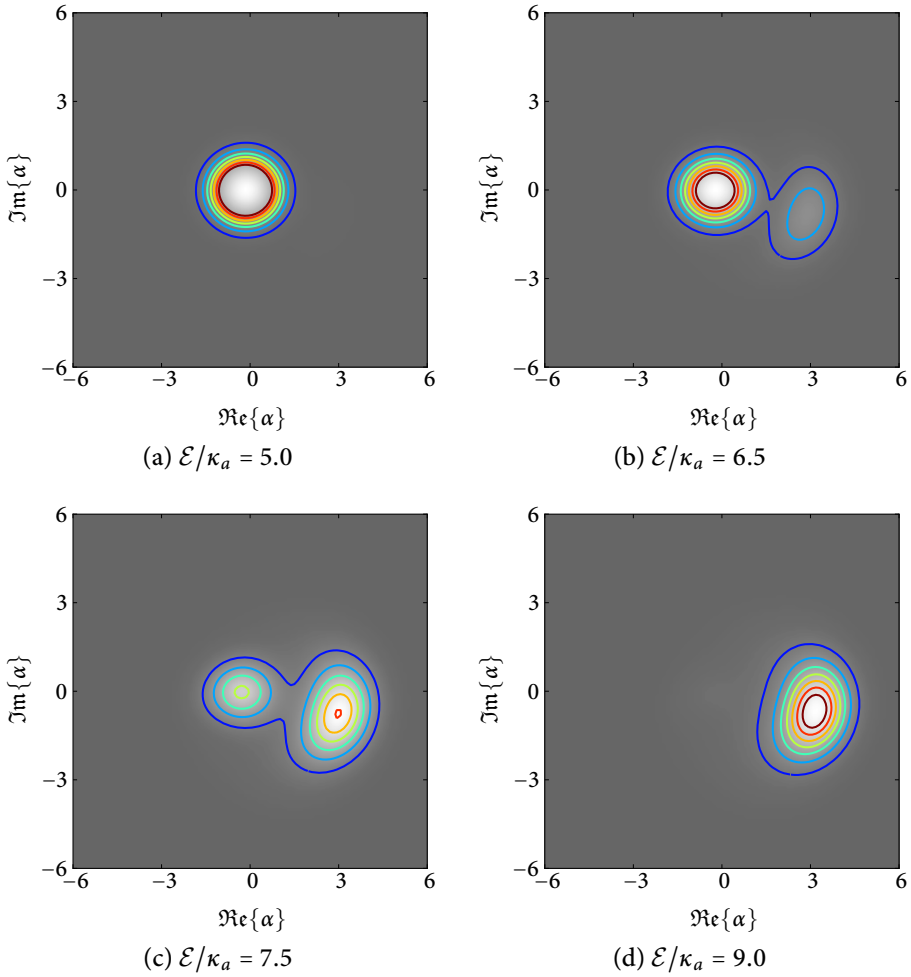

(a) $\mathcal{E}/\kappa_a = 5.0$ (b) $\mathcal{E}/\kappa_a = 6.5$

(c) $\mathcal{E}/\kappa_a = 7.5$ (d) $\mathcal{E}/\kappa_a = 9.0$

FIGURE 8.4: Q-functions, computed from steady state solutions of the master equation (8.2), using the parameters in table 8.1. Contour lines are plotted at $Q(\alpha) = 0, 0.2, 0.4, \ldots, 0.14$. The cavity mode is truncated at the 29-photon level, while the transmon is truncated at the 4-excitation level.

8.2.1 Jump trajectories

Due to the quantum fluctuations present in the master equation treatment, the system state is able to "tunnel" between the two metastable states. Suppose we were to select one of the parameter regimes depicted in Fig. 8.4 where the bimodality is present, and perform an experiment wherein we continuously monitor the light output from the transmission line resonator. In this case, we should be able to observe the system switching between a low-output and a high-output state, corresponding to the "tunnelling" between the two metastable states of the system. We cannot observe this process using the master equation: if we were to calculate some quantity such as $\langle \hat{a}^\dagger \hat{a}(t) \rangle$ using the master equation, we would simply obtain a mean somewhere between the two metastable states, as we did in Fig. 8.3. This is because the master equation constitutes a statistical average over all the possible trajectories of the quantum state. In order to observe the system switching between its two metastable states, we must appeal to quantum trajectory theory (section 2.4).

The master equation (8.2) has dissipators $\mathcal{D}[\hat{a}]\rho$ and $\xi\mathcal{D}[\hat{b}]\rho$, for the damping of the resonator mode and the relaxation of the transmon excitations respectively. These dissipators lead to two jump operators

$$\hat{\jmath}_a = \hat{a}\,, \quad \hat{\jmath}_b = \sqrt{\xi}\hat{b}\,, \tag{8.24}$$

corresponding to direct detection of photons from the resonator and the transmon.[1] The non-Hermitian effective Hamiltonian, which generates the coherent evolution of the unnormalised conditioned wavefunction $|\tilde{\Psi}_c(t)\rangle$ between jumps, is therefore given by

$$H_{\text{eff}} = H - \mathrm{i}\hbar\frac{1}{2}(\hat{\jmath}_a^\dagger \hat{\jmath}_a + \hat{\jmath}_b^\dagger \hat{\jmath}_b)\,, \tag{8.25}$$

where the system Hamiltonian H is given by (8.3). By applying the Monte Carlo algorithm outlined in section 2.4.4, and using RK4 integration between the jumps, we obtain the quantum trajectory simulations of the mean photon number $\langle \hat{a}^\dagger \hat{a} \rangle$ shown in Fig. 8.5. Note the visible switching, at driving strengths $\mathcal{E}/\kappa_a = 6.5$ and $\mathcal{E}/\kappa_a = 7.5$, between the states with low and high mean photon numbers. The noise in the high mean photon number state is simply shot noise.

8.2.2 Heterodyne current records

We seek an unravelling of the master equation (8.2) which models the type of measurement made in optical heterodyne detection. Consider the schematic "experiment" depicted in Fig. 8.6, in which the light output from the transmission line resonator interferes with a coherent

[1] If the photons are not actually detected, in the case of the transmon for example, the jump operators remain the same. The Lindblad master equation is Markovian, so photons emitted into the environment by relaxation of the transmon levels will not affect the evolution of the system after their emission; they can thus, in principle, be detected at any time without changing the state of the system.

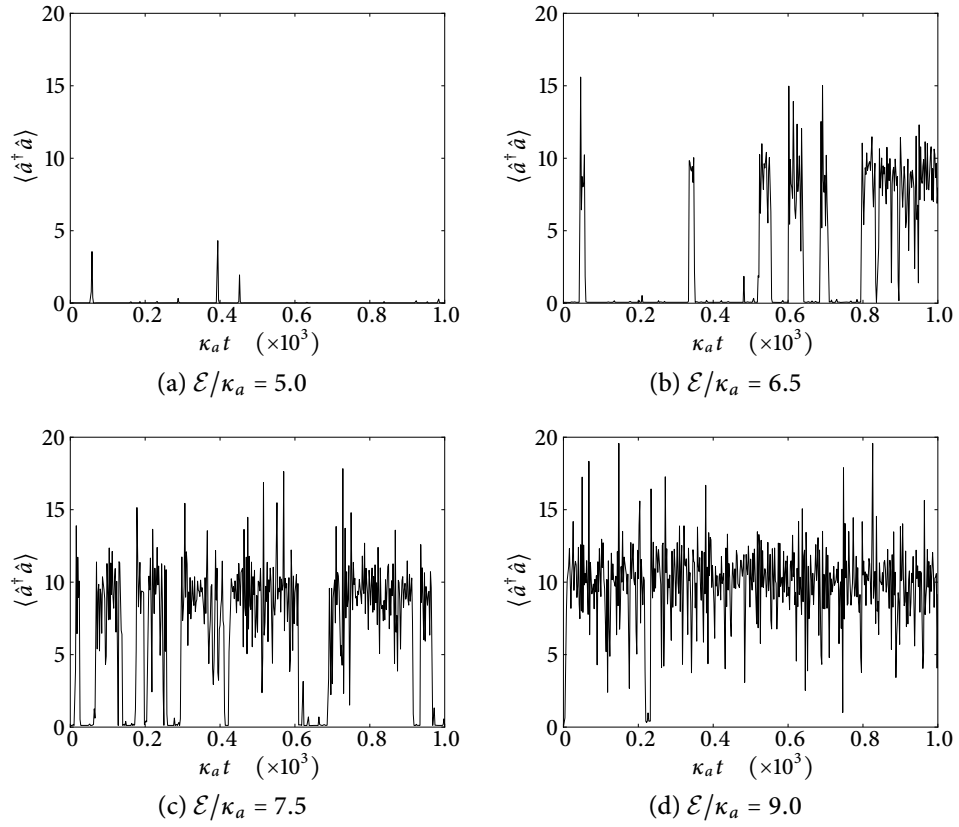

(a) $\mathcal{E}/\kappa_a = 5.0$ (b) $\mathcal{E}/\kappa_a = 6.5$

(c) $\mathcal{E}/\kappa_a = 7.5$ (d) $\mathcal{E}/\kappa_a = 9.0$

FIGURE 8.5: Monte Carlo simulations of quantum trajectories with photoelectron counting, computed using the parameters in table 8.1. The mean photon number in the transmission line resonator is shown for four driving field strengths. The cavity mode is truncated at the 29-photon level, while the transmon is truncated at the 4-excitation level.

local oscillator field. The local oscillator field has complex amplitude

$$\mathcal{E}_{\mathrm{lo}} = |\mathcal{E}_{\mathrm{lo}}| \, \mathrm{e}^{\mathrm{i}\theta} \, . \tag{8.26}$$

In this situation, the transmon levels relax as usual; this is taken into account by way of the jump operator

$$\hat{\jmath}_b = \sqrt{\xi} \hat{b} \, , \tag{8.27}$$

just as in the case of the jump trajectory. If the photons from the resonator were to be directly detected, we would have the jump operator

$$\hat{\jmath}_a = \hat{a} \, , \tag{8.28}$$

however in this case the cavity output is not observed directly, but is rather measured using heterodyne detection. In place of the single jump operator $\hat{\jmath}_a$ we now have – taking into account

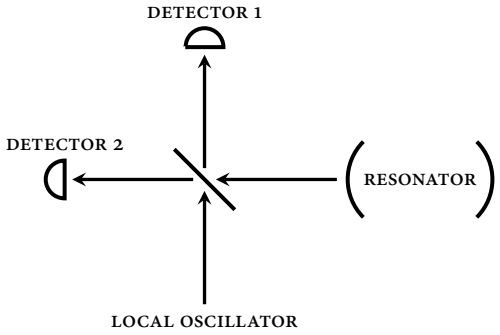

FIGURE 8.6: Schematic depiction of optical heterodyne detection. A strong local oscillator field is superposed on the output from the transmission line resonator at a 50/50 beam splitter.

the two detectors and the 50/50 beam splitter shown in Fig. 8.6 – two jump operators [9],

$$\hat{\jmath}_+ = \frac{1}{\sqrt{2}}(\mathcal{E}_{\mathrm{lo}} + \hat{\jmath}_a) = \frac{1}{\sqrt{2}}(|\mathcal{E}_{\mathrm{lo}}|\,\mathrm{e}^{\mathrm{i}\theta} + \hat{\jmath}_a)\,, \tag{8.29a}$$

$$\hat{\jmath}_- = \frac{1}{\sqrt{2}}(\mathcal{E}_{\mathrm{lo}} - \hat{\jmath}_a) = \frac{1}{\sqrt{2}}(|\mathcal{E}_{\mathrm{lo}}|\,\mathrm{e}^{\mathrm{i}\theta} - \hat{\jmath}_a)\,. \tag{8.29b}$$

The non-Hermitian Hamiltonian which generates the coherent evolution of $|\tilde{\Psi}_c(t)\rangle$ between jumps is therefore given by

$$\begin{aligned} H_{\mathrm{eff}} &= H - \mathrm{i}\hbar\frac{1}{2}(\hat{\jmath}_+^\dagger\hat{\jmath}_+ + \hat{\jmath}_-^\dagger\hat{\jmath}_- + \hat{\jmath}_b^\dagger\hat{\jmath}_b) \\ &= H - \mathrm{i}\hbar\frac{1}{2}(\hat{\jmath}_a^\dagger\hat{\jmath}_a + \hat{\jmath}_b^\dagger\hat{\jmath}_b + |\mathcal{E}_{\mathrm{lo}}|^2)\,. \end{aligned} \tag{8.30}$$

We may neglect the term $-\mathrm{i}\hbar\frac{1}{2}|\mathcal{E}_{\mathrm{lo}}|^2$, as it has no effect on the normalised conditioned state [9].

In the case of homodyne detection, which we do not consider in detail here, the phase θ of the local oscillator is constant. Under heterodyne detection, the local oscillator phase is time-dependent, $\theta(t)$, and varies rapidly at a rate $\Omega \gg 1$ (not to be confused with the Rabi frequency). Thus, we have

$$\hat{\jmath}_+ = \frac{1}{\sqrt{2}}(|\mathcal{E}_{\mathrm{lo}}|\,\mathrm{e}^{-\mathrm{i}\Omega t} + \hat{\jmath}_a)\,, \tag{8.31a}$$

$$\hat{\jmath}_- = \frac{1}{\sqrt{2}}(|\mathcal{E}_{\mathrm{lo}}|\,\mathrm{e}^{-\mathrm{i}\Omega t} - \hat{\jmath}_a)\,, \tag{8.31b}$$

with $\theta(0) = 0$.

We have the jump operators $\hat{\jmath}_\pm$ from (8.31), as well as $\hat{\jmath}_b$; the corresponding probabilities for a jump to occur in the interval $[t, t + \Delta t)$ are given by

$$p_{c,i} = \langle\Psi_c(t)|\hat{\jmath}_i^\dagger\hat{\jmath}_i|\Psi_c(t)\rangle\Delta t\,, \tag{8.32}$$

for $i = \pm, b$. We have, broadly, two different types of "jump": those due to relaxation of the transmon levels $\hat{\jmath}_b$, and heterodyne-type detections $\hat{\jmath}_\pm$. From the integration kernel (2.77) of

the quantum trajectory we see that we can divide up the time-evolution of the conditioned state into intervals delineated by jumps in the transmon state, $\hat{j}_b$. In between the jumps due to $\hat{j}_b$, we have evolution generated by H_{eff} as well as heterodyne detections.

A derivation of the stochastic Schrödinger equation (SSE) for heterodyne detection[2] has been given by Carmichael [9]. We will not repeat the derivation here, as it is lengthy; instead we refer the reader to the literature. In our notation, the SSE for heterodyne detection is given by

$$\mathrm{d}\left|\bar{\Psi}_c(t)\right\rangle = \left[\frac{1}{\mathrm{i}\hbar}H_{\text{eff}}\,\mathrm{d}t + (Ge\,|\mathcal{E}_{\text{lo}}|)^{-1}\mathrm{e}^{\mathrm{i}\Omega t}\hat{j}_a\,\mathrm{d}q\right]\left|\bar{\Psi}_c(t)\right\rangle\,, \tag{8.33a}$$

with the charge $\mathrm{d}q$ deposited in the detector circuit in the interval t to $t+\mathrm{d}t$ given by

$$\mathrm{d}q = Ge\,|\mathcal{E}_{\text{lo}}|\left[\left\langle \mathrm{e}^{-\mathrm{i}\Omega t}\hat{j}_a^\dagger + \mathrm{e}^{\mathrm{i}\Omega t}\hat{j}_a\right\rangle(t)\,\mathrm{d}t + \mathrm{d}W(t)\right]\,, \tag{8.33b}$$

where G is the detector gain and e is the electronic charge; $\mathrm{d}W(t)$ is an infinitesimal Wiener increment [14] satisfying

$$\mathrm{E}[\mathrm{d}W(t)] = 0\,,\quad \mathrm{d}W(t)^2 = \mathrm{d}t\,. \tag{8.34}$$

All we really know about the rate Ω is that it is large. Assuming that it is very large compared with the bandwidth of the source-field fluctuations, we define the slowly-varying charge increment

$$\mathrm{d}\tilde{q} \equiv \mathrm{e}^{\mathrm{i}\Omega t}\mathrm{d}q\,, \tag{8.35}$$

and neglect the rapidly-oscillating term $e^{2\mathrm{i}\Omega t}\,\langle\hat{j}_a\rangle$ that appears on the right-hand side of (8.33b). We also make the substitution

$$\mathrm{e}^{\mathrm{i}\Omega t}\mathrm{d}W(t) \to \mathrm{d}Z(t)\,, \tag{8.36}$$

where

$$\mathrm{d}Z(t) = \frac{1}{\sqrt{2}}\left[\mathrm{d}W_x(t) + \mathrm{i}\,\mathrm{d}W_y(t)\right] \tag{8.37}$$

is a complex-valued Wiener increment with covariances

$$\overline{\mathrm{d}Z(t)\mathrm{d}Z(t)} = \overline{\mathrm{d}Z^*(t)\mathrm{d}Z^*(t)} = 0\,,\quad \overline{\mathrm{d}Z^*(t)\mathrm{d}Z(t)} = \mathrm{d}t\,, \tag{8.38}$$

and $\mathrm{d}W_x(t)$ and $\mathrm{d}W_y(t)$ are statistically independent real-valued Wiener increments with

[2] For related work on homodyne trajectories, see Wiseman and Milburn [10, 11] and Carmichael [12]. Wiseman [13] also considers homodyne and heterodyne detection in the context of quantum trajectory theory.

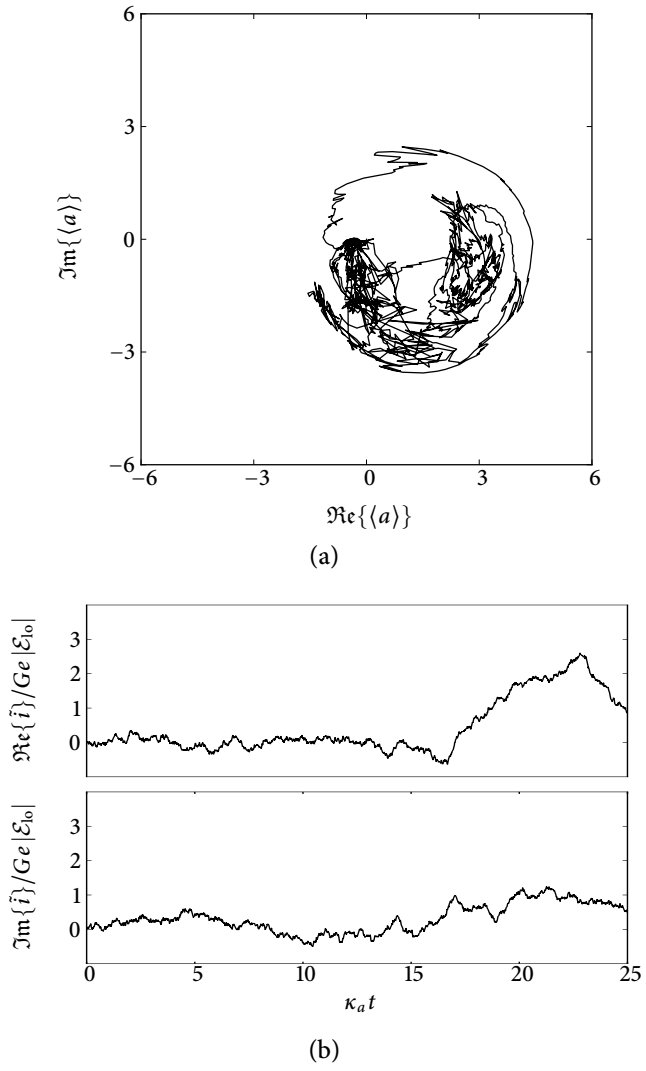

FIGURE 8.7: (a) Monte Carlo simulation of a quantum trajectory with photoelectron counting for the transmon, and heterodyne current records for the transmission line resonator, computed using the parameters in table 8.1, with $\mathcal{E}/\kappa_a = 7.5$. The cavity mode is truncated at the 29-photon level, while the transmon is truncated at the 4-excitation level. The trajectory shown was integrated for a total time $25{\kappa_a}^{-1}$. (b) The filtered heterodyne current record obtained from the same simulation, performed with parameters $G\,|\mathcal{E}_{\rm lo}|\,/\kappa_a = 1$ and ${\tau_d}^{-1}/\kappa_a = 0.25$.

covariances

$$\overline{\mathrm{d}W_x(t)\mathrm{d}W_x(t)} = \overline{\mathrm{d}W_y(t)\mathrm{d}W_y(t)} = \mathrm{d}t\,, \quad \overline{\mathrm{d}W_x(t)\mathrm{d}W_y(t)} = 0\,. \tag{8.39}$$

Substituting in $\mathrm{d}\tilde{q}$ and $\mathrm{d}Z$, we obtain the new SSE for heterodyne detection,

$$\mathrm{d}\left|\bar{\Psi}_c(t)\right\rangle = \left[\frac{1}{\mathrm{i}\hbar}H_{\rm eff}\,\mathrm{d}t + (Ge\,|\mathcal{E}_{\rm lo}|)^{-1}\hat{j}_a\,\mathrm{d}\tilde{q}\right]\left|\bar{\Psi}_c(t)\right\rangle\,, \tag{8.40}$$

with

$$\mathrm{d}\tilde{q} = Ge\,|\mathcal{E}_{\rm lo}|\left[\left\langle\hat{j}_a^\dagger\right\rangle(t)\,\mathrm{d}t + \mathrm{d}Z(t)\right]\,. \tag{8.41}$$

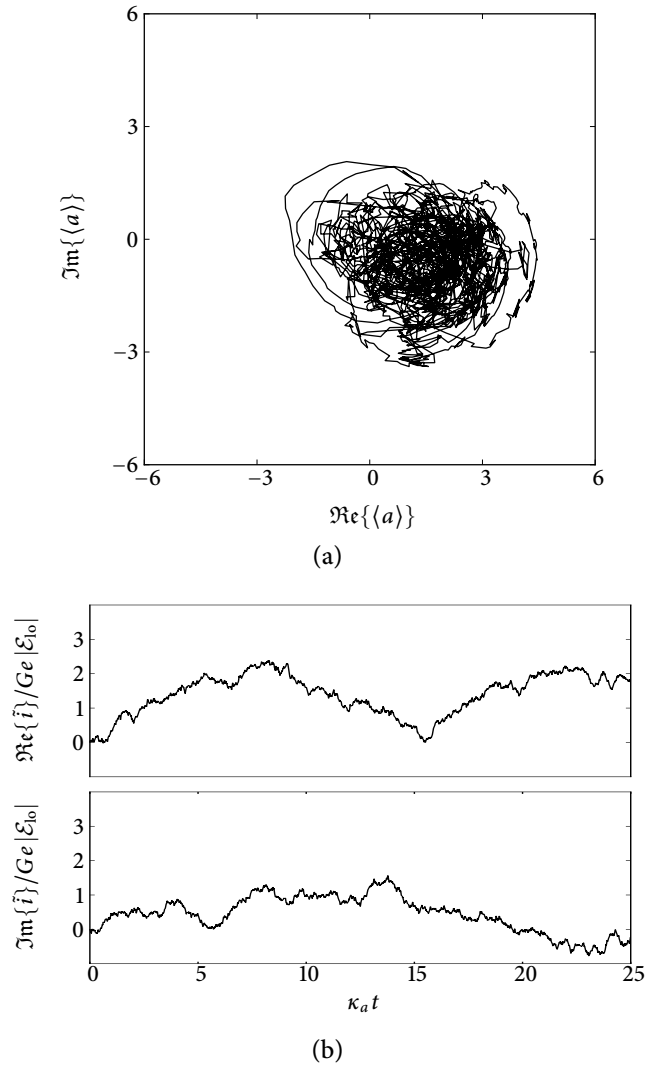

FIGURE 8.8: (a) Monte Carlo simulation of a quantum trajectory with photoelectron counting for the transmon, and heterodyne current records for the transmission line resonator. (b) The filtered heterodyne current record obtained from the same simulation. All parameters are the same as those used in Fig. 8.8.

The stochastic Schrödinger equation (8.40) defines the evolution between quantum jumps due to relaxation of the transmon levels, $\hat{j}_b$. We also define the *filtered heterodyne current* $\tilde{i}(t)$, which satisfies the stochastic differential equation

$$\mathrm{d}\tilde{i} = -\tau_d{}^{-1}(\tilde{i}\mathrm{d}t - \mathrm{d}\tilde{q})\,, \tag{8.42}$$

where $\tau_d{}^{-1}$ is the detection bandwidth. Heterodyne detection provides us, by way of the complex-valued heterodyne current $\tilde{i}(t)$, with a measurement of the complex amplitude of the resonator field. In the presence of shot noise $\mathrm{d}Z$, the detection bandwidth $\tau_d{}^{-1}$ has a substantial effect on the measurement [15].

We perform quantum trajectory simulations, using the stochastic Schrödinger equation (8.40) to generate the evolution between jumps due to $\hat{j}_b$. The SSE is integrated using the Euler

method, and we use pseudorandom numbers to generate $\mathrm{d}Z$. Of course, t is replaced with $\kappa_a t$ throughout due to our use of the dimensionless master equation (8.2). An example trajectory is shown in Fig. 8.7a, and the corresponding time series of the filtered heterodyne current is shown in Fig. 8.7b; a second example is shown in Fig. 8.8. Due to the time-consuming Euler numerical integration we have used in these simulations, the time-scale on which we are able to examine the dynamics of the system is much shorter than that required to clearly see the bimodality in the cavity field. As such, this avenue of investigation remains inconclusive. A clear direction for future investigation is to perform further Monte Carlo simulations of heterodyne current records, or alternatively to implement a higher-order integration method to make simulations on longer time scales numerically tractable.

8.3 Summary

Our semiclassical treatment of the driven transmon-resonator circuit QED system established that, in the semiclassical approximation, the system displays dispersive optical bistability. Inclusion of the quantum fluctuations bears out this conclusion: the Q-functions displayed in Fig. 8.4 demonstrate the bimodality of the cavity field, as do our Monte Carlo simulations of quantum trajectories with photoelectron counting. Figure 8.5, which was obtained from these simulations, shows the mean photon number in the resonator alternating between two metastable states. Our Monte Carlo simulations of quantum trajectories with heterodyne current records, the results of which are shown in Figs. 8.7 and 8.8, remain inconclusive due to numerical constraints.

References

[1] P. Meystre and M. Sargent III. *Elements of Quantum Optics*, chapter 7. Springer-Verlag, second edition, 1991.

[2] R. J. Schoelkopf and S. M. Girvin. Wiring up quantum systems. *Nature*, 451:664–669, 2008.

[3] P. D. Drummond and D. F. Walls. Quantum theory of optical bistability. I: Nonlinear polarisability model. *Journal of Physics A: Mathematical and General*, 13:725–741, 1980.

[4] D. F. Walls and G. J. Milburn. *Quantum Optics*, sections 8.2.3, 9.4 & 13.1. Springer-Verlag, 1994.

[5] M. Tabor. *Chaos and integrability in nonlinear dynamics: An introduction*, section 1.4. Wiley, 1989.

[6] H. J. Carmichael. *Statistical Methods in Quantum Optics 1: Master Equations and Fokker-Planck Equations*. Springer, 1999.

[7] H. J. Carmichael. *Statistical Methods in Quantum Optics 2: Non-Classical Fields*. Springer, 2008.

[8] D. F. Walls and G. J. Milburn. *Quantum Optics*, sections 4.2.3. Springer-Verlag, 1994.

[9] H. J. Carmichael. *Statistical Methods in Quantum Optics 2: Non-Classical Fields*, section 18.2. Springer, 2008.

[10] H. M. Wiseman and G. J. Milburn. Quantum theory of field-quadrature measurements. *Physical Review A*, 47:642–662, 1993.

[11] H. M. Wiseman and G. J. Milburn. Interpretation of quantum jump and diffusion processes illustrated on the Bloch sphere. *Physical Review A*, 47:1652–1666, 1993.

[12] H. J. Carmichael. *An Open Systems Approach to Quantum Optics*. Springer-Verlag, 1993.

[13] H. M. Wiseman. Quantum trajectories and quantum measurement theory. *Quantum and Semiclassical Optics*, 8:205–222, 1996.

[14] C. W. Gardiner. *Handbook of Stochastic Methods*, section 4.2. Springer-Verlag, 1985.

[15] H. J. Carmichael. *Statistical Methods in Quantum Optics 2: Non-Classical Fields*, section 18.2.3. Springer, 2008.

9

Conclusion

In this thesis we have investigated two new directions in cavity quantum electrodynamics: two-mode cavity QED, and circuit QED. We shall summarise our work in each area separately.

Two-mode cavity QED

We have investigated the dynamics of a cavity QED system in which two optical cavity modes with orthogonal linear polarisations interact with a single atom, via an $F = 3 \leftrightarrow F' = 4$ transition. We took into account the full atomic level structure for this transition, including the Zeeman energy shift.

We found that in a certain parameter regime, a semiclassical treatment of the driven mode of the cavity was a good approximation. Treating the driven mode as a complex number reduces the dimensionality of the system Hilbert space, making numerical analysis more tractable. We used numerical integration of the master equation derived from this semiclassical model, along with a standard quantum regression formula, to compute second-order photon correlation functions for the non-driven mode of the cavity. We found that the system displayed quantum beats: interference fringes in the second-order photon correlation function caused by the Larmor precession of the atom in an applied magnetic field. We also extended our treatment of the two-mode cavity QED system to allow for motion of a single atom through the cavity, and performed calculations showing the effect of this motion on the quantum beats.

We simulated the strong driving behaviour of this system, and found that the mean photon number in the non-driven mode of the cavity began to decrease beyond a certain threshold driving field strength. We explained this behaviour qualitatively by way of an analogy to a simple model derived from the Jaynes-Cummings Hamiltonian, involving a two-level atom in a single-mode cavity.

Currently, our work on two-mode cavity QED considers only a single atom interacting with the modes of a cavity. Future work might include an extension of our model to simulate the behaviour of an atomic beam, including multi-atom effects.

Circuit QED

We investigated the emerging field of circuit quantum electrodynamics: an implementation of cavity QED in a superconducting circuit. We considered a specific circuit QED system consisting of a transmission line cavity coupled to a superconducting charge qubit, and starting

from the basic principles of quantum mechanics and electrical circuit theory, we developed the background physics of this circuit QED system.

In the circuit QED system we investigated, the cavity consists of a superconducting wire placed between two ground plates; gaps in the wire are the "mirrors" that define a microwave cavity. The electric fields of the transmission line are coupled to a Josephson charge qubit known as a transmon, which behaves in many ways more similarly to an anharmonic oscillator than a pure qubit. We derived a Hamiltonian for the transmon and considered the nature of its coupling to the transmission line resonator, making connections to the Jaynes-Cummings model of cavity QED. Damping of the circuit QED system was introduced by way of the Lindblad master equation.

As an application of the theory we developed, we investigated dispersive optical bistability in our model of the circuit QED system. A semiclassical treatment, along with a linearised stability analysis, was the first step: this analysis was indicative of optical bistability. We went on to carry out a full quantum treatment, plotting Q-functions to visualise the bimodality of the resonator field. We performed Monte Carlo simulations based on a quantum trajectory unravelling of the master equation. These simulations demonstrated the expected "tunnelling" between metastable states due to quantum fluctuations, confirming optical bistability in the circuit QED system.

As our work on heterodyne measurement of the circuit QED system remains inconclusive, an obvious avenue of future investigation would be to perform further Monte Carlo simulations of heterodyne current records. Based on our other investigations of dispersive optical bistability in the circuit QED system, we would expect to see further evidence of bimodality in the resonator field.

Appendix A

Quantisation of the LC oscillator

An LC circuit, consisting of an inductor L and a capactior C, forms an electrical harmonic oscillator, which can be described quantum-mechanically. We will now outline the quantisation of the LC oscillator, which is analogous to the usual harmonic oscillator quantisation procedure: see, for example, Sakurai [1].

For a lossless parallel LC circuit, such as that depicted in Fig. A.1, the potential differences V across the capacitor and inductor are equal, giving

$$V = \frac{Q}{C} = L\frac{\mathrm{d}J}{\mathrm{d}t}\,, \tag{A.1}$$

where J is the current passing through the inductor. The current passing through the capacitor is $\dot{Q} = -J$. The sign conventions for the voltage and current are as displayed in Fig. A.1. The energy stored in the capacitor is $H_C = \frac{1}{2}CV^2$, while the energy stored in the inductor is $H_L = \frac{1}{2}LJ^2$. Hence, the Hamiltonian for the LC oscillator is given by

$$H = \frac{1}{2}CV^2 + \frac{1}{2}LJ^2\,. \tag{A.2}$$

The charge stored in the capacitor is given by $Q = CV$, and the flux stored in the inductor is $\Phi = LJ$. Thus, the Hamiltonian can be written

$$H = \frac{Q^2}{2C} + \frac{\Phi^2}{2L}\,. \tag{A.3}$$

Differentiating (A.3), we find

$$\frac{\partial H}{\partial Q} = \frac{Q}{C} = L\frac{\mathrm{d}J}{\mathrm{d}t} = \dot{\Phi} \tag{A.4a}$$

$$\frac{\partial H}{\partial \Phi} = \frac{\Phi}{L} = J = -\dot{Q}\,. \tag{A.4b}$$

Equations (A.4) are Hamilton's equations with generalised coordinate Φ and canonical conjugate momentum Q. Because these variables are canonical conjugates, when we replace the classical variables with their corresponding operators, we obtain the commutator

$$\left[\hat{\Phi}, \hat{Q}\right] = \mathrm{i}\hbar\,. \tag{A.5}$$

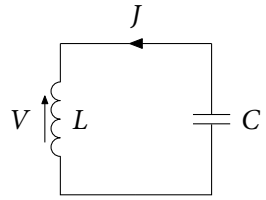

FIGURE A.1: A parallel LC circuit.

The Hamiltonian for a particle moving in a harmonic potential is given by

$$H = \frac{p^2}{2m} + \frac{m\omega^2 x^2}{2}\,. \tag{A.6}$$

Comparison with (A.3) gives us the analogous quantities for the LC oscillator system: $m \leftrightarrow C$ and $\omega \leftrightarrow 1/\sqrt{LC}$. We define photon annihilation and creation operators

$$\hat{a} = \frac{1}{\sqrt{2\hbar Z_0}}\left(\hat{\Phi} + \mathrm{i}Z_0\hat{Q}\right), \tag{A.7a}$$

$$\hat{a}^\dagger = \frac{1}{\sqrt{2\hbar Z_0}}\left(\hat{\Phi} - \mathrm{i}Z_0\hat{Q}\right), \tag{A.7b}$$

where $Z_0 = \sqrt{L/C}$ is the on-resonance impedance of the oscillator. It is easily verified that these operators have the required commutation relation

$$\left[\hat{a}, \hat{a}^\dagger\right] = 1\,. \tag{A.8}$$

It is also simple to show that the LC oscillator Hamiltonian (A.3) can be written

$$H = \hbar\omega\left(\hat{a}^\dagger\hat{a} + \frac{1}{2}\right), \tag{A.9}$$

where $\omega = 1/\sqrt{LC}$.

There is of course a symmetry between the canonical coordinates: we can arrange the sign conventions in the circuit such that the commutator comes out as $\left[\hat{\Phi}, \hat{Q}\right] = -\mathrm{i}\hbar$, giving $x \leftrightarrow Q$ and $p \leftrightarrow \Phi$, but the results are all the same. For further information see, for example, Devoret [2].

References

[1] J. J. Sakurai. *Modern Quantum Mechanics*, section 2.3. Addison-Wesley, revised edition, 1994.

[2] M. H. Devoret. Quantum fluctuations in electrical circuits. In S. Reynaud, E. Giacobino, and J. Zinn-Justin, editors, *Quantum Fluctuations*, pages 351–386. Les Houches (session LXIII, 1995), Elsevier, 1997.

Appendix B

Theory of superconductivity & the Josephson effect

This chapter contains a brief review of the basic theory of superconductivity necessary to understand the content of chapters 6–8. We review the microscopic BCS theory of superconductivity [1–3], as well as the Ginzburg-Landau theory [4]. For further reading on superconductivity, see Tinkham [5], Fossheim and Sudbø [6], Atland and Simons [7].

B.1 BCS theory

Here we briefly describe the microscopic theory of superconductivity, without going into any great mathematical detail. This theory, originally developed by Bardeen, Cooper and Schrieffer [1–3], describes superconductivity as a consequence of the formation of *Cooper pairs*. A Cooper pair is a pair of electrons bound together in a particular manner first described by Cooper [1], who showed that a weak attractive interaction between the electrons can cause pairs of electrons to form bound states. To see how this binding comes about, one may refer to, for example, Tinkham [8].

To see how the phenomenon of superconductivity arises as a result of such pairing, we follow the treatments of Tinkham [9] and Atland and Simons [10]. We adopt a model based on the so-called *pairing Hamiltonian*,

$$H = \sum_{\mathbf{k}\sigma} \epsilon_{\mathbf{k}} \hat{n}_{\mathbf{k}\sigma} + \sum_{\mathbf{kl}} V_{\mathbf{kl}} \hat{c}^{\dagger}_{\mathbf{k}\uparrow} \hat{c}^{\dagger}_{-\mathbf{k}\downarrow} \hat{c}_{-\mathbf{l}\downarrow} \hat{c}_{\mathbf{l}\uparrow} \,, \tag{B.1}$$

which should be interpreted as describing the physics of a thin shell of states centred around the Fermi surface, comprising electrons paired as $(\mathbf{k}\uparrow, -\mathbf{k}\downarrow)$. The creation operator $\hat{c}^{\dagger}_{\mathbf{k}\uparrow}$ creates an electron of momentum $\mathbf{k}$ and spin up. The number operator is given by $\hat{n}_{\mathbf{k}\sigma} = \hat{c}^{\dagger}_{\mathbf{k}\sigma}\hat{c}_{\mathbf{k}\sigma}$, where σ labels the spin index.

The Fermi sea is unstable against the formation of a bound Cooper pair. As more Cooper pairs condense, the state of the system will eventually become so greatly changed that the binding energy for an additional pair will go to zero, and the system will reach an equilibrium. We assume therefore that the so-called *BCS ground state* $|\psi_G\rangle$, which describes the state of the system at this equilibrium point, contains a macroscopic number of Cooper pairs. Thus, operators such as $\hat{c}_{-\mathbf{k}\downarrow}\hat{c}_{\mathbf{k}\uparrow}$ have nonzero expectation values in $|\psi_G\rangle$, and we define

$$b_{\mathbf{k}} = \langle \psi_G | \hat{c}_{-\mathbf{k}\downarrow} \hat{c}_{\mathbf{k}\uparrow} | \psi_G \rangle \,, \quad b^{*}_{\mathbf{k}} = \left\langle \psi_G \middle| \hat{c}^{\dagger}_{\mathbf{k}\uparrow} \hat{c}^{\dagger}_{-\mathbf{k}\downarrow} \middle| \psi_G \right\rangle \,. \tag{B.2}$$

We substitute

$$\hat{c}_{-\mathbf{k}\downarrow}\hat{c}_{\mathbf{k}\uparrow} = b_{\mathbf{k}} + \underbrace{\hat{c}_{-\mathbf{k}\downarrow}\hat{c}_{\mathbf{k}\uparrow} - b_{\mathbf{k}}}_{\text{small}} \tag{B.3}$$

and its Hermitian conjugate into the pairing Hamiltonian (B.1), neglecting quantities bilinear in the small fluctuation term. Adding in a chemical potential term, which is equivalent to taking the zero of kinetic energy to be at the level of the Fermi surface, gives the *model Hamiltonian*

$$H_M = H - \mu\hat{N} \approx \sum_{\mathbf{k}\sigma} \xi_{\mathbf{k}}\hat{n}_{\mathbf{k}\sigma} + \sum_{\mathbf{kl}} V_{\mathbf{kl}}\left(\hat{c}^{\dagger}_{\mathbf{k}\uparrow}\hat{c}^{\dagger}_{-\mathbf{k}\downarrow}b_{\mathbf{l}} + b^{*}_{\mathbf{k}}\hat{c}_{-\mathbf{l}\downarrow}\hat{c}_{\mathbf{l}\uparrow} - b^{*}_{\mathbf{k}}b_{\mathbf{l}}\right), \tag{B.4}$$

where $\xi_{\mathbf{k}} \equiv \epsilon_{\mathbf{k}} - \epsilon_F$ and $\hat{N}$ is the total particle-number operator. Furthermore, we can define

$$\Delta_{\mathbf{k}} = -\sum_{\mathbf{l}} V_{\mathbf{kl}}b_{\mathbf{l}}, \tag{B.5}$$

and substitute (B.5) into (B.4) to obtain

$$H_M = \sum_{\mathbf{k}}\left[\xi_{\mathbf{k}}\sum_{\sigma}\hat{c}^{\dagger}_{\mathbf{k}\sigma}\hat{c}_{\mathbf{k}\sigma} - \left(\Delta_{\mathbf{k}}\hat{c}^{\dagger}_{\mathbf{k}\uparrow}\hat{c}^{\dagger}_{-\mathbf{k}\downarrow} + \Delta^{*}_{\mathbf{k}}\hat{c}_{-\mathbf{k}\downarrow}\hat{c}_{\mathbf{k}\uparrow} - \Delta_{\mathbf{k}}b^{*}_{\mathbf{k}}\right)\right]. \tag{B.6}$$

The Hamiltonian (B.6) may be diagonalised by a suitable unitary transformation,[1] which involves the definition of new Fermi operators $\hat{\alpha}_{\mathbf{k}\sigma}$. The creation operators $\hat{\alpha}^{\dagger}_{\mathbf{k}\sigma}$ create elementary excitations known as *Bogoliubov quasi-particles*; the corresponding quasi-particle annihilation operators annihilate the BCS ground state. This diagonalisation yields the transformed model Hamiltonian

$$H_M = \sum_{\mathbf{k}\sigma}\lambda_{\mathbf{k}}\hat{\alpha}^{\dagger}_{\mathbf{k}\sigma}\hat{\alpha}_{\mathbf{k}\sigma} + \sum_{\mathbf{k}}\left(\xi_{\mathbf{k}} - \lambda_{\mathbf{k}} + \Delta_{\mathbf{k}}b^{*}_{\mathbf{k}}\right), \tag{B.7}$$

where

$$\lambda_{\mathbf{k}} \equiv \left(|\Delta_{\mathbf{k}}|^2 + \xi^2_{\mathbf{k}}\right)^{1/2}. \tag{B.8}$$

The second term in (B.7) is a constant, while the first gives the increase in energy above the ground state in terms of the number operators $\hat{\alpha}^{\dagger}_{\mathbf{k}\sigma}\hat{\alpha}_{\mathbf{k}\sigma}$ for the Bogoliubov quasi-particles. The energy of an elementary excitation of momentum $\hbar\mathbf{k}$ is $\lambda_{\mathbf{k}}$, given by (B.8). As such, $\Delta_{\mathbf{k}}$ plays the role of an *energy gap* – a minimum excitation energy – since even at the surface of the Fermi sphere, where $\xi_{\mathbf{k}} = 0$, the excitation energy $\lambda_{\mathbf{k}} = |\Delta_{\mathbf{k}}| > 0$. It is easy enough to determine the temperature-dependence of the energy gap $\Delta(T)$, but in the interest of brevity we shall not do so here. If the energy gap is larger than the thermal energy of the lattice, the Cooper pair fluid is not scattered by the lattice and can flow without dissipation, resulting in superconductivity.

The *critical temperature* T_c is the temperature at which the energy gap $\Delta(T) \to 0$. In this case, $\lambda_{\mathbf{k}} \to |\xi_{\mathbf{k}}|$ and the excitation spectrum is the same as in the normal, non-superconducting

[1] See Bogoliubov [11, 12], Valatin [13], or Tinkham [14] and references therein.

state. Values for the critical temperature derived using the BCS theory of superconductivity have been closely verified by experiment [15].

Not all superconductors are thought to be described by the microscopic BCS theory. BCS theory places an upper limit on the critical temperature T_c of about 30 K, but in 1986 the first high-T_c superconductor was discovered [16]. High-T_c superconductors possess critical temperatures far exceeding 30 K. The mechanism underlying high-temperature superconductivity remains unknown.

B.2 Ginzburg-Landau theory

The microscopic BCS theory treated in section B.1 is a highly successful theory in those cases where it is applicable, that is, those in which the energy gap Δ is constant in space. The Ginzburg-Landau (GL) theory is a more macroscopic theory of superconductivity which is useful in situations where the BCS theory becomes cumbersome [4]. The theory was originally proposed as having a phenomenological foundation: a pseudowavefunction $\psi(\mathbf{r})$ was introduced as a complex order parameter, with $|\psi(\mathbf{r})|^2$ originally thought to represent the local density of superconducting electrons, $\rho_s(\mathbf{r})$.

Gor'kov subsequently showed that the GL theory was derivable as a limiting case of the microscopic theory, generalised to the spatially inhomogeneous regime [17]. It turns out that $\psi(\mathbf{r})$ is directly proportional to the gap parameter $\Delta(\mathbf{r})$.[2]

B.2.1 The phenomenological approach

The basic postulate of the phenomenological GL theory is that near the superconducting transition (that is, near T_c), and for small ψ that varies slowly in space, the free energy F of the superconductor has the form (in SI units)

$$F = F_n + \alpha |\psi|^2 + \frac{\beta}{2} |\psi|^4 + \frac{1}{2m'} \left| \left(-i\hbar\nabla - e'\mathbf{A}\right) \psi \right|^2 + \frac{|\mathbf{B}|^2}{2\mu_0}, \tag{B.9}$$

where F_n is the free energy in the normal phase (absent any magnetic fields), $\mathbf{A}$ is the electromagnetic vector potential, and $\mathbf{B} = \nabla \times \mathbf{A}$ [19, 20]. The term $|B|^2 / 2\mu_0$ represents the magnetic field energy in the vacuum. The values of the mass m' and charge e' were not initially known.

In the absence of any external fields or gradients in ψ, from (B.9) we have

$$F - F_n = \alpha |\psi|^2 + \frac{\beta}{2} |\psi|^4 , \tag{B.10}$$

from which we can tell that in order for the free energy to have a minimum for finite ψ, β must always be positive. On the other hand, α can be either positive or negative. If $\alpha > 0$, the minimum free energy occurs at $|\psi|^2 = 0$, corresponding to the normal, non-superconducting state. If $\alpha < 0$, corresponding to the superconducting state, the minimum occurs when

[2] For an accessible microscopic derivation of the Ginzburg-Landau differential equations, using Green's functions, see Fetter and Walecka [18].

$|\psi|^2 = |\psi_\infty|^2 = -\alpha/\beta$. Here ψ_∞ represents the order parameter infinitely deep within the superconductor, where it is screened from any surface fields or currents. Thus, $\alpha(T)$ must change from positive to negative at the critical temperature T_c.

The parameters e' and m' respectively represent the charge and mass of the superconducting charge carriers. From the microscopic pairing theory of superconductivity, we now know that the charge carriers are Cooper pairs, with charge $e' = 2e$. The effective mass can be taken to be $m' = 2m$.

We would also like to define the density of superconducting charge carriers $\rho_s' = \frac{1}{2}\rho_s = |\psi|^2$ where ρ_s as before is the density of superconducting electrons, but in real metals, the situation can be substantially more complicated, and fixing $m' = 2m$ sometimes means that ρ_s' can no longer be interpreted as a particle density. It is conventional, however, to simply take $m' = 2m$ without worrying about the details of real metals and dirty superconductors; see Tinkham [21] for details.

B.2.2 The Ginzburg-Landau differential equations

When external fields or currents are imposed on the superconductor, $\psi(\mathbf{r}) = |\psi(\mathbf{r})|\,\mathrm{e}^{\mathrm{i}\varphi(\mathbf{r})}$ and the vector potential $\mathbf{A}(\mathbf{r})$ adjust themselves to minimise the overall free energy. As such, we must minimise the total free energy with respect to both of the parameters mentioned above. Using the free energy F from (B.9), we set

$$\mathcal{F} = \int F \,\mathrm{d}\mathbf{r}\,, \tag{B.11}$$

where the integration runs over the volume of the superconductor, and vary $\psi(\mathbf{r})$ by $\delta\psi(\mathbf{r})$ and $\mathbf{A}(\mathbf{r})$ by $\delta\mathbf{A}(\mathbf{r})$. The variation in the free energy is thus given by

$$\begin{aligned}\delta\mathcal{F} = \int \mathrm{d}\mathbf{r} \left\{ \delta\psi^* \left[\alpha\psi + \beta\,|\psi|^2\,\psi + \frac{1}{2m'}\left(-\mathrm{i}\hbar\nabla - e'\mathbf{A}\right)^2 \psi \right] + \text{c.c.} \right\} \\ + \int \mathrm{d}\mathbf{r}\; \delta\mathbf{A} \cdot \left\{ \frac{1}{\mu_0}\nabla\times\mathbf{B} - \frac{e'}{2m'}\left[\psi^*\left(-\mathrm{i}\hbar\nabla - e'\mathbf{A}\right)\psi + \text{c.c.}\right] \right\}, \end{aligned} \tag{B.12}$$

where it has been assumed that no current passes through the boundary, giving the boundary condition

$$\left(-\mathrm{i}\hbar\nabla - e'\mathbf{A}\right)\psi\big|_{\hat{\mathbf{n}}} = 0\,, \tag{B.13}$$

and where surface contributions have been neglected, and integration by parts has been performed. Setting $\delta\mathcal{F} = 0$, and using Maxwell's equation $\nabla\times\mathbf{B} = \mu_0\mathbf{J}$ (with negligible displacement current, for example when $\mathbf{E} = 0$) we obtain from (B.12) the *Ginzburg-Landau differential*

equations:

$$\alpha\psi + \beta\left|\psi\right|^2\psi + \frac{1}{2m'}\left(-\mathrm{i}\hbar\nabla - e'\mathbf{A}\right)^2\psi = 0\,, \tag{B.14}$$

$$\mathbf{J} = -\mathrm{i}\hbar\frac{e'}{2m'}\left(\psi^*\nabla\psi - \psi\nabla\psi^*\right) - \frac{e'^2}{m'}\left|\psi\right|^2\mathbf{A}\,. \tag{B.15}$$

For more details of the above calculation, see Fossheim and Sudbø [6], de Gennes [22], or Landau et al. [23].

The first Ginzburg-Landau equation (B.14) has a form similar to the time-independent Schrödinger equation for a particle of mass m' and charge e' in an electromagnetic field, aside from the nonlinear term; the second equation (B.15) is the usual quantum-mechanical expression for a current of such particles [24].

Consider the first Ginzburg-Landau equation (B.14). In the simplified case where no fields are present and as such $\mathbf{A} = 0$, the GL equation (B.14) becomes

$$-\frac{\hbar^2}{2m'}\nabla^2\psi + \alpha\psi + \beta\left|\psi\right|^2\psi = 0\,, \tag{B.16}$$

We now write $\psi(\mathbf{r}) = \left|\psi(\mathbf{r})\right|\mathrm{e}^{\mathrm{i}\varphi(\mathbf{r})}$, and introduce the normalised wavefunction

$$f(\mathbf{r}) = \left|\psi(\mathbf{r})\right| / \left|\psi_\infty\right|\,, \tag{B.17}$$

where $\left|\psi_\infty\right|^2 = -\alpha/\beta > 0$ in the superconducting state, and thus $\left|\psi_\infty\right| = \left(\left|\alpha\right|/\beta\right)^{1/2}$. After a few manipulations, (B.16) becomes

$$\xi^2(T)\nabla^2 f(\mathbf{r}) + f(\mathbf{r}) - f(\mathbf{r})^3 = 0\,, \tag{B.18}$$

where

$$\xi^2(T) = \frac{\hbar^2}{2m'\left|\alpha(T)\right|}\,, \tag{B.19}$$

$\xi(T)$ being a characteristic length known as the Ginzburg-Landau coherence length.

B.3 Flux quantisation

Suppose that some region of a superconductor is in the normal, non-superconducting state. In order for the order parameter $\psi = \left|\psi\right|\mathrm{e}^{\mathrm{i}\varphi}$ to be single-valued, the phase φ must change by integral multiples of 2π in making a complete circuit of the normal region. More specifically, the line integral of the gradient $\nabla\varphi$ around a closed contour C enclosing the normal domain must be equal to an integral multiple of 2π, that is

$$\oint_C \nabla\varphi\cdot\mathrm{d}\mathbf{s} = 2\pi N\,, \quad N \in \mathbb{Z}\,. \tag{B.20}$$

In the presence of a magnetic field, this is slightly modified. The magnetic field couples to the superconducting order parameter via the vector potential **A**, so as to modify the phase of the order parameter according to the usual minimal coupling scheme [24]. The resulting gauge-invariant phase of the order parameter has gradient given by

$$\nabla\varphi \to \nabla\varphi - \frac{e'}{\hbar}\mathbf{A}\,. \tag{B.21}$$

The condition for the order parameter to be single-valued now becomes

$$\oint_C \left(\nabla\varphi - \frac{e'}{\hbar}\mathbf{A}\right)\cdot \mathrm{d}\mathbf{s} = 2\pi N\,. \tag{B.22}$$

In the case where the region of the superconductor in question would otherwise be in the superconducting state, and the normal state results entirely from the magnetic flux passing through the superconductor, we obtain the relation

$$\frac{2\pi}{\Phi_0}\oint_C \mathbf{A}\cdot \mathrm{d}\mathbf{s} = 2\pi N\,, \tag{B.23}$$

where we have defined the flux quantum, $\Phi_0 = h/2e$, and used $e' = 2e$. The flux through the surface S enclosed by the contour C is known as the *fluxoid*, denoted Φ, and is given by

$$\Phi = \int_S \mathbf{B}\cdot \mathrm{d}\mathbf{a} = \int_S (\nabla\times\mathbf{A})\cdot \mathrm{d}\mathbf{a}\,. \tag{B.24}$$

Using Stokes' theorem, we obtain

$$\Phi = \oint_C \mathbf{A}\cdot \mathrm{d}\mathbf{s} = N\Phi_0\,, \tag{B.25}$$

demonstrating the quantisation of flux. It is clear that $\Phi = 0$ for any path which encloses no hole but only superconducting material. For further reading see Fossheim and Sudbø [25], Tinkham [26].

B.4 The Josephson effect

The maximum dissipationless supercurrent that a superconductor can support is known as the *critical current* J_c. Whenever two strongly superconducting electrodes are brought into contact in such a way that the critical current in the contact region is much lower than that of the individual constituents, the contact is called a *weak link* [27, 28].

Josephson [29, 30, 31] predicted in 1962 that such a junction should be able to sustain a supercurrent without the application of a voltage, and furthermore that if a voltage difference were to be maintained across the junction, high frequency electromagnetic waves would be radiated.

The Josephson effect can be described starting from the microscopic pairing theory of superconductivity. However, we will not do so here. A good description of the microscopic

theory of the Josephson effect is available in Ketterson and Song [32], and of course in the original papers [29, 33–35].

B.4.1 DC Josephson effect

As the Josephson effect is a general property of weak links, it can be derived from the Ginzburg-Landau theory by considering a simple special case. We consider two superconducting electrodes separated by a short, one-dimensional link of length $L \ll \xi$, all of the same superconductor. From (B.18) we know that the one-dimensional GL equation describing the link can be written as

$$\xi^2 \frac{\mathrm{d}^2}{\mathrm{d}z^2} f(z) + f(z) - f(z)^3 = 0\,. \tag{B.26}$$

We can assume without loss of generality that the massive electrodes are in equilibrium, and that $|f| = 1$ in both of them (from the definition of ψ_∞); however the phases of the order parameters may differ by a phase γ. As such, the solution of (B.26) should match the boundary conditions $f = 1$ at $z = 0$ and $f = \mathrm{e}^{\mathrm{i}\gamma}$ at $x = L$. As noted by Aslamazov and Larkin [36], so long as $L \ll \xi$, the first term in (B.26) dominates due to the fact that it is larger than the other two terms by a factor which scales with $(\xi/L)^2$ for any nonzero γ. In this limit, the problem reduces to Laplace's equation in one dimension $\mathrm{d}^2 f(z)/\mathrm{d}z^2 = 0$, which has general solution $f(z) = A + Bz$. Applying the boundary conditions at both ends of the bridge, we obtain the solution for the order paramter in the bridge,

$$f(z) = 1 + \frac{\mathrm{e}^{\mathrm{i}\gamma} - 1}{L} z\,. \tag{B.27}$$

Substitution of (B.27) into the one-dimensional version of the Ginzburg-Landau current equation (B.15), again in the case where no fields are present, gives

$$J = J_c \sin\gamma\,, \tag{B.28}$$

with the critical current J_c given by

$$J_c = \frac{e'\hbar\,|\psi_\infty|^2}{m'} \frac{\mathcal{A}}{L}\,, \tag{B.29}$$

where $\mathcal{A}$ is the cross-sectional area of the superconducting link. The relation (B.28) is known as the *DC Josephson current-phase relation*; it tells us that a supercurrent is driven across the weak link separating the two superconductors simply by the difference in the phase of the superconducting order parameter across the barrier.

B.4.2 AC Josephson effect

Consider a Josephson junction in a magnetic field $\mathbf{B} = \nabla \times \mathbf{A}$. To derive the form of the AC Josephson current which arises in the presence of a potential difference across the barrier,

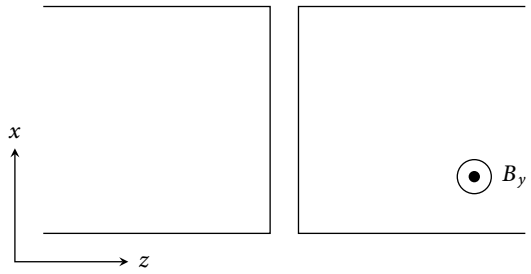

FIGURE B.1: Schematic depiction of a tunnel junction – a type of weak link – in the presence of a magnetic field.

we need to take into account the role of the vector potential **A**. Therefore, we need to use a gauge-invariant form of the phase difference across the junction, which – as we noted in section B.3 – is given by

$$\nabla\varphi - \frac{2e}{\hbar}\mathbf{A} = \nabla\varphi - \frac{2\pi}{\Phi_0}\mathbf{A}\,. \tag{B.30}$$

To obtain the gauge-invariant phase difference between the two sides ("right" and "left") of the junction, we integrate from left to right and get

$$\gamma_{\mathrm{l}\to\mathrm{r}} = \int_{\mathrm{l}}^{\mathrm{r}} \left(\nabla\varphi - \frac{2\pi}{\Phi_0}\mathbf{A}\right)\cdot \mathrm{d}\mathbf{s}\,. \tag{B.31}$$

Adopting the geometry depicted in Fig. B.1, we consider the case where $\mathbf{A} = A_z(x)\hat{\mathbf{z}}$, which corresponds to placing the magnetic field **B** parallel to the contact plane, and pointing along the y-axis, with $\mathbf{B} = B_y(x)\hat{\mathbf{y}}$ and $B_y(x) = \partial A_z/\partial x$.

On integration of (B.31) we obtain

$$\gamma \equiv \gamma_{\mathrm{l}\to\mathrm{r}} = (\varphi_{\mathrm{r}} - \varphi_{\mathrm{l}}) - \frac{2\pi}{\Phi_0}\int_{\mathrm{l}}^{\mathrm{r}} A_z\,\mathrm{d}z\,, \tag{B.32}$$

where φ_{r} and φ_{l} are fixed phases which exist in the absence of any AC current or applied voltage.[3] For later convenience, we define $\gamma_0 = \varphi_{\mathrm{r}} - \varphi_{\mathrm{l}}$.

Note that in the Coulomb gauge the transverse component of the electric field is given by $\mathbf{E}_{\mathrm{T}} = -\partial\mathbf{A}/\partial t$ [37]. Taking the time derivative of (B.32), we find, using $E_z = -\partial A_z/\partial t$,

$$\begin{aligned}\frac{\partial}{\partial t}\gamma &= -\frac{2\pi}{\Phi_0}\int_{\mathrm{l}}^{\mathrm{r}}\frac{\partial}{\partial t}A_z\,\mathrm{d}z = \frac{2\pi}{\Phi_0}\int_{\mathrm{l}}^{\mathrm{r}} E_z\,\mathrm{d}z \\ &= \frac{2\pi}{\Phi_0}V \equiv \omega_J\,,\end{aligned} \tag{B.33}$$

where ω_J is known as the *Josephson frequency*. The relation (B.33) demonstrates that the Josephson junction emits electromagnetic radiation at the Josephson frequency; integrating

[3] Even though the phases in the two electrodes comprising the junction, and within the junction itself, are not well defined, we can write the integral of the gradient as the difference between the phases of the endpoints (by the second fundamental theorem of calculus), and neglect any $2\pi N$ contribution, which will of course not affect the order parameter itself.

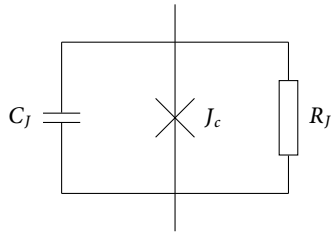

FIGURE B.2: Equivalent circuit of the RCSJ model. The ideal Josephson junction, depicted as a cross, is described by (B.35).

this relation gives

$$\gamma = \gamma_0 + \omega_J t\,. \tag{B.34}$$

Substitution of (B.34) into the previously obtained Josephson current relation (B.28) gives

$$J = J_c \sin\left(\gamma_0 + \omega_J t\right)\,. \tag{B.35}$$

It is this oscillatory supercurrent which generates the electromagnetic radiation.

B.4.3 The RCSJ model

A physical Josephson junction can be modelled by an idealised description known as the RCSJ (resistively and capacitively shunted junction) model. In the RCSJ model, the physical junction is modelled by an ideal junction described by (B.35), shunted by a resistance R_J and a capacitance C_J (the term "shunted" refers to components placed in parallel), as depicted in Fig. B.2. The resistance R_J builds in dissipation[4] in the finite voltage regime (that is, when a voltage V is applied across the junction) without affecting the lossless DC regime (zero voltage) described in (B.28) – see section B.4.1. The capacitance C_J takes into account the geometric capacitance between the electrodes, rather than the capacitance of the electrodes to ground.

In the RCSJ model, the time dependence of the phase γ in the presence of an external bias current J is given by the current through each of the three parallel channels seen in Fig. B.2, giving

$$J = J_c \sin\gamma + \frac{V}{R_J} + C_J\frac{\mathrm{d}V}{\mathrm{d}t}\,. \tag{B.36}$$

We already know from (B.33) that in the presence of a potential difference V across the junction, γ evolves in time according to $\dot{\gamma} = 2\pi V/\Phi_0$; substitution for V in (B.36) yields a second-order differential equation for γ. We obtain

$$\frac{\mathrm{d}^2\gamma}{\mathrm{d}\tau^2} + \mathcal{Q}^{-1}\frac{\mathrm{d}\gamma}{\mathrm{d}\tau} + \sin\gamma = \frac{J}{J_c}\,, \tag{B.37}$$

[4]See Tinkham [38] and references therein for a discussion of why this is the *only* dissipation term present in the model.

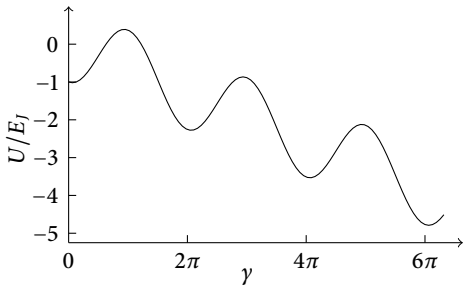

FIGURE B.3: The tilted-washboard potential, with $J/J_c = 0.2$.

where we have defined $\tau = \omega_p t$, with ω_p – the *plasma frequency* of the junction – given by

$$\omega_p = \left(\frac{2\pi J_c}{\Phi_0 C_J} \right)^{\frac{1}{2}} ; \tag{B.38}$$

the quality factor of the junction $\mathcal{Q}$ is given by

$$\mathcal{Q} = \omega_p R_J C_J . \tag{B.39}$$

In the case where the junction is dissipationless (or approximately so), we can neglect the resistor channel in the RCSJ equivalent circuit (Fig. B.2) (which is equivalent to letting $R_J \to \infty$) causing the terms in (B.36) and (B.37) involving R^{-1} and $\mathcal{Q}^{-1}$ respectively to drop out. We refer to this set-up as the *capacitively shunted junction*, or CSJ model.

B.4.4 The tilted-washboard model

The equation of motion (B.37) can be written

$$C_J \left(\frac{\Phi_0}{2\pi} \right)^2 \frac{\mathrm{d}^2\gamma}{\mathrm{d}t^2} = -\frac{1}{R_J} \left(\frac{\Phi_0}{2\pi} \right)^2 \frac{\mathrm{d}\gamma}{\mathrm{d}t} - \frac{\partial}{\partial\gamma} U(\gamma) , \tag{B.40}$$

where

$$U(\gamma) = -E_J \left(\cos\gamma + \frac{J}{J_c}\gamma \right) , \tag{B.41}$$

and $E_J \equiv J_c(\Phi_0/2\pi)$ is the Josephson coupling energy.

The form (B.40) is the same as the equation of motion of a particle of effective mass $C_J(\Phi_0/2\pi)^2$ moving along the γ axis in an effective potential $U(\gamma)$, and subject to a viscous drag force $-R_J^{-1}(\Phi_0/2\pi)^2\dot{\gamma}$. The potential $U(\gamma)$ has the form of a "tilted washboard", as we see in Fig. B.3.

The significance of J_c is that when $J < J_c$, the potential has local minima in which the motion of γ can be localised, and bound states exist. When $J = J_c$, the local minima become points of inflection, so that for $J \gtrsim J_c$, no stable equilibrium points and thus no bound states exist.

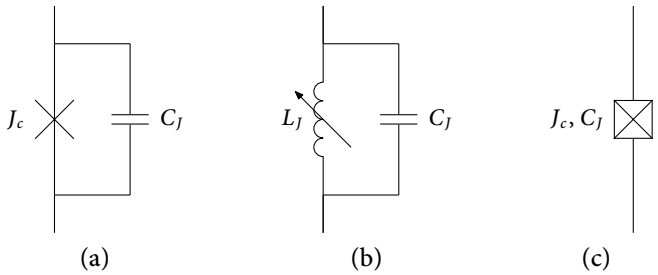

FIGURE B.4: Three different ways of depicting the CSJ (capacitively shunted junction) model of a physical Josephson junction.

B.4.5 The Josephson junction as a nonlinear inductor

Taking the time derivative of (B.28) yields

$$\frac{\mathrm{d}J}{\mathrm{d}t} = J_c \cos\gamma \frac{\partial\gamma}{\partial t}\,, \tag{B.42}$$

and combining the above result with (B.33) gives

$$\frac{\mathrm{d}J}{\mathrm{d}t} = V\frac{2\pi J_c}{\Phi_0}\cos\gamma\,. \tag{B.43}$$

The time-varying voltage across an inductor with inductance L is given by [39]

$$V = -L\frac{\mathrm{d}J}{\mathrm{d}t}\,, \tag{B.44}$$

which then leads to the inductance of the Josephson junction

$$|L_J| = \frac{\Phi_0}{2\pi}\frac{1}{J_c\cos\gamma} = \frac{\Phi_0}{2\pi}\left(J_c^2 - J^2\right)^{-1/2}\,. \tag{B.45}$$

As we can see, the Josephson junction behaves as a nonlinear inductor. A capacitively shunted junction (CSJ) will have a resonant frequency

$$\omega(J) = \frac{1}{\sqrt{L_J C_J}} = \left(\frac{2\pi J_c}{\Phi_0 C_J}\right)^{1/2}\left(1 - \frac{J^2}{J_c^2}\right)^{1/4}\,. \tag{B.46}$$

Compare the above with the plasma frequency of the junction ω_p, from (B.38).

B.5 SQUID devices

B.5.1 The DC SQUID

A DC SQUID (superconducting quantum interference device) employs a geometry with two Josephson junctions in parallel, forming a loop structure – such a circuit is depicted schematically in Fig. B.5a. We consider this geometry in the following section.

In the case where the *magnitude* of the superconducting order parameter $\psi(\mathbf{r})$ does not vary with position, we can write $\psi(\mathbf{r}) = |\psi| \, \mathrm{e}^{\mathrm{i}\varphi(\mathbf{r})}$. As such, the Ginzburg-Landau current relation (B.15) becomes

$$\mathbf{J} = \frac{e}{m} |\psi|^2 \left(\hbar \nabla \varphi - 2e\mathbf{A} \right) . \tag{B.47}$$

We consider a contour inside the two-junction DC SQUID loop, deep enough within the superconducting material that the supercurrent can be taken to be *zero*.[5] Thus, we obtain

$$\nabla \varphi - 2\pi \Phi_0^{-1} \mathbf{A} = 0 . \tag{B.48}$$

Integrating around the contour described above, we obtain

$$\gamma_1 - \gamma_2 = 2\pi \Phi_0^{-1} \oint \mathbf{A} \cdot \mathrm{d}\mathbf{s} = 2\pi \frac{\Phi}{\Phi_0} \pmod{2\pi} , \tag{B.49}$$

where γ_1 and γ_2 are the respective phase differences across the two junctions, and Φ is the flux in the DC SQUID loop.

The total current J in the lumped DC SQUID can be written as a sum of the currents across the junctions 1 and 2, which are taken to have identical critical currents, giving

$$\begin{aligned} J &= J_c \sin \gamma_1 + J_c \sin \gamma_2 \\ &= 2J_c \cos \left(\pi \frac{\Phi}{\Phi_0} \right) \sin \left(\gamma_2 + \pi \frac{\Phi}{\Phi_0} \right) . \end{aligned} \tag{B.50}$$

The relation (B.49) implies that the phases γ_1 and γ_2 cannot both have the value $\pi/2$, which would give the total current in the lumped circuit element a maximum value of $2J_c$. In reality, the relation (B.50) means that the maximum value of J is given by

$$J_{\max} = 2J_c \left| \cos \left(\pi \Phi / \Phi_0 \right) \right| . \tag{B.51}$$

From (B.37), we find that for a resistively shunted junction for which the geometric capacitance C_J is small so that the quality factor $\mathcal{Q} \ll 1$, the equation of motion of the phase difference across the junction reduces to the first-order differential equation

$$\frac{\mathrm{d}\gamma}{\mathrm{d}t} = \frac{2e}{\hbar} R_J J_c \left(\frac{J}{J_c} - \sin \gamma \right) . \tag{B.52}$$

Integrating the above equation yields the analytic solution[6]

$$J \tan \frac{\gamma}{2} = J_c + \frac{V_0}{R_J} \tan \frac{\omega_{J0} t}{2} , \tag{B.53}$$

[5] This is a reasonable assumption providing the superconducting material forming the junction is thicker than the penetration depth of the flux into the junction. See Tinkham [40], Fossheim and Sudbø [41].

[6] For more information, see Waldram [42, 43].

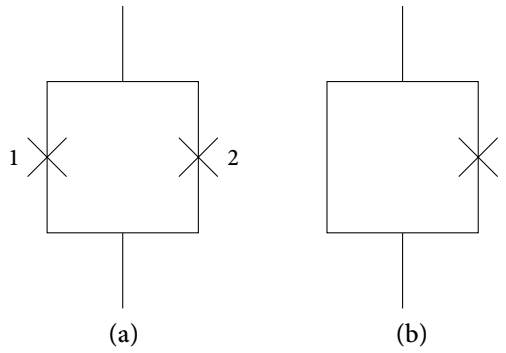

FIGURE B.5: Schematic diagram of (a) a DC SQUID, and (b) a RF SQUID.

where $\omega_{J0} \equiv 2\pi V_0/\Phi_0$, and

$$V_0 = R_J\sqrt{J^2 - J_c^2} \tag{B.54}$$

is the time-averaged voltage across the lumped DC SQUID circuit element. Thus, from (B.51) and (B.54) we obtain an approximate relation for the average DC voltage across the DC SQUID,

$$V = \frac{R}{2}\sqrt{J^2 - \left[2J_c\cos\left(\pi\Phi/\Phi_0\right)\right]^2}\,, \tag{B.55}$$

where $R/2$ is the resistance of the two resistively shunted junctions in parallel. This relation tells us that the DC SQUID is a flux-to-voltage transducer.

For more information about the DC SQUID, see Fossheim and Sudbø [44], Tinkham [45], and references therein.

B.5.2 The RF SQUID

An RF SQUID, depicted schematically in Fig. B.5b, consists of a loop interrupted by a single Josephson junction. The Josephson element is shorted by the loop when DC current is passed through the device, so the single-junction SQUID must be monitored using an RF current coupled into the SQUID loop. For more information about the RF SQUID, and its practical operation, see Tinkham [46].

References

[1] L. N. Cooper. Bound electron pairs in a degenerate fermi gas. *Physical Review*, 104: 1189–1190, 1956.

[2] J. Bardeen, L. N. Cooper, and J. R. Schrieffer. Microscopic theory of superconductivity. *Physical Review*, 106:162–164, 1957.

[3] J. Bardeen, L. N. Cooper, and J. R. Schrieffer. Theory of superconductivity. *Physical Review*, 108:1175–1204, 1957.

[4] L. D. Landau. On the theory of superconductivity. In D. ter Haar, editor, *Men of physics: L. D. Landau*, pages 138–167. Pergamon Press, 1965.

[5] M. Tinkham. *Introduction to Superconductivity*. McGraw-Hill, second edition, 1996.

[6] K. Fossheim and A. Sudbø. *Superconductivity: Physics and Applications*. John Wiley and Sons, 2004.

[7] A. Atland and B. Simons. *Condensed Matter Field Theory*. Cambridge University Press, 2006.

[8] M. Tinkham. *Introduction to Superconductivity*, sections 3.1 & 3.2. McGraw-Hill, second edition, 1996.

[9] M. Tinkham. *Introduction to Superconductivity*, section 3.5. McGraw-Hill, second edition, 1996.

[10] A. Atland and B. Simons. *Condensed Matter Field Theory*, sections 6.4.1-3. Cambridge University Press, 2006.

[11] N. N. Bogoliubov. On a new method in the theory of superconductivity. *Il Nuovo Cimento*, 7:794–805, 1958.

[12] N. N. Bogoliubov. A new method in the theory of superconductivity. *Soviet Physics – Journal of Experimental and Theoretical Physics*, 7:41–46, 1958.

[13] J. G. Valatin. Comments on the theory of superconductivity. *Il Nuovo Cimento*, 7:843–857, 1958.

[14] M. Tinkham. *Introduction to Superconductivity*, page 60. McGraw-Hill, second edition, 1996.

[15] M. Tinkham. *Introduction to Superconductivity*, page 63. McGraw-Hill, second edition, 1996.

[16] J. G. Bednorz and K. A. Müller. Possible high-T_c superconductivity in the Ba–La–Cu–O system. *Zeitschrift für Physik B*, 64:189–193, 1986.

[17] L. P. Gor'kov. Microscopic derivation of the Ginzburg-Landau equations in the theory of superconductivity. *Soviet Physics – Journal of Experimental and Theoretical Physics*, 9: 1364–1367, 1959.

[18] A. L. Fetter and J. D. Walecka. *Quantum Theory of Many-Particle Systems*, chapters 51 & 53. McGraw-Hill, 1971.

[19] M. Tinkham. *Introduction to Superconductivity*, section 4.1. McGraw-Hill, second edition, 1996.

[20] A. Zee. *Quantum field theory in a nutshell*, chapters v.3 & v.4. Princeton University Press, 2003.

[21] M. Tinkham. *Introduction to Superconductivity*, pages 114–115. McGraw-Hill, second edition, 1996.

[22] P. G. de Gennes. *Superconductivity of metals and alloys*, chapter 6. W. A. Benjamin, 1966. Translated from the French by P. A. Pincus.

[23] L. D. Landau, E. M. Lifshitz, and L. P. Pitaevskiĭ. *Statistical Physics, Part 2*, volume 9 of *Course of Theoretical Physics*, section 45. Pergamon Press, 1980. Translated from the Russian by J. B. Sykes and M. J. Kearsley.

[24] J. J. Sakurai. *Modern Quantum Mechanics*, pages 130–139. Addison-Wesley, revised edition, 1994.

[25] K. Fossheim and A. Sudbø. *Superconductivity: Physics and Applications*, section 4.7.3.

John Wiley and Sons, 2004.

[26] M. Tinkham. *Introduction to Superconductivity*, section 4.5. McGraw-Hill, second edition, 1996.

[27] K. Fossheim and A. Sudbø. *Superconductivity: Physics and Applications*, section 5.1. John Wiley and Sons, 2004.

[28] M. Tinkham. *Introduction to Superconductivity*, section 6.1. McGraw-Hill, second edition, 1996.

[29] B. D. Josephson. Possible new effects in superconductive tunnelling. *Physics Letters*, 1: 251–253, 1962.

[30] B. D. Josephson. Supercurrents through barriers. *Advances in Physics*, 14:419–451, 1965.

[31] B. D. Josephson. The discovery of tunnelling supercurrents. *Reviews of Modern Physics*, 46:251–254, 1974.

[32] J. B. Ketterson and S. N. Song. *Superconductivity*, chapter 30. Cambridge University Press, 1999.

[33] J. Bardeen. Tunneling into superconductors. *Physical Review Letters*, 9:147–149, 1962.

[34] V. Ambegaokar and A. Baratoff. Tunneling between superconductors. *Physical Review Letters*, 10:486–489, 1963.

[35] V. Ambegaokar and A. Baratoff. Tunneling between superconductors. *Physical Review Letters*, 11:104, 1963.

[36] L. G. Aslamazov and A. I. Larkin. Josephson effect in superconducting point contacts. *Journal of Experimental and Theoretical Physics Letters*, 9:87–91, 1969.

[37] R. Loudon. *The quantum theory of light*, section 4.1. Oxford University Press, third edition, 2000.

[38] M. Tinkham. *Introduction to Superconductivity*, page 204. McGraw-Hill, second edition, 1996.

[39] D. J. Griffiths. *Introduction to Electrodynamics*, page 313. Prentice Hall, third edition, 1999.

[40] M. Tinkham. *Introduction to Superconductivity*, page 214. McGraw-Hill, second edition, 1996.

[41] K. Fossheim and A. Sudbø. *Superconductivity: Physics and Applications*, page 134. John Wiley and Sons, 2004.

[42] J. R. Waldram. The Josephson effects in weakly coupled superconductors. *Reports on Progress in Physics*, 39:751–827, 1976.

[43] J. R. Waldram. *Superconductivity of metals and cuprates*. IOP, 1996.

[44] K. Fossheim and A. Sudbø. *Superconductivity: Physics and Applications*, sections 5.4 & 11.1. John Wiley and Sons, 2004.

[45] M. Tinkham. *Introduction to Superconductivity*, section 6.5.1. McGraw-Hill, second edition, 1996.

[46] M. Tinkham. *Introduction to Superconductivity*, section 6.5.2. McGraw-Hill, second edition, 1996.

Appendix C

Cooper pair box: analytic solution

The Hamiltonian for the Cooper pair box in the phase basis (section 7.1.1) leads to a time-independent Schrödinger equation which can be solved analytically. Here we present a brief derivation of the solutions to this equation, based on the work of Cottet [1] and Koch et al. [2].

From (7.13), the Cooper pair box Hamiltonian in the phase basis is given by

$$H = E_c \left(-\mathrm{i}\frac{\partial}{\partial \gamma} - n_g \right)^2 - E_J \cos \hat{\gamma} \,. \tag{C.1}$$

Thus, the phase-space energy eigenfunction $\psi_k(\gamma) \equiv \langle \gamma | E_k \rangle$ and its associated energy E_k satisfy the time-independent Schrödinger equation,

$$\left[E_c \left(-\mathrm{i}\frac{\partial}{\partial \gamma} - n_g \right)^2 - E_J \cos \gamma \right] \psi_k(\gamma) = E_k \psi_k(\gamma) \,, \tag{C.2}$$

with the periodic boundary condition

$$\psi_k(\gamma) = \psi_k(\gamma + 2\pi) \,. \tag{C.3}$$

Using the commutation relation $[\hat{\gamma}, \hat{n}] = \mathrm{i}$, and proceeding in a manner analogous to the standard examination of translation in quantum mechanics,[1] one obtains the equation

$$\exp\left(\mathrm{i}\hat{\gamma} \cdot \mathrm{d}n\right) |n\rangle = |n + \mathrm{d}n\rangle \,. \tag{C.4}$$

Because of this relation, we have

$$\exp\left(-\mathrm{i}n_g\hat{\gamma}\right) H(n_g) \exp\left(\mathrm{i}n_g\hat{\gamma}\right) = H(n_g' = 0) \,. \tag{C.5}$$

Following Koch et al. [2] and Cottet [4], we therefore introduce the function

$$\psi_k'(\gamma) = \mathrm{e}^{-\mathrm{i}n_g\gamma} \psi_k(\gamma) \,, \tag{C.6}$$

which satisfies the Schrödinger equation

$$-E_c \frac{\partial^2}{\partial \gamma^2} \psi_k'(\gamma) - E_J \cos(\gamma) \psi_k'(\gamma) = E_k \psi_k'(\gamma) \,. \tag{C.7}$$

[1] See, for example, Sakurai [3].

If we define

$$x \equiv \frac{1}{2}\gamma\,, \tag{C.8a}$$

$$u(x) \equiv \psi_k'(2x)\,, \tag{C.8b}$$

$$q \equiv -\frac{2E_J}{E_c}\,, \tag{C.8c}$$

$$a \equiv \frac{4E_k}{E_c}\,, \tag{C.8d}$$

we can recast the equation (C.7) in the form

$$\frac{\mathrm{d}^2u}{\mathrm{d}x^2} + \left[a - 2q\cos\left(2x\right)\right]u = 0\,, \tag{C.9}$$

which is the canonical form of *Mathieu's differential equation* [5]. The function $u(x)$ is π-periodic on x. Mathieu's differential equation possesses well-known analytic solutions.

The following is adapted from Cottet [4] and Abramowitz and Stegun [6]. For a given q, there exists a set of special values of a, called *characteristic values*, which yield the desired periodic solutions of (C.9). The characteristic values which yield even solutions of Mathieu's equation are denoted $a(v,q)$, while those that yield odd solutions are denoted $b(v,q)$.

Floquet's theorem[2] tells us that there exist solutions to (C.9) of the form

$$F_v(x) = \mathrm{e}^{\mathrm{i}vx}P(x)\,, \tag{C.10}$$

where $v(a,q)$ is a real parameter (known as the *characteristic exponent*) and $P(x)$ is a π-periodic function. Similarly,

$$F_v(-x) = \mathrm{e}^{-\mathrm{i}vx}P(-x) \tag{C.11}$$

satisfies (C.9) whenever (C.10) does. A further property is

$$u(x+m\pi) = \begin{cases} \mathrm{e}^{\mathrm{i}vm\pi}u(x) & \text{when } u(x) = F_v(x) \\ \mathrm{e}^{-\mathrm{i}vm\pi}u(x) & \text{when } u(x) = F_v(-x)\,; \end{cases} \tag{C.12}$$

solutions having this property are known as *Floquet solutions*. Choosing the former Floquet-type solution above, and back-substituting for $\psi_k(\gamma)$, we obtain

$$\begin{aligned} \psi_k(x) &= \frac{1}{\sqrt{2}}\exp(\mathrm{i}n_g\gamma)F_v\left(a,q,\frac{\gamma}{2}\right) \\ &= \frac{1}{\sqrt{2}}\exp\left[\mathrm{i}\left(n_g+\frac{v}{2}\right)\gamma\right]P\left(\frac{4E_k}{E_c},-\frac{2E_J}{E_c},\frac{\gamma}{2}\right). \end{aligned} \tag{C.13}$$

[2] See Abramowitz and Stegun [6] and references therein.

The corresponding energy eigenvalues E_k are given by

$$\begin{aligned} E_k &= \frac{E_c}{4} a\left(v, q\right) \\ &= \frac{E_c}{4} a\left(v, -\frac{2E_J}{E_c}\right). \end{aligned} \tag{C.14}$$

Expressions for the Floquet solutions F_z and the corresponding eigenvalues a are available in Abramowitz and Stegun [6].

From (C.13), applying the periodic boundary condition (C.3) gives

$$n_g + \frac{v}{2} \in \mathbb{Z}. \tag{C.15}$$

As such, for each value of n_g, only a set of certain discrete values of v, which we will call v_k with $k \in \mathbb{N}$, are possible. Each value v_k can be associated to an eigenfunction ψ_k; this can be done in such a way that E_k increases with k. See Koch et al. [2] and Cottet [4] for appropriate expressions for v_k in terms of k and n_g.

References

[1] A. Cottet. *Implementation of a quantum bit in a superconducting circuit*. PhD thesis, l'Université Paris VI, 2002.

[2] J. Koch, T. M. Yu, J. Gambetta, A. A. Houck, D. I. Schuster, J. Majer, A. Blais, M. H. Devoret, S. M. Girvin, and R. J. Schoelkopf. Charge-insensitive qubit design derived from the Cooper pair box. *Physical Review A*, 76:042319, 2007.

[3] J. J. Sakurai. *Modern Quantum Mechanics*, pages 44–50. Addison-Wesley, revised edition, 1994.

[4] A. Cottet. *Implementation of a quantum bit in a superconducting circuit*, section 1.1.3. PhD thesis, l'Université Paris VI, 2002.

[5] J. Meixner, F. W. Schäfke, and G. Wolf. *Mathieu Functions and Spheroidal Functions and Their Mathematical Foundations, Further Studies*. Springer-Verlag, 1980.

[6] M. Abramowitz and I. A. Stegun, editors. *Handbook of mathematical functions with formulas, graphs and mathematical tables*, chapter 20. Wiley, tenth edition, 1972.